Internally consistent thermodynamic data for aqueous species in the system Na-K-Al-Si-O-H-Cl

Author(s):
Miron, George D.; Wagner, Thomas; Kulik, Dmitrii A.; Heinrich, Christoph A.

Publication date:
2016-08-15

Permanent link:
https://doi.org/10.3929/ethz-b-000117090

Originally published in:
Geochimica et Cosmochimica Acta 187, https://doi.org/10.1016/j.gca.2016.04.026

Internally consistent thermodynamic data for aqueous species in the system Na-K-Al-Si-O-H-Cl

George D. Miron[a.b], Thomas Wagner[b], Dmitrii A. Kulik[c], Christoph A. Heinrich[a]

[a]Institute of Geochemistry and Petrology, ETH Zurich, Switzerland, dan.miron@erdw.ethz.ch
[b]Department of Geosciences and Geography, University of Helsinki, Finland
[c]Laboratory for Waste Management, Paul Scherrer Institut, 5232 Villigen PSI, Switzerland

Submitted to: Geochimica et Cosmochimica Acta

Date: 10 April 2016

Abstract

A large amount of critically evaluated experimental data on mineral solubility, covering the entire Na-K-Al-Si-O-H-Cl system over wide ranges in temperature and pressure, was used to simultaneously refine the standard state Gibbs energies of aqueous ions and complexes in the framework of the revised Helgeson-Kirkham-Flowers equation of state. The thermodynamic properties of the solubility-controlling minerals were adopted from the internally consistent dataset of Holland and Powell (2002; Thermocalc dataset ds55). The global optimization of Gibbs energies of aqueous species, performed with the GEMSFITS code (Miron et al., 2015), was set up in such a way that the association equilibria for ion pairs and complexes, independently derived from conductance and potentiometric data, are always maintained. This was achieved by introducing reaction constraints into the parameter optimization that adjust Gibbs energies of complexes by their respective Gibbs energy effects of reaction, whenever the Gibbs energies of reactant species (ions) are changed. The optimized thermodynamic dataset is reported with confidence intervals for all parameters evaluated by Monte Carlo trial calculations. The new thermodynamic dataset is shown to reproduce all available fluid-mineral phase equilibria and mineral solubility data with good accuracy and precision over wide ranges in temperature (25 to 800°C), pressure (1 bar to 5 kbar) and composition (salt concentrations up to 5 molal). The global data optimization process adopted in this study can be readily repeated any time when extensions to new chemical elements and species are needed, when new experimental data become available, or when a different aqueous activity model or equation of state should be used. This work serves as a proof of concept that our optimization strategy is feasible and successful in generating a thermodynamic dataset reproducing all fluid-mineral and aqueous speciation equilibria in the Na-K-Al-Si-O-H-Cl system within their experimental uncertainties. The new dataset resolves the long-standing discrepancies between thermodynamic data of minerals and those of aqueous ions and complexes, by achieving an astonishing degree of consistency between a large number of fluid-mineral equilibrium data. All of this at the expense of changing the standard state properties of aqueous species, manly the Gibbs energy of formation. Using the same strategy, the core dataset for the system Na-K-Al-Si-O-H-Cl can be extended with additional rock-forming elements such as Ca, Mg, Fe, Mn, Ti, S, C, B. In future, the standard-state properties of minerals and aqueous species should be simultaneously optimized, to create the next-generation of fully internally consistent data for fluid-mineral equilibria. Although we employ the widely used HKF equations for this study, the same computational approach can be readily applied to any other speciation-based equation of state for multicomponent aqueous solutions.

1. Introduction

Fluid-rock reactions play a key role in a wide range of geological processes such as mass transfer and hydrothermal convection at mid-ocean ridges, melting and fluid transfer in subduction zones, metamorphic devolatilization in compressional orogenic belts, the formation of hydrothermal ore deposits, and fluid circulation and permeability evolution in natural and engineered geothermal reservoirs. Detailed insight into fluid-rock reactions can be gained from quantitative field studies, high-temperature and -pressure laboratory experiments, and numerical geochemical and reactive transport simulations. Geochemical modeling combined with experimental studies of the equilibrium solubility of minerals and mineral assemblages are essential for constraining the transport capacity of natural aqueous fluids, for evaluating mass fluxes in fluid-rock systems, and for understanding reaction progress during hydrothermal alteration (e.g. Helgeson, 1969; Reed, 1982; Engi, 1992; Stefánsson, 2001; Zhu and Anderson, 2002; Anderson, 2005; Bénézeth et al., 2009; Sverjensky, 2014).

Numerical reactive transport modeling is a powerful approach for simulating geochemical processes in natural fluid-rock systems (e.g. Lichtner et al., 1997; Xu et al., 2001; Steefel and Maher, 2009; Zheng et al., 2009; Xu et al., 2011; Leal et al., 2014; Zhang et al., 2015), which are inaccessible to direct field studies and too complex for controlled laboratory experimentation. Reactive transport models rely critically on the robustness of the geochemical models and, hence, on the availability, accuracy, precision and consistency of parameters such as standard state properties of minerals and aqueous species, equilibrium constants for solubility reactions, activity and equation of state parameters for non-ideal multicomponent phases (mineral solid-solutions, aqueous solutions, fluid and gas mixtures), and kinetic rate constants for mineral dissolution and precipitation (Engi, 1992; André et al., 2006; Schott et al., 2009; Thien et al., 2014).

Considerable progress in the thermodynamic description of minerals and their solid-solutions at high temperatures and pressures has been driven by the development of internally consistent thermodynamic datasets (Holland and Powell, 1985; Powell and Holland, 1985; Berman et al., 1986; Berman, 1988; Chatterjee et al., 1994; Gottschalk, 1997; Chatterjee et al., 1998; Holland and Powell, 1998; Holland and Powell, 2011). Typically, properties of minerals and fluids that are known from high-precision experiments or sufficiently accurate estimation techniques (Berman and Brown, 1985; Holland, 1989) such as heat capacity, molar volume, thermal expansion and compressibility, are accepted without further modification, and only enthalpies of formation (and sometimes entropies) as the most critical and least accurately known parameters are refined during the global fitting process.

If changes are applied to the formation Gibbs energies of mineral endmembers, adjustments of similar magnitude should be applied to Gibbs energies of formation the respective aqueous ions

and complexes, to maintain the internal consistency. Adjustment of aqueous species data should be done in a simultaneous manner, by considering numerous mineral solubility experiments and always taking care that the complex electrolyte association equilibria known from conductance, electromotive force or spectroscopic experiments are maintained. However, aqueous electrolyte fluids at elevated temperatures and pressures have never been subject to any simultaneous derivation of internally consistent data, because such fitting needs to combine very diverse types of experimental data including mineral solubility as well as direct fluid property measurements. Instead, all thermodynamic databases commonly used for aqueous geochemistry, such as SUPCRT92 (Johnson et al., 1992; Shock et al., 1997; Sverjensky et al., 1997), the LLNL database (Delany and Lundeen, 1990), and the FreeGs database (Bastrakov et al., 2005), are based on sequential evaluation of individual solubility equilibria or fitting of a few selected reactions (Pokrovskii and Helgeson, 1995, 1997a, b).

As a consequence, large discrepancies between modeled and experimentally determined mineral solubilities and speciation equilibria may persist in these datasets. Paradoxically, the situation is becoming worse, because the mineral data present in the geochemical databases have since been refined by new algorithms and simultaneous fitting against solid-solid phase equilibria experiments but without including mineral solubility (Holland and Powell, 1998; Holland and Powell, 2011). Prominent examples illustrating these discrepancies are the large mismatch between predicted and measured fluid compositions in the feldspar-mica-quartz system (Montoya and Hemley, 1975; Popp and Frantz, 1980; Gunter and Eugster, 1981; Sverjensky et al., 1991; Haselton et al., 1995), substantial disagreement between calculated and accurately measured carbonate mineral solubility products (Bénézeth et al., 2009, 2011), and the poor description of ion association equilibria of major aqueous electrolytes such as HCl, KCl, NaOH, KOH and $CaCl_2$ (Tagirov et al., 1997; Ho and Palmer, 1996, 1997; Ho et al., 2001; Méndez de Leo and Wood, 2005). Reasons that have prevented developing internally consistent datasets for aqueous and hydrothermal geochemistry are the strong interrelation between standard state and activity model data (Helgeson et al., 1981), limitations in computational techniques and capacities required for the global fitting of very large datasets, and the uneven distribution of high-precision experimental data in temperature – pressure – composition space.

The body of experimental data for fluid-rock equilibria has grown considerably since the last concerted effort by Helgeson et al. (1981), Tanger and Helgeson (1988), Johnson et al. (1992), Sverjensky et al. (1997), and Shock et al. (1997). Of particular importance are high-precision experimental studies of electrolyte association using conductance methods. The experimental studies have covered most of the major aqueous electrolytes that are present in natural geofluids such as

NaCl, KCl, HCl, NaOH, and KOH (Ho et al., 1994; 2000a, 2000b, 2001; Ho and Palmer, 1996, 1997). The experiments were conducted with modern high-precision static and flow-through conductance instruments using very dilute salt solutions, which makes the derived ion pair association constants largely independent of the aqueous activity model that was used. In addition, these studies used improved and theoretically sound conductance models for data processing, which resulted in much more reliable and accurate equilibrium constants (Sharygin et al., 2001, 2002). The speciation equilibria for the most important constituents of natural geofluids are now well constrained by high-quality experimental data that cover wide ranges in temperature and pressure.

Connecting the thermodynamic properties of aqueous species with those of the rock-forming minerals requires experimental data for mineral solubility in aqueous solutions. A large amount of solubility measurements under crustal conditions at temperatures and pressures up to 600 °C and 10 kbar has been accumulated, including the solubility of rock-forming oxides, silicates, aluminosilicates and carbonates in pure water, aqueous salt solutions and H_2O-CO_2 mixtures. New solubility experiments of corundum and aluminum hydroxides (Bénézeth et al., 2001; Palmer et al., 2001), quartz (Manning, 1994; Newton and Manning, 2000; Shmulovich et al., 2001) and aluminosilicates (Shinohara and Fujimoto, 1994; Haselton et al., 1995; Manning et al., 2010; Wohlers et al., 2011) have become available. Most importantly, phase equilibria experiments have been performed in the multicomponent system Na-K-Al-Si-O-H-Cl at temperatures and pressures up to 650 °C and 2 kbar, involving the solubility of synthetic metapelite (K-feldspar, albite, aluminosilicate, quartz) in moderately saline aqueous solutions (Hauzenberger et al., 2001; Pak et al., 2003).

In summary, it is timely to develop a new approach to derive the first internally consistent thermodynamic dataset for fluid-rock equilibria that will resolve the discrepancies of the existing data. Our long-term vision is to develop a fully consistent dataset that covers at least the system Na-K-Ca-Fe-Mg-Mn-Al-Si-Ti-C-S-Cl-F-B-O-H, with possible extension to important ore metals and other trace elements. This dataset should simultaneously describe all experimentally determined mineral reaction equilibria, solubility measurements, spectroscopic data, and potentiometric and conductance constraints on aqueous speciation within experimental accuracy. As a first step towards that vision, we derive in this study an internally consistent dataset of the thermodynamic properties for aqueous species in the core system Na-K-Al-Si-O-H-Cl by simultaneously refining the standard state molal Gibbs energies of aqueous ions and complexes utilizing a large database of critically evaluated solubility, conductance and potentiometric experiments that cover a wide range in temperature, pressure and composition. The properties of the aqueous ions and complexes are derived using the Holland-Powell mineral dataset (Holland and Powell, 1998) as a given basis. The mineral properties from this dataset are assumed to be fully consistent and no adjustments were allowed to

their thermodynamic properties. The dynamic approach to dataset regression makes it possible to repeat the procedure whenever new and improved experimental constraints become available or when more aqueous species and chemical elements are added.

2. Thermodynamic framework

The standard state convention for aqueous species adopted in this study is the ideal one molal solution referenced to infinite dilution. For water solvent, the standard state is pure water at any pressure and temperature, and water activity is based on the mole fraction concentration scale. For minerals, the standard state is unit activity of pure solids at any pressure or temperature (Oelkers et al., 1995). The standard partial molal Gibbs energies applied for aqueous species in this study are the apparent standard partial molal Gibbs energies, defined as (Helgeson et al., 1981):

$$\Delta G^0_{T,P} = \Delta_f G^0_{T_r,P_r} + (G^0_{T,P} - G^0_{T_r,P_r}) \quad (1)$$

where $\Delta_f G^0_{T_r,P_r}$ represents the standard state partial molal Gibbs energy of formation (at reference temperature T_r = 298.15 K and reference pressure P_r = 1 bar) of the substance from the elements at their standard states at 298.15 K and 1 bar, and $(G^0_{T,P} - G^0_{T_r,P_r})$ represents the difference in the standard partial molal Gibbs energy of the substance at the temperature (T) and pressure (P) of interest and that at the reference temperature (T_r) and pressure (P_r).

The molar properties of minerals in this study were calculated from the Holland-Powell internally consistent thermodynamic dataset (Holland and Powell, 1998; updated Thermocalc 2002 dataset ds55) and the thermodynamic framework of this dataset. This dataset is referred to as HP02 in the remainder of this paper. The Gibbs energy of minerals at elevated temperatures and pressures is calculated by temperature integration of a 4-term heat capacity equation and pressure integration of a Murnaghan equation of state for molar volume. For phases with order-disorder transitions, a Landau model term is added (Holland and Powell, 1998). The following minerals were used during regression of solubility data: albite, andalusite, corundum, diaspore, kaolinite, kyanite, microcline, muscovite, nepheline, paragonite, pyrophyllite, quartz, sanidine, sillimanite, and topaz. The thermodynamic data for these minerals can be found in the electronic supplementary material (Table EA1). Recently, a new updated mineral dataset has been published (Holland and Powell, 2011), but we have preferred to use the previous dataset because it is supported by comprehensive solid-solution models for all relevant rock-forming minerals (feldspars, micas, amphibole, chlorite, pyroxene, epidote etc.) and the data for key minerals of the system Na-K-Al-Si-O-H-Cl are more consistent with

calorimetric constraints and the aqueous species data (Holland and Powell, 1998; Dolejs and Wagner, 2008). This results in smaller adjustments to the standard state properties of aqueous species during regression of the large body of experimental solubility data in this study.

Thermodynamic properties of water were calculated with the IAPS-84 equation of state (Kestin et al., 1984). The calculated Gibbs energies of H_2O liquid using this model were compared with the values calculated using the compensated Redlich-Kwong (CORK) model that is used in the HP02 dataset (Holland and Powell, 1991). The standard Gibbs energy per mole of H_2O calculated using the CORK model is slightly more positive than that calculated using IAPS-84 (in the range of 100-1000 °C and 1 bar to 5 kbar) with an average difference of 130 ± 90 J/mol. This difference is considerably smaller than the uncertainty of the experimental data that were used to derive both equations of state (Kestin et al., 1984; Holland and Powell, 1991) and thermodynamic properties predicted from both models are fully consistent with each other.

The properties of aqueous species were modeled within the framework of the revised Helgeson-Kirkham-Flowers (HKF) equation of state (Helgeson and Kirkham, 1974a, 1974b; Tanger and Helgerson, 1988; Shock et al., 1992). The HKF equation of state accounts for solvation and non-solvation properties of aqueous ions and complexes. The thermodynamic properties are calculated from $\Delta_f G^0_{298,1}$, $S^0_{298,1}$ and seven empirical coefficients (a_1, a_2, a_3, a_4, c_1, c_2, ω_0), which describe the temperature and pressure dependence of partial molal volume and heat capacity. HKF equation of state parameters were derived for a large number of aqueous species by regression of experimentally determined equilibrium constants, volume and heat capacity data (Tanger and Helgeson, 1988; Shock and Helgeson, 1988; Shock et al., 1989; Shock et al., 1997; Sverjensky et al., 1997; Sverjensky et al., 2014). Subsequently, empirical correlations between the partial molal properties were developed and used to predict the properties of a large number of aqueous species for which no or insufficient experimental data are available (Shock and Helgeson, 1988; Shock et al., 1989; Sassani and Shock, 1992; Shock et al., 1997; Sverjensky et al., 1997; Plyasunov and Shock, 2001; Sverjensky et al., 2014). These data were incorporated into the SUPCRT92 dataset (Johnson et al., 1992), which has become a de facto standard in geochemical modeling. We therefore use the SUPCRT92 dataset as a reference when comparing the calculations with our new dataset with experimental mineral solubility and phase stability data.

The activity coefficients for charged aqueous species were calculated with the extended Debye-Hückel equation (Helgeson et al., 1981):

$$\log_{10}\gamma_j = \frac{-A_\gamma z_j^2\sqrt{I}}{1+\mathring{a}B_\gamma\sqrt{I}} + b_\gamma I + \log_{10}\frac{n_{jw}}{n_w} \qquad (2)$$

where $A_{\square}$ and $B_{\square}$ represent the Debye-Hückel solvent parameters, $\mathring{a}$ stands for the ion size parameter, $b_{\square}$ is a semi-empirical extended term parameter, I represents the true ionic strength (corrected for ion pairing and complexing), and the last term represents the conversion from mole fraction to molality (with n_{jw} being the mole amount of water solvent, and n_w the total mole amount of the aqueous phase including water-solvent). In the model of Helgeson et al. (1981), $\mathring{a}$ and $b_{\square}$ are common for all charged aqueous species in the predominant electrolyte. Revised models that account for the temperature and pressure dependence of $b_{\square}$ for the four major background electrolytes (NaCl, KCl, NaOH, KOH) (Oelkers and Helgeson, 1990; Pokrovskii and Helgeson, 1995; Pokrovskii and Helgeson, 1997b; Pokrovskii and Helgeson, 1997a) were used in this study. In this model framework, the ion-size parameters are pressure and temperature dependent as well (Shock et al., 1992). The activity model is thought to be applicable for true ionic strengths up to 1-3 molal, but due to the formation of ion pairs with increasing temperature it can be used to total salt concentrations of up to 5 mol/kg (Oelkers and Helgeson, 1990; Sharygin et al., 2002; Dolejs and Wagner, 2008). For neutral species, the activity coefficient is assumed to be a linear function of the effective ionic strength:

$$\log_{10}\gamma_j = b_g I + \log_{10}\frac{n_{jw}}{n_w} \tag{3}$$

where b_g is the empirical Setchenow coefficient and is approximated to be equal to the common third parameter $b_{\square}$ used for the charged species. The activity coefficient of water is calculated from the osmotic coefficient as in Helgeson et al. (1981):

$$\ln a_w = -\frac{\phi\, m_\Sigma}{55.508435} \tag{4}$$

where m_Σ is the sum of molalities of all aqueous species, and ϕ is the osmotic coefficient, calculated as in Helgeson et al. (1981).

An additional thermodynamic constraint was to retain the properties of the Cl^- ion as reported in Shock and Helgeson (1988). This was done because for each chemical element in an internally consistent thermodynamic dataset, one anchor substance is needed, whose thermodynamic properties are accepted from calorimetric data (Holland and Powell 1990; 1998). Chlorine is a fluid volatile element and there are no chlorine-bearing silicate mineral phases in the HP02 dataset that would be suitable as anchor phases; the properties of halite (NaCl) in the HP02 dataset were adapted from Robie and Hemingway (1995) without being linked to other mineral phases by reaction equilibria. The standard state partial molal Gibbs energy, enthalpy, and entropy of Cl^- originate from the CODATA compilation (Cox et al., 1989) and were determined using electromotive force data at different temperatures (Bates and Kirschman, 1919; Bates and Bower, 1954; Cerquetti et al., 1968)

and heat of solution data of gaseous hydrogen chloride (Vanderzee and Nutter, 1963). The values of the standard state partial molal heat capacity and volume of Cl^- were estimated by regressing standard partial molal volume, isothermal compressibility and isobaric heat capacity data (up to 100 °C) for aqueous HCl electrolyte solutions (Tanger and Helgeson, 1988), which were then used to derive the HKF parameters (Shock and Helgeson, 1988).

The H_2O dissociation constants calculated with the properties of the OH^- ion from the SUPCRT92 database differ by as much as 0.3-0.4 log units from those calculated from the density equation of Marshall and Franck (1981). However, the values for the H_2O dissociation constant calculated with the SUPCRT92 data are much closer to the data obtained from the new formulation by Bandura and Lvov (2006). This formulation is now recommended by the International Association for the Properties of Water and Steam as a replacement of the older formulation by Marshall and Franck (1981). The average deviation between the values calculated using the SUPCRT92 data for the OH^- ion and the formulation of Bandura and Lvov (2006) is better than 0.1 log units, which is well within the original experimental uncertainty. Consequently, we have retained the properties of the aqueous OH^- ion from the SUPCRT92 database.

3. Ion association properties of major electrolytes

Revision of the ion pair association constants for major electrolytes (NaCl, KCl, NaOH, KOH) was required due to many contradicting data and new high precision conductance experiments at high temperatures and pressures that became available since the major reviews by Sverjensky et al. (1997) and Shock et al. (1997). The partial molal standard state properties and HKF parameters of the neutral ion pairs $NaCl^0$, KCl^0, $NaOH^0$, and KOH^0 were refined using the OptimB optimization program (Shvarov, 2015), using equilibrium constants derived from recent conductance experiments. These experimental data have the advantage over the older datasets that the conductance was measured in very dilute solutions (Ho and Palmer 1997; Ho et al., 2000a, b; Ho et al., 2001; Sharygin et al., 2002; Zimmerman et al., 2007; Arcis et al., 2014) and that equilibrium constants were derived with more theoretically sound models for the conductivity of electrolyte solutions (Tagirov et al., 1997; Ho and Palmer 1997; Ho et al., 2000 a, b; Ho et al., 2001; Tagirov et al., 1997; Zimmerman et al., 2007; Plumridge et al., 2015). This makes the equilibrium constants retrieved from the conductance data largely independent from the aqueous activity model employed.

3.1. $NaCl^0$ association constant

A considerable body of experimental data on the association constant of $NaCl^0$ has become available that was not used in the data analysis by Sverjensky et al. (1997). The association constant of $NaCl^0$

has been determined by high-precision conductance measurements of dilute aqueous NaCl solutions (with both a static and a flow-through cell) over wide ranges of temperature and pressure of 250-600 °C and 0.1-3.4 kbar (Ho et al., 1994, 2000a; Zimmermann et al., 1995; Gruszkiewicz and Wood, 1997). In addition, the association constant has been derived from mean stoichiometric activity coefficients in the temperature interval 200-350 °C at saturated water vapor pressure (Plyasunov, 1988). We have obtained thermodynamic properties of $NaCl^0$ from regression of the association constants based on the new conductance data only. The association constants calculated with the new thermodynamic properties of $NaCl^0$ are fairly consistent with the ones derived in the supercritical region (400-800 °C, 0.5-4.0 kbar) by Oelkers and Helgeson (1988) from the older conductance data of Quist and Marshall (1969). Figure 1A shows a comparison between the calculated values from this study, those calculated with the data from SUPCRT92 (Sverjensky et al., 1997), and the experimental data of Ho et al. (1994).

3.2. KCl^0 association constant

Substantial experimental datasets were published after the comprehensive data analysis presented by Sverjensky et al. (1997). The association constant of KCl^0 has been determined using high-precision conductance measurements (Ho and Palmer, 1997; Ho et al., 2000a) in the temperature range of 50-600 °C at pressures from saturated water vapor pressure (SWVP) to 3.4 kbar. In addition, association constants for KCl^0 were derived from mean stoichiometric activity coefficients in the temperature range 100-325 °C at saturated water vapor pressure (Pokrovskii and Helgeson, 1997a). The conductance data below 300 °C (Ho et al., 2000a) have a very large associated error and are inconsistent with those at higher temperatures. The association constants derived from mean stoichiometric activity coefficients at low temperatures were found to be inconsistent with the conductance data of Ho and Palmer (1997) and introduce larger errors in the properties of KCl^0 when included into the regression. Therefore, we have only considered dissociation constants derived from the conductance data above 300 °C for retrieving new thermodynamic properties of KCl^0 (Fig. 1B).

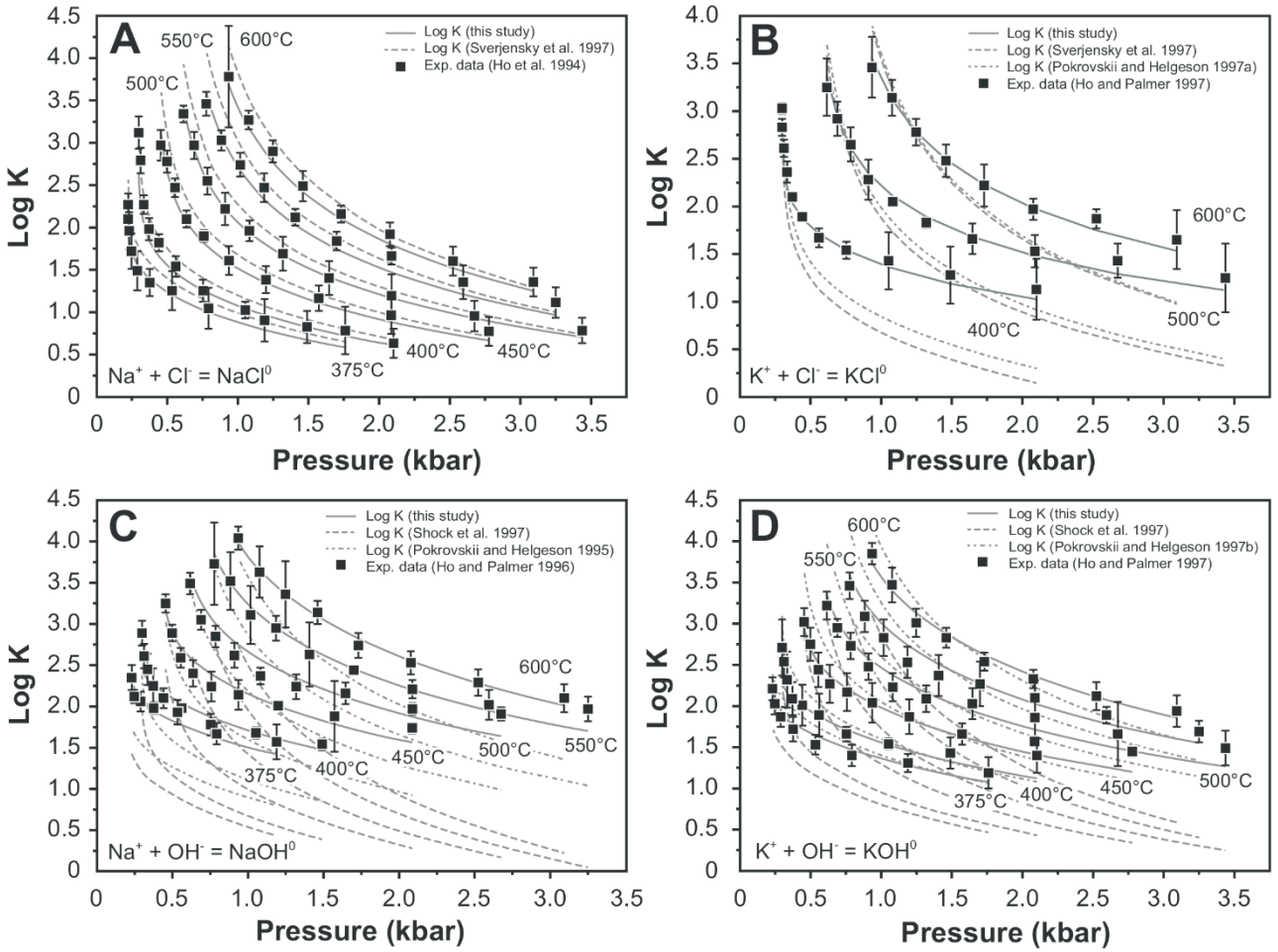

Figure 1. Comparison between calculated and experimentally determined (Ho et al., 1994; Ho and Palmer, 1996; Ho and Palmer, 1997) association constants for the major electrolytes (**A**) NaCl, (**B**) KCl, (**C**) NaOH and (**D**) KOH. Calculated association constants are from this study, the SUPCRT92 dataset (Shock et al., 1997; Sverjensky et al., 1997) and critical assessments of individual systems (Pokrovskii and Helgeson, 1995, 1997a, 1997b).

3.3. $NaOH^0$ association constant

The thermodynamic properties for $NaOH^0$ derived by Shock et al. (1997) are mainly based on few experiments at low temperatures and saturated water vapor pressure. Predictions of the association constants in the supercritical region at temperatures exceeding 400 °C are in gross disagreement with newer experimental data that extend to higher pressures and temperatures. The dissociation constant of $NaOH^0$ was recently determined using conductance measurements at temperatures of 100-600 °C and pressures of 0.1-3.1 kbar (Ho and Palmer, 1996; Ho et al., 2000b). Additional data were derived from mean stoichiometric activity coefficients in the temperature range 25-250 °C at saturation pressure (Pokrovskii and Helgeson, 1995) but, like in the case of KCl^0, they introduce larger errors for the properties of $NaOH^0$ at supercritical conditions when fitted together with the conductance data. We have therefore retrieved thermodynamic properties of $NaOH^0$ from dissociation constants based on the conductance data above 300 °C (Fig. 1C).

3.4. KOH^0 association constant

The thermodynamic data for KOH^0 given by Shock et al. (1997) are essentially based on correlations and estimations. Pokrovskii and Helgeson (1997b) have obtained thermodynamic data for KOH^0 from regression of association constants that were derived from conductance measurements of Franck (1956) and Lukashov et al. (1975). The conductance models employed by Franck (1956) and Lukashov et al. (1975), which were used to extract the limiting equivalent conductance and association constants from the experiments, were shown to be very inaccurate compared to more recent studies (e.g., Ho et al., 2000b; Sharygin et al. 2001; Sharygin et al. 2002). Consequently, association constants in the supercritical region calculated with the models of Shock et al. (1997) and Pokrovskii and Helgeson (1997b) are in considerable disagreement with the most recent experimental data. The association constants of KOH^0 were derived from high-precision conductance measurements in the temperature range 100-600 °C and at pressures of 0.14-3.4 kbar (Ho and Palmer 1997; Ho et al., 2000b). We have retrieved the thermodynamic properties of KOH^0 from regression of those new experimental data (Fig. 1D).

3.5. HCl^0 association constant

Based on the consideration of available datasets, we have concluded that the critical assessment of the properties of HCl^0 given by Tagirov et al. (1997) is the most consistent with the majority of experimental data, and we have accepted this dataset. The data that were derived by Tagirov et al. (1997) represent virtually all the experimental data available at the time when the evaluation was performed (e.g., Frantz and Marshall, 1984; Ruaya and Seward, 1987; Simonson et al., 1990; Sverjensky et al., 1991; Sretenskaya, 1992; Tagirov et al., 1997), except the experimental data points from Frantz and Marshall (1984) in the low-density region. Furthermore, the data from Tagirov et al. (1997) are in excellent agreement with recent potentiometric measurements by Reukov and Zotov (2006) and reasonably consistent with the new conductance measurements by Ho et al. (2001). Note that most of the experiments by Ho et al. (2001) were performed in the low-density region (350-400 °C, 0.26-0.31 kbar) where calculations using the revised HKF model are not accurate.

4. Selection of experimental solubility data

A large range of experimental mineral solubility datasets was reviewed prior to regression of the thermodynamic properties of aqueous species. Not all the experimental datasets could be used for fitting, because of mutual inconsistencies between different solubility datasets and, sometimes,

insufficient documentation of the experimental conditions. The critical evaluation of experimental data was based on the following set of criteria:

(1) *Proof of attainment of equilibrium*. Preferred solubility experiments were the ones performed from both undersaturated and supersaturated conditions. In case where solubility equilibrium was only approached from undersaturated conditions, the documentation of the experimental conditions was carefully screened for sufficiently long run times and proper demonstration that indeed equilibrium solubility was measured.

(2) *Potential problems encountered during the experiments*. The documentation of the experimental conditions (where possible) was checked for possible reactions with the capsule or autoclave material, presence of contaminant phases or impurities in the reactants, or precipitation of mineral phases during quench.

(3) *Experimental and analytical methods*. The simplest way to perform solubility measurements is by the weight loss method, where only the weight loss of the reactant mineral is measured before and after the experiment (Morey et al., 1962; Manning, 1994). Using this method, it is impossible to demonstrate attainment of equilibrium from both undersaturated and supersaturated conditions, but the problem is often addressed by investigating the required time for attainment of equilibrium or by comparison with reversed equilibrium experiments (Anderson and Burnham, 1965). The potentially largest source of error in weight loss experiments is mineral precipitation during the quench of the solutions (Manning, 1994). Therefore, experiments that use a fast quench method are preferred. Experimental settings that avoid problems due to quenching are the ones that extract the aqueous solution to be analyzed at run temperature and pressure. The analytical methods used for analyzing the elemental composition of the aqueous solutions can have a great impact on the accuracy of the measurements. Some elements, like aluminum, have very low concentrations under most experimental conditions studied. We have therefore preferred studies that demonstrate the reproducibility of measured dissolved element concentrations using different analytical techniques.

(4) *Consistency of the experiments*. The agreement between different independent measurements of the same quantity and the agreement between data obtained with different experimental methods served as an important selection criterion. In cases where many experimental studies have investigated one chemical system over the same range in pressure and temperature, it is critical that the reported values are consistent with each other within their stated uncertainty. However, the observation that several experimental datasets are consistent with each other while another dataset is not, is not a proof that the inconsistent dataset is the incorrect one. Therefore, our strategy was based on identifying at least one high quality dataset that would meet the strictest quality criteria (reversed equilibria, well documented experimental conditions and results, accurate analytical techniques) as a

basis for evaluating the quality of other datasets. The high quality datasets would also need to show reasonably consistent trends in temperature, pressure and composition space and not a large scatter of the measured properties.

In a number of cases, the experimental uncertainty associated with the data is not specified, or it is difficult to assess. Commonly, the total error of the experiments does not account for the accuracy of the experimental conditions and the accuracy of the analytical methods. The selected high quality studies would always report the total errors, while others would not report them. For this reason, in our study the experimental errors could not be directly applied as weights in the optimization routine.

Due to the limitation of the revised HKF model (Tanger and Helgeson 1988) to pressures up to 5 kbar, only experiments at conditions equal or below 5 kbar were used during data regression (and experiments at pressures above 5 kbar are not considered in the following experimental data review). Sverjensky et al. (2014) proposed an extension of the HKF model to much higher pressures based on a different equation of state for water properties (Zhang and Duan, 2005) and an empirical expression for the dielectric constant of water valid up to 60 kbar. In their model, they used new correlations for the pressure dependence of the HKF parameters, as well as different speciation models for silica and aluminum including dimers and polymers that are needed for the high pressure systems. Understanding of the solubility and aqueous speciation of rock-forming elements at very high temperatures and pressures is still far from complete, and substantially more experimental data are needed to resolve some of the disagreements between different studies (Audetat and Keppler, 2005; Antignano and Manning, 2008; Dolejs and Manning, 2010; Hayden and Manning, 2011; Mookherjee et al., 2014).

Because the extended Debye-Hückel activity model (Helgeson et al., 1981; Oelkers and Helgeson, 1990; Pokrovskii and Helgeson, 1995; Pokrovskii and Helgeson, 1997b; Pokrovskii and Helgeson, 1997a) used in our study is only valid up to salt concentrations of about 5 molal, experiments at higher concentrations (Sharygin et al., 2002) were excluded from the regression. A restriction of 2 and 3 molal for the calculated effective ionic strength was placed on experiments below and above 100 °C, respectively. Appelo et al. (2015) showed that the calculated activity coefficient for NaCl solutions starts to deviate from the measured values above 2 molal NaCl concentration at 25 °C. Nevertheless, we do compare the calculated mineral solubility data with their experimental counterparts at higher salt concentrations to evaluate the extrapolation capability of our thermodynamic model.

4.1. Quartz solubility

The solubility of quartz in water and salt solutions has been extensively studied over a wide range of pressure and temperature using various experimental methods and analytical techniques. A summary of the experimental datasets selected for the final database is presented in Table 2. These datasets were divided into three categories.

The first category contains experiments for which the authors demonstrated solubility equilibrium by approaching it both from undersaturated and supersaturated conditions (Morey et al., 1962; Crear and Anderson, 1971; Walther and Orville, 1983). These experiments involved the usage of pressure bombs or extraction-quench vessels and sampling of the solution in equilibrium with quartz at run conditions.

The second category of experiments were those where equilibrium was reached only from undersaturated conditions, but they employed (depending on the conditions) run times on the order of several days or even weeks (sufficient time to reach equilibrium). Equilibrated solution in these experiments was sampled at run conditions (Lier et al., 1960; Rimstidt, 1997) or for experiments above 100 °C after fast quenching (in less than 1 minute) (Siever, 1962; Hemley et al., 1980). Because of the slow dissolution rate of quartz, experiments at low temperatures require equilibration times on the order of many days, sometimes years (Rimstidt, 1997). Rimstidt (1997) studied the solubility of quartz at ambient conditions by analyzing the solution in equilibrium with quartz at 21 °C after more than 13 years. The thermodynamic data derived from these experiments are consistent with the ones obtained from amorphous silica solubility experiments widely investigated due to the technological importance for the glass manufacturing industry (Rimstidt, 1997). Rimstidt (1997) convincingly argued that the previously determined value for quartz solubility at ambient conditions (Morey et al., 1962) is incorrect because equilibrium was not attained.

The third category of experiments considered were those that used weight loss of a single quartz crystal and employed a very fast quenching procedure (less than 1 minute). This included the experiments from Manning (1994) and Newton and Manning (2000). Their approach minimized the possibility of silica precipitation on the primary quartz crystal or on the capsule walls. All

Table 1. Standard state properties (partial molal entropy, heat capacity and volume) and HKF parameters of neutral ion pairs derived from association constant data based on new conductance experiments.

Species	$S^0_{298,1}$ (J/mol·K)	$Cp^0_{298,1}$ (J/mol·K)	$V^0_{298,1}$ (J/bar)	$a_1 \cdot 10$ (cal/mol/bar)	$a_2 \cdot 10^{-2}$ (cal/mol)	a_3 (cal·K/mol/bar)	$a_4 \cdot 10^{-4}$ (cal·K/mol)	c_1 (cal/mol/K)	$c_2 \cdot 10^{-4}$ (cal·K/mol)	$\omega_0 \cdot 10^{-5}$ (cal/mol)
[(1)]$NaCl^0$	110.8	47.52	2.4	5.0828	4.6290	3.9306	-2.9704	13.6339	-0.7212	0.0889
[(1)]$NaOH^0$	42.4	113.5	-0.023	1.7792	-3.4372	7.1010	-2.6369	22.8222	2.6543	0.1189
[(1)]KCl^0	182.16	33.32	2.99	5.8341	7.0550	2.9771	-3.0707	-5.7084	7.6228	0.1996
[(1)]KOH^0	90.6	41.47	1.41	3.7562	1.3900	5.2037	-2.8365	13.4990	-1.0192	0.1665
[(2)]HCl^0	1.76	149.5	1.64	16.1573	-11.4311	-46.1866	-2.3036	46.4716	-5.2811	0.0000

[(1)] Optimized using association constant data.
[(2)] Taken from Tagirov et al. (1997).

Table 2. Summary of the quartz and corundum solubility experiments selected for the global optimization.

Reference	System	Number of data points used (total number)	[(1)]Direction of equilibrium	Temperature range (deg. C)	Pressure range (kbar)	Dataset total error (Eq. 10)
Morey et al. (1962)	Quartz-H_2O	20 (41)	U+S	45 – 300	SWVP – 1.0	0.009
Crear and Anderson (1971)	Quartz-H_2O-NaOH	18 (38)	U+S	179 – 329	SWVP	0.028
Fournier et al. (1982)	Quartz-H_2O-NaCl	30 (35)	U+S	350	0.2 – 0.5	0.012
Walther and Orville (1983)	Quartz-H_2O	13 (20)	U+S	350 – 550	1 – 2	0.018
Lier et al. (1960)	Quartz-H_2O	5 (5)	U	65 – 100	SWVP	0.014
Siever (1962)	Quartz-H_2O	4 (16)	U	125 – 182	SWVP	0.015
Adcock (1985)	Quartz-H_2O	1 (1)	U	400	1.0	0.035
Manning (1994)	Quartz-H_2O	4 (52)	U	500 – 900	5 – 20	0.097
Rimstidt (1997)	Quartz-H_2O	5 (10)	U	21 – 96	SWVP	0.029
Newton and Manning (2000)	Quartz-H_2O	4 (10)	U	500 – 900	2 – 15	0.078
Becker et al. (1983)	Corundum-H_2O	10	U	670	2 – 20	0.053
Tropper and Manning (2007)	Corundum-H_2O	2	U	700 – 1100	5 – 20	0.041
Anderson and Burnham (1967)	Corundum-H_2O-KOH	6	U	600 – 900	2 – 6	0.081
Pascal and Anderson (1989)	Corundum-H_2O-NaOH-KOH	21	U	600 – 700	2 – 2.6	0.023
Barns et al. (1963)	Corundum-H_2O-NaOH-KOH	5	U	430 – 600	1.45	0.156

[(1)] U: equilibrium approached from undersaturation; S: equilibrium approached from supersaturation.
[(2)] SWVP: Saturated water vapor pressure.

experimental data from categories 1 through 3 discussed above were included into the final experimental database.

Several studies determined quartz solubility using the weight loss method (Kennedy, 1950; Wyart and Sabatier, 1955; Kitahara, 1960; Weill and Fyfe, 1964; Novgorodov, 1975; Novgorodov, 1977) at conditions between 160 and 400 °C, from saturated water vapor pressure up to 2 kbar. Kennedy (1950) and Weill and Fyfe (1964) demonstrated the attainment of equilibrium by performing a series of dissolution rate experiments, thereby establishing the time required for obtaining a stable value for the concentration of dissolved silica. A drawback of their experimental procedure was the slow quench time used, increasing the risk of silica precipitation. Another important source of error was the determination of water present in the capsule at different conditions, which is essential for calculating the correct solubility (Weill and Fyfe, 1964). When compared with the preferred datasets reviewed above (Table 2), these experiments show systematically lower solubility. This most likely reflects problems related to silica precipitation during slow quenching, and we have therefore not included these data into the final experimental database.

A number of studies have measured quartz solubility by weight loss in perforated gold capsules containing quartz grains (Anderson and Burnham, 1965, 1967; Shmulovich et al., 2001, 2006). These capsules were enclosed in larger sealed gold capsules during the experiments. The difference in weight of the inner capsule after the completion of the runs was then taken as the amount of quartz dissolved in the solution of the outer capsule. Using this method, the fluid in the outer capsule is partially separated from the quartz in the inner capsule, preventing the precipitation of silica on the quartz crystal during quench (Anderson and Burnham, 1965). The authors approximated the time required to attain equilibrium by performing time series dissolution experiments (Anderson and Burnham, 1965) or by allowing relative large run times for equilibration (Shmulovich et al., 2001; Shmulovich et al., 2006). When compared with the datasets that employed a fast quench method or measured the solubility of quartz from both undersaturated and supersaturated conditions, the measured quartz solubility of these experiments is systematically lower. Manning (1994) reports on average about 10% higher quartz solubility for experiments above 600 °C compared to Anderson and Burnham (1965). One possible explanation for the lower solubility reported by Anderson and Burnham (1965) is the precipitation of quartz in the outer capsule during quench (Manning 1994). Shmulovich et al. (2001) report that in some of their experiments quartz could have precipitated on the cold end of the quartz crystal due to a small temperature gradient present in their capsules. These data were therefore not included into the final experimental database.

The dataset of Morey et al. (1962) shows considerably lower solubility at temperatures below 130 °C, compared to the trend of the data at higher temperatures. This most likely reflects that

equilibrium was not attained in the lower temperature experiments. Therefore, the experimental data below 130 °C were not included into the final experimental database.

Experimental measurements of quartz solubility in NaOH solutions were performed by Crear and Anderson (1971) and agree with those done in pure H_2O when considering Si-Na complexation. The quartz solubility in KOH solutions reported by Cloke (1954) shows a large scatter of ±1 log units, which is possibly due to corrosion of the experimental capsule. When compared with quartz solubility in pure water, the values reported by Anderson and Burnham (1967) and Pascal and Anderson (1989) for quartz solubility in KOH solutions are higher by 0.1 log units, indicating the presence of a K-Si complex. The quartz solubility experiments performed by Ostapenko et al. (1969) in NaOH solutions show better agreement with the selected data for quartz solubility in pure water. However, Ostapenko et al. (1969) used a slow quench method, which casts doubt on their results. The data of Ostapenko et al. (1969) were therefore not included into the final experimental database.

The solubility of quartz in NaCl solutions has been investigated in a number of studies (see review by Akinfiev and Diamnond, 2009). The well-documented experiments of Fournier et al. (1982) were done using a gold bag hydrothermal apparatus. Equilibrium was reached both from undersaturated and supersaturated conditions, and the experimental solution was extracted at run conditions, quenched to below 80 °C and analyzed. This dataset also agrees with the experimental data for quartz solubility in H_2O and NaOH solutions reviewed above, and was therefore included into the final experimental database. A second dataset accepted for the final experimental database was that of Newton and Manning (2000), which was performed with the weight loss method but with a fast quench technique. The quartz solubility experiments in NaCl, KCl, and HCl solutions of Anderson and Burnham (1967) were not included into the final experimental database, because of the slow quench method used.

4.2. Corundum solubility

Corundum solubility in water and aqueous electrolyte solutions has been extensively studied and reviewed by Pokrovskii and Helgeson (1995, 1997b). There are several experimental studies of corundum solubility in pure water at elevated temperatures and pressures. The datasets included into the final experimental database are summarized in Table 2. Most of these experiments used the weight loss method (Anderson and Burnham, 1967; Burnham et al., 1973; Becker et al., 1983; Tropper and Manning, 2007). Ragnarsdóttir and Walther (1985) and Walther (1997) used an extraction-quench technique and measured the equilibrium concentration from both undersaturated and supersaturated conditions. The difference between these two datasets is around one order of magnitude. The solubility experiments of Walther (1997) yielded about 1.2-1.5 log units higher Al concentrations

than those of Becker et al. (1983) and Tropper and Manning (2007). The experiments of Becker et al. (1983) and Tropper and Manning (2007) are in excellent agreement with each other and were used in several studies to model corundum solubility at high pressures and temperatures (Dolejs and Manning 2010; Sverjensky et al. 2014). Ragnarsdóttir and Walther (1985) report the presence of 0.3 wt.% of Na_2O impurity in their starting material. Although they discarded their first runs (yielding 2 orders of magnitude higher Al solubility than the subsequent ones), even a small amount of Na_2O could dramatically influence the pH of the solution, the Al speciation and thus the total Al solubility.

The low solubility of corundum in water, as well as the very slow equilibration rates, result in generally rather poor reproducibility of dissolved aluminum concentrations in solubility experiments. The large scatter and the substantial disagreement between different datasets could be due to different grain sizes of the starting solid materials used, different sample treatment to remove contamination, or due to the formation of other stable phases during the experiments such as aluminum hydroxides which would substantially increase the solubility. The datasets of Walther (1997) and Ragnarsdóttir and Walther (1985) are in gross disagreement with other experiments and new high pressure experiments (Dolejs and Manning, 2010) and were therefore not included into the final experimental database.

The solubility of corundum in both KOH and NaOH solutions was studied by Barns et al. (1963), Anderson and Burnham (1967), and Pascal and Anderson (1989). Azaroual et al. (1996) studied corundum solubility in KOH solutions, and Yalman et al. (1960) and Yamaguchi et al. (1962) in NaOH solutions. All studies employed a weight loss method. The experiments of Yamaguchi et al. (1962) employed a very slow quench technique, making it likely that Al minerals precipitated during quench and that the measured solubility is lower than the equilibrium solubility. The corundum solubility data in NaOH solutions at 400 °C and 276 bars obtained by Yalman et al. (1960) are systematically lower by around 0.1 log units, compared with the other datasets. We suspect that equilibrium was not reached in their experiments. The solubility measurements of corundum in KOH solutions at 400 °C and 0.5-2.0 kbar performed by Azaroual et al. (1996) are somewhat lower (0.1 log units) than those predicted from the thermodynamic model of Pokrovskii and Helgeson (1997b). The calculated values using the model of Pokrovskii and Helgeson (1997b) reproduce the experimental data of Pascal and Anderson (1989), Anderson and Burnham (1967), and Barns et al. (1963) within their uncertainty. Therefore, we have selected only these data for the final experimental database.

Additional corundum solubility experiments were done by Walther (2001) in NaCl solutions and Korzhinskiy (1987) in HCl solutions. The resulting solubilities are much higher than in pure water, up to 2 log units in NaCl solutions (Walther, 2001) and up to 4 log units in HCl solutions

(Korzhinskiy, 1987). To explain these elevated solubilities, the authors considered the possibility of chloro-aluminum complexes at their experimental conditions. Because the number of experimental data points was too small for refining the properties of Al-Cl species, we have not included these datasets into the final experimental database.

4.3. Gibbsite, boehmite and diaspore solubility

Several reviews of the solubility of aluminum hydroxide minerals have been published in the past decades (Apps et al., 1988; Apps and Neill, 1990; Hemingway et al., 1991; Verdes et al., 1992; Wesolowski, 1992; Pokrovskii and Helgeson, 1995; Pokrovskii and Helgeson, 1997b; Tagirov and Schott, 2001; Tutolo et al., 2014). Because of the intrinsic experimental difficulties related to measurement of Al solubility, new high quality studies have been performed quite recently (Palmer et al., 2001; Bénézeth et al., 2001). Reflecting the availability of new data, we have performed a critical analysis of all available experimental datasets that report the solubility of aluminum hydroxide phases.

4.3.1. Gibbsite solubility

We selected a number of datasets that report the solubility of gibbsite in NaOH solutions for our final experimental database (Table 3). Gibbsite solubility was determined from both undersaturated and supersaturated sides by Ikkatai and Okada (1962) in NaOH solutions and by Wesolowski (1992) in NaOH, NaCl, KOH, and KCl solutions. Russell et al. (1955) collected a large consistent dataset allowing for very long run times (up to 11 days at 40 °C). Only the experiments above 120 °C were excluded because they reported decomposition of gibbsite to boehmite at these conditions. The experimental datasets of Tsirlina (1936) and Lyapunov et al. (1964) show rather close agreement with the results from the experimental studies discussed above. The dataset of Tsirlina (1936) was included while the one of Lyapunov et al. (1964) was excluded because of the high concentration of NaOH used in their study that exceeded the ion strength limit of 3 molal (where the activity model employed is considered appropriate). The gibbsite solubility data reported by Palmer and Wesolowski (1992)

Table 3. Summary of the gibbsite, boehmite and diaspore solubility experiments selected for the global optimization.

Reference	System	Number of data points used (total number)	[(1)]Direction of equilibrium	Temperature range (deg. C)	[(2)]Pressure range (kbar)	Dataset total error (Eq. 10)
Ikkatai and Okada (1962)	Gibbsite-H_2O-NaOH	14	U+S	40 – 130	SWVP	0.133
Wesolowski et al. (1992)	Gibbsite-H_2O-NaOH-NaCl	28	U+S	25 – 80	0.001	0.021
Russell et al. (1955)	Gibbsite-H_2O-NaOH	34	U	40 – 120	SWVP	0.040
Tsirlina (1936)	Gibbsite-H_2O-NaOH	6	U	95	0.001	0.042
Palmer and Wesolowski (1992)	Gibbsite-H_2O-NaCl-HCl	51	U	30 – 70	0.001	0.051
Bénézeth et al. (2001)	Boehmite-H_2O-NaOH-NaCl-HCl	392	U+S	100 – 290	SWVP	0.040
Palmer et al. (2001)	Boehmite-H_2O-NaOH-NaCl-HCl	108	U+S	100 – 290	SWVP	0.061
Castet et al. (1993)	Boehmite-H_2O-NaOH-NaCl-HCl	57	U+S	90 – 350	SWVP	0.053
Verdes et al. (1992)	Boehmite-H_2O-NaOH-NaCl	18	U	135 – 300	SWVP	0.031
Diakonov et al. (1996)	Boehmite-H_2O-NaOH-NaCl	16	U	125 – 350	SWVP	0.007
Salvi et al. (1998)	Boehmite-H_2O-NaOH	2	U	300	SWVP	0.017
Kuyunko et al. (1983)	Boehmite-H_2O-NaOH	8	U	200 – 250	SWVP	0.031
Bernshtein and Matsenok (1961)	Boehmite-H_2O-NaOH	6	U	250 – 300	SWVP	0.037
Russell et al. (1955)	Boehmite-H_2O-NaOH	33	U	80 – 170	SWVP	0.180
Druzhinina (1955)	Boehmite-H_2O-NaOH	4	U	200	SWVP	0.084
Verdes et al. (1992)	Diaspore-H_2O-NaOH-NaCl	26	U	135 – 300	SWVP	0.040
Wefers (1967)	Diaspore-H_2O-NaOH	19	U	250 – 330	SWVP	0.168
Bernshtein and Matsenok (1965)	Diaspore-H_2O-NaOH	4	U	250 – 300	SWVP	0.042
Druzhinina (1955)	Diaspore-H_2O-NaOH	5	U	200 – 220	SWVP	0.099

[(1)] U: equilibrium approached from undersaturation; S: equilibrium approached from supersaturation.
[(2)] SWVP: Saturated water vapor pressure.

are in good agreement with the other selected datasets and thus were included into the final experimental database.

By contrast to the studies reviewed in the section above, the experimental results of Fricke and Jucaitis (1930) and Sato (1954) show systematically higher solubilities and were not included into the final experimental database (Fig. 2). The data of Berecz and Szita (1970) are in close agreement with other studies at lower temperatures, but show systematically higher solubilities at 50-60 °C, and therefore the dataset was not included. The experiments of Apps (1970) in dilute NaOH solutions show a large scatter and were discarded because of a suspected contamination of the run materials with bayerite (Apps et al., 1988). The experimental study of Hitch et al. (1980), although done from both undersaturated and supersaturated conditions, reports gibbsite solubilities that are higher by as much as 0.12 log units (Wesolowski, 1992). The systematically higher solubility could be due to the small grain size (<38 µm) used in their experiments, which can enhance the solubility due to surface energy effects (Wesolowski, 1992). Their dataset was therefore not included into the final database.

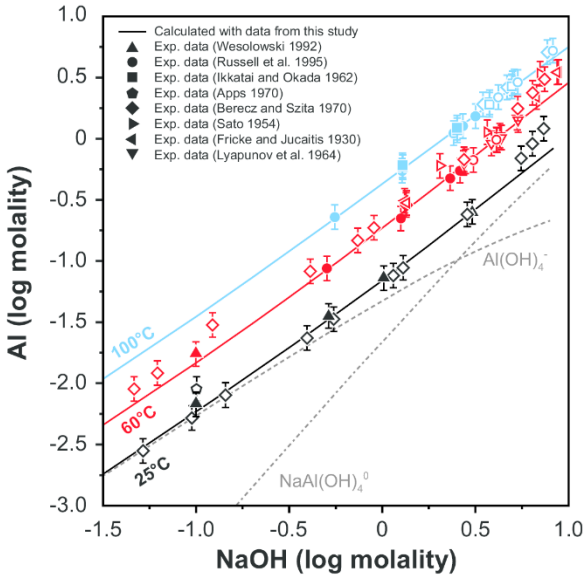

Figure 2. Comparison between calculated and experimental gibbsite solubility (Al concentration) data in NaOH solutions. Full symbols represent experimental data points used in the global data regression, while hollow symbols represent experimental data points which were not used. The grey dashed and dash-dotted lines show the relative contributions of the $Al(OH)_4^-$ and $NaAl(OH)_4^0$ species to total solubility.

4.3.2. Boehmite solubility

Boehmite solubility experiments in H_2O-NaOH solutions were all performed from undersaturated conditions (Table 3). The datasets of Russell et al. (1955), Druzhinina (1955), Bernshtein and Matsenok (1961), Kuyunko et al. (1983), Diakonov et al. (1996), and Salvi et al. (1998) are all in

good agreement with each other and show consistent trends with temperature and NaOH concentration. Therefore, they were included into the final experimental database. The data collected by Magarshak (1938) at 200 °C are in excellent agreement with those of Kuyunko et al. (1983) at the same temperature, but the experiments at 150 °C show a systematically higher solubility; thus the dataset was not selected. The experiments of Apps (1970) were also not selected due to large scatter and disagreement with the datasets discussed above. Castet et al. (1993) and Verdes et al. (1992) performed boehmite solubility experiments in mixed NaOH and NaCl solutions from both undersaturated and supersaturated conditions. Solubility experiments in acidic solutions were performed by Castet et al. (1993), Palmer et al. (2001) and Bénézeth et al. (2001).

Both Palmer et al. (2001) and Bénézeth et al. (2001) collected an extensive dataset of boehmite solubility over a wide range in pH conditions (2-10) between 100 and 290 °C at SWVP, and at 0.03, 0.1, 0.3, 1, and 5 molal NaCl concentration, from both undersaturated and supersaturated solutions. The measurements were performed in a hydrogen-electrode concentration cell, providing continuous in situ recording of hydrogen ion molality. The concentration of aluminum was measured from samples extracted at run conditions using ion chromatography and spectrophotometry (Palmer et al., 2001). The boehmite solubility experiments measured by Bénézeth et al. (2001) at 0.03 molal NaCl concentration were all included into the final experimental database, with the exception of the data at 290 °C. We noted that when calculating the equilibrium aluminum concentration using thermodynamic properties of boehmite from Hemingway et al. (1991), the data from Bénézeth et al. (2001) above 250 °C are not in agreement with the trend obtained from the experimental results of Bénézeth et al. (2001) at lower temperatures. The experimental data above 250 °C were therefore not included into the final database. Palmer et al. (2001) measured the solubility of boehmite as function of increasing NaCl concentration, from 0.1 to 5 molal NaCl. Their calibration for determining the hydrogen ion concentration does not take into account the formation of the neutral species HCl^0 (Palmer et al., 2001). When the neutral ion pair HCl^0 is included in calculation of the equilibrium solubility and speciation, its proportion increases with increasing temperature and Cl concentration. The fraction of HCl^0 in 1 molal NaCl solutions is around 10% of the total dissolved hydrogen at 154 °C and around 30% at 203 °C. When calculating the total Al concentration for the complete datasets of Bénézeth et al. (2001) and Palmer et al. (2001), it was not possible to reproduce all data in the acidic to neutral pH range with one set of thermodynamic properties for the Al hydroxide species. This likely reflects differences in the calculation of hydrogen ion concentration between the experimental studies and our modeling, related to the effect of the HCl^0 ion pair formation. Our calculations predict different H^+ concentrations in the acidic region above 0.03 molal NaCl, compared to the values reported by Palmer et al. (2001). This problem was not observed for the data at alkaline

pH, and we have therefore only included the experimental data above a pH value of 6 from the study of Palmer et al. (2001) into the final experimental database. From the data reported by Bénézeth et al. (2001) we included all experimental points with the exception of the experimental data above 250 °C.

4.3.3. Diaspore solubility

Solubility experiments of diaspore in dilute and concentrated NaOH and NaOH-NaCl solutions were performed from undersaturated conditions (Druzhinina, 1955; Bernshtein and Matsenok, 1965; Wefers, 1967; Chang et al., 1979; Apps et al., 1988; Verdes et al., 1992). The data above 150 °C are in fair agreement with each other with the exception of the dataset of Chang et al. (1979) which shows systematically lower Al concentrations (Pokrovskii and Helgeson, 1995). The experiments below 150 °C show a very large scatter, likely related to the low equilibration rate of the dissolution reaction and too short run times. The data of Chang et al. (1979) were therefore not considered. Table 3 summarizes the experimental datasets included into the final experimental database.

4.4. Solubility of feldspars, aluminosilicates, and silicate assemblages

Experimental solubility studies of aluminosilicates, feldspars and micas (and assemblages of several phases) are of particular importance, because they provide simultaneous constraints on the thermodynamic properties of several aqueous species. The experimental datasets that were included into the final database are summarized in Table 4.

4.4.1. Feldspar solubility

The solubility of feldspars has been investigated in a number of studies. Because of the incongruent dissolution of feldspars and difficulties in attaining equilibrium, these experiments are very challenging (Antignano and Manning, 2003; Azimov and Bushmin, 2007). Incongruent dissolution of feldspars can produce a number of different solid hydrolysis products that may include micas, aluminosilicates, corundum, leucite, and nepheline. Solubility experiments of albite and microcline were performed by Currie (1968) and Adcock (1985) using a dynamic flow through method. They reported that nepheline formed by incongruent dissolution of albite, which however is not in agreement with the measured ratios of dissolved element concentrations (Azimov and Bushmin, 2007). In the microcline solubility experiments, the reported Na concentrations are very close to those of K, probably due to the presence of Na in the natural microcline samples (up to 2.7 wt.% Na_2O).

Table 4. Summary of the aluminosilicate and Na-K-Al-Si mineral assemblage solubility experiments selected for the global optimization.

Reference	System	Number of data points used (total number)	[(1)]Direction of equilibrium	Temperature range (deg. C)	Pressure range (kbar)	Dataset property error (Eq. 10)
Davis (1972)	Albite-paragonite-H_2O	12	U	500 – 700	2 – 5	Si: 0.047 Al: 0.027 Na: 0.021
Hemley et al. (1980)	Pyrophyllite-kaolinite-andalusite-corundum-disapore-boehmite-H_2O	24	U	200 – 500	1 – 2	Si: 0.045
Hemley (1959)	Muscovite-K-feldspar-Quartz-H_2O-KCl	4	U	400 – 500	1	Log(K/H): 0.104
Sverjensky et al. (1991)	K-feldspar-muscovite-kaolinite-pyrohyllite-andalusite-quartz-H_2O-KCl	21	U+S	300 – 600	0.5 – 2	Log(K/H): 0.101
Haselton et al. (1995)	K-feldspar-muscovite-abdalusite-quartz-H_2O-KCl	4	U+S	400 – 500	1	Log(K/H): 0.099
Montoya and Hemley (1975)	Albite-paragonite-andalusite-quartz-H_2O	3	U	300 – 500	1	Log(Na/H): 0.025
Hauzenberger et al. (2001)	K-feldspar-albite-andalusite-quartz-H_2O-KCl-NaCl	33	U+S	600	2	Na: 0.073 K: 0.057 K/Na: 0.147
Pak et al. (2003)	K-feldspar-albite-andalusite-quartz-H_2O-KCl-NaCl	22	U+S	650	2	Na: 0.072 K: 0.052 K/Na: 0.096

[(1)] U: equilibrium approached from undersaturation; S: equilibrium approached from supersaturation.

Even a very small albite component in microcline can have a large influence on the total solubility in this system, and the measured Na and K concentrations will reflect equilibrium with an albite-microcline solid-solution. To avoid such complications, we have only considered feldspar solubility studies where it was demonstrated that pure phases have been used.

Davis (1972) studied the solubility of albite in H_2O using a static tube-in-tube technique. Reflecting the incongruent dissolution behavior of albite, a residue of pragonite was found in experiments that were inside the paragonite stability field. These experiments show consistent pressure and temperature trends, and were done using both natural and synthetic albite samples. Where the experimental conditions of Davis (1972) overlap with the ones from Currie (1968), the latter show systematically lower solubility (Anderson and Burnham, 1983). The lower measured solubility in the experiments of Currie (1968) and Adcock (1985) could have been caused by reprecipitation, due to high flow rate in their experiments, or due to the formation of other secondary phases (nepheline) (Adcock, 1985). Therefore, we have only included the albite solubility experiments of Davis (1972) into our final database.

4.4.2. Aluminosilicate solubility

The solubility experiments involving aluminosilicates such as kyanite, andalusite and sillimanite (Brown and Fyfe, 1971; Ostapenko and Arapova, 1971; Ostapenko et al., 1978) are affected by incongruent dissolution behavior in a similar way as the feldspar experiments. This results in preferential transfer of silica into solution and precipitation of secondary corundum (Azimov and Bushmin, 2007). In all aluminosilicate solubility studies only the concentration of silica was determined, but not the concentration of aluminum. There is also a considerable scatter between different datasets, likely due to difficulties in reaching equilibrium (Azimov and Bushmin, 2007). Reflecting these issues, we have not included the aluminosilicate solubility experiments into the final database.

4.4.3. Solubility of silicate mineral assemblages

Solubility experiments in the system SiO_2-Al_2O_3-H_2O with two-mineral assemblages were conducted by Hemley et al. (1980). They used well-characterized pure natural minerals and a cold-seal bomb quench method (30 seconds quench time to room temperature, followed by extraction and analysis of the solution). Their experiments were included into the final database.

When using three-mineral assemblages that buffer the composition of the solution, the uncertainties concerning the phase assemblages are eliminated and the solution is more likely to be in equilibrium with the solid phases (Azimov and Bushmin, 2007). Experiments containing potassium

feldspar, muscovite and quartz were done by Walther and Woodland (1993), but the analyzed Na concentration in solution was similar to that of K or even higher, suggesting contamination by Na from the natural microcline sample used. Solubilities in the system K_2O-Al_2O_3-SiO_2-H_2O were also studied by Anderson et al. (1987). They used natural mineral samples where the microcline had 97% orthoclase component and the corundum contained up to 1.2 wt.% Fe. Because of the presence of impurities, these datasets were not included into the final database.

Woodland and Walther (1987) determined the solubility of albite, paragonite and quartz in supercritical H_2O. The authors used relatively pure natural mineral samples and sampled the equilibrium solution at run conditions with an extraction-quench technique. Their experimental design should have provided for a reversal of solubility equilibrium based on the changes in element concentrations when going from one temperature-pressure state point to the next one (decrease in T would result in approach to equilibrium from supersaturation and increase from undersaturation). Although we could not identify any obvious issues in their experimental setup, the measured Si, Al, and Na concentrations show a substantial overlap between isotherms at pressures above 1-1.5 kbar. Furthermore, the trends with temperature and pressure displayed by the data are not in agreement with trends expected from thermodynamic relations. Therefore, we have not included these data into the final experimental database.

It is well known that the solubility and transport of many elements in crustal fluids is controlled by the chlorinity (Roedder, 1984; Yardley, 1997, 2005). The solubility of silicate mineral assemblages in aqueous chloride solutions has therefore been determined by several experimental studies. Haselton et al. (1995) studied the stability of muscovite, andalusite, sanidine and quartz in 1 molal KCl solutions. Similar phase equilibria were studied by Haselton et al. (1988) but in topaz-bearing assemblages. Experiments investigating feldspar-mica-quartz equilibria in NaCl and KCl solutions were reported by Hemley (1959), Montoya and Hemley (1975), and Sverjensky et al. (1991). These studies used both synthetic and natural minerals. The experiments reported by Sverjensky et al. (1991) were done using extraction of the equilibrium solution at run conditions. This dataset is in good agreement with that of Montoya and Hemley (1975), who used a standard cold-seal vessel technique and sampled the solution after quench. The studies discussed above obtained reversed phase equilibrium by starting from Na- or K-rich solutions with lower HCl content than the equilibrium value, or from HCl concentrations higher than the equilibrium value. Except for the topaz-bearing assemblages (Haselton et al., 1988), these experimental data were all included into the final database.

Other experiments in similar systems were not included into the final dataset, but are shown in plots that compare solubilities and phase equilibria calculated with the final thermodynamic dataset

with their experimental counterparts. These are the studies of Popp and Frantz (1980) and Shinohara and Fujimoto (1994) in the system Na_2O-Al_2O_3-SiO_2-H_2O-HCl. Popp and Frantz (1980) used the Ag-AgCl buffer technique to control the activity of HCl, making the reproduction of the initial system composition technically impossible when using GEMS3. Shinohara and Fujimoto (1994) studied the composition of the vapor and liquid phases for NaCl concentrations from 0.05 to 1.0 molal at 600 °C and pressures 0.5 and 2 kbar. They determined HCl concentrations several times higher than those obtained by Popp and Frantz (1980) for very similar pressure-temperature conditions. A likely explanation could be the slow quench method used in their study, despite the fact that their results for different quench times were rather consistent. Other experimental data in the system K_2O-Al_2O_3-SiO_2-H_2O-HCl that were not included into the final database were those by Gunter and Eugster (1981), Wintsch et al. (1980), and Shade (1974). Gunter and Eugster (1981) used the Ag-AgCl buffer technique to control the activity of HCl. Wintsch et al. (1980) performed the experiments in very dilute KCl solutions (0.02 molal), which introduced a large error when using the assumption that the ratio of K/H of the quench solution is the same as at the experimental pressure-temperature conditions. This is very different in experimental studies at 1 molal KCl concentrations (Haselton et al., 1995), because at low chlorinity the amount of total hydrogen at experimental conditions is sufficiently small to be affected by changes in the solution speciation during quench (Haselton et al., 1995). Shade (1974) used natural impure natural muscovite (with paragonite content of 10%) and potassium feldspar (with 10 % albite content) samples as starting materials.

High quality reversed solubility experiments at 600 and 650 °C and 2 kbar involving synthetic metapelite (assemblage potassium feldspar, albite, andalusite, and quartz) in moderately saline solutions were recently reported by Hauzenberger et al. (2001) and Pak et al. (2003). They used a rapid quench technique, accurate analytical methods and documented the experimental conditions very well. The four-mineral assemblage used was able to buffer all components in the system, and the concentrations of dissolved Na, K, Al and Si in the fluid were analyzed. We have specifically included their precise measurements of K/Na ratios in solution into the final experimental database.

5. Parameter optimization methods

The standard state Gibbs energies of aqueous species were regressed with the GEMSFITS code (Miron et al., 2015); http://gems.web.psi.ch/GEMSFITS, which uses the GEMS3K Gibbs energy minimization code (Kulik et al., 2013) and the TsolMod library of activity and equation of state models (Wagner et al., 2012). The chemical system definitions (lists of phases and species; initial thermodynamic properties of each species; bulk composition, pressure and temperature for each experimental data point) were prepared using the GEM-Selektor v.3 code (GEMS3) package

(http://gems.web.psi.ch/GEMS3) and then exported into text files that can be read by GEMS3K and GEMSFITS codes (Miron et al., 2015). The starting composition of each experimental data point was specified in terms of the amounts of oxides, water and salts. If reported, the fluid/solid mass ratio in the experiment was specified as in the experimental studies; otherwise a fluid/mineral ratio of 0.1 was selected to make sure that the calculated equilibria would always remain mineral-buffered.

A weighted least-squares minimization method was used for the global fitting of the standard state molal Gibbs energies $\Delta_f G^0_{298,1}$ of several aqueous species. The standard state volume ($V^0_{298,1}$), entropy ($S^0_{298,1}$), heat capacity ($Cp^0_{298,1}$), and HKF parameters (a_1, a_2, a_3, a_4, c_1, c_2, ω_0) were fixed to the values collected from several sources (Tables 1 and 5) or obtained from regression of equilibrium constants in this study. This mainly concerned the Al species $Al(OH)_3^0$ and the neutral ion pairs $NaCl^0$, KCl^0, $NaOH^0$, KOH^0 and HCl^0.

The weighting scheme was not directly retrieved from the experimental errors or the quality of the datasets. However, relative weights were used in order to obtain an accurate refinement of parameters and make the fit sufficiently sensitive to those experiments, which have only small contributions to the total sum of squared residuals. The relative and/or absolute change in the total sum of squared residuals from one fitting iteration to the next one can be small enough for the minimization algorithm to converge before accurately refining the properties of some minor but important species. For example, the number of experiments that constrain the properties of the $KAlO_2^0$ species is small compared to the total number of experiments processed in the global fit and hence the contribution of this species to the total sum of squared residuals is small. Consequently, the algorithm would converge before accurately refining the $KAlO_2^0$ properties to the desired precision. A solution to this problem was to increase the weight of those experiments that constrain the properties of the $KAlO_2^0$ species.

As stated in the thermodynamic framework section, the properties of the minerals are accepted from the Holland and Powell (1998) database as revised in the Thermocalc dataset ds55 (referred to as HP02). The standard state thermodynamic properties of boehmite and gibbsite are not part of this dataset, and were taken from Hemingway et al. (1991) and Robie and Hemingway (1995), respectively. Different thermodynamic data have been used for boehmite by Verdes et al. (1992), Castet et al. (1993), and Bénézeth et al. (2001), when retrieving the thermodynamic properties of aluminum species. These studies used values for the standards state entropy and heat capacity of 48.4

Table 5. Standard state properties (partial molal entropy, heat capacity and volume) and HKF parameters of aqueous species used in this study. These values were not adjusted during the global optimization process but taken from their original references or from separate regression of association constant and solubility data.

Species	$S^0_{298,1}$ (J/mol·K)	$Cp^0_{298,1}$ (J/mol·K)	$V^0_{298,1}$ (J/bar)	$a_1 \cdot 10$ (cal/mol/bar)	$a_2 \cdot 10^{-2}$ (cal/mol)	a_3 (cal·K/mol/bar)	$a_4 \cdot 10^{-4}$ (cal·K/mol)	c_1 (cal/mol/K)	$c_2 \cdot 10^{-4}$ (cal·K/mol)	$\omega_0 \cdot 10^{-5}$ (cal/mol)
[(1)]Al^{3+}	-339.74	-119.34	4.53	-3.3984	-16.0789	12.0699	-2.1143	14.4295	-8.8523	2.7403
[(1)]$AlOH^{2+}$	-181.13	-37.44	-2.06	-0.4532	-8.8878	9.2434	-2.4116	15.4131	-4.8618	1.5897
[(1)]$Al(OH)_2^+$	-27.53	40.86	0.385	2.4944	-1.6909	6.4146	-2.7091	16.7439	-1.0465	0.5324
[(2)]$Al(OH)_3^0$	5.16	248.56	3.07	6.1977	8.2816	2.4950	-3.1214	71.1003	-1.0644	1.0461
[(1)]$Al(OH)_4^-$	103.55	96.54	4.63	8.4938	12.9576	0.6570	-3.3147	55.7265	-11.4047	1.0403
[(1)]$NaAl(OH)_4^0$	204.18	134.56	5.36	9.1267	14.3411	0.1121	-3.3719	60.7157	-14.0523	0.0000
[(1)]$AlH_3SiO_4^{2+}$	56.78	-300.67	1.396	0.1600	-7.2300	8.6100	-2.4800	37.0700	-49.6600	0.8800
[(3)]$KAlO_2^0$	149.37	18.05	3.114	6.0070	6.8858	3.0436	-3.0637	1.3940	1.2120	-0.0500
[(4)]K^+	101.04	8.39	0.901	3.559	-1.4730	5.4350	-2.7120	7.4000	-1.7910	0.1927
[(4)]Na^+	58.41	38.12	-0.121	1.8390	-2.2850	3.2560	-2.7260	18.1800	-2.9810	0.3306
[(5)]$NaHSiO_3^0$	41.84	102.95	1.273	3.4928	0.7500	5.4483	-2.8100	20.2395	1.9785	-0.0380
[(6)]$HSiO_3^-$	19.7	-38.47	0.5	3.3090	-0.5201	5.9467	-2.7575	15.0000	-4.9202	1.5583
[(7)]SiO_2^0	75.31	-318.4	1.61	1.9000	1.7000	20.0000	-2.7000	29.1000	-51.2000	0.1291
[(4)]Cl^-	56.74	122.49	1.734	4.0320	4.8010	5.5630	-2.8470	-4.4000	-5.7140	1.4560
[(4)]OH^-	10.71	136.34	-0.471	1.2527	0.0738	1.8423	-2.7821	4.1500	-10.3460	1.7246
[(4)]H^+	0	0	0	0	0	0	0	0	0	0

[(1)] Taken from Tagirov and Schott (2001).
[(2)] Derived in this study using the standard state molar volume and heat capacity from Pokrovskii and Helgeson (1995), the boehmite solubility data from Benezeth et al. (2001) and the corundum solubility data at 5 kbar from Becker et al. (1983) and Tropper and Manning (2007).
[(3)] Taken from Pokrovskii and Helgeson (1995).
[(4)] Taken from Shock and Helgeson (1988).
[(5)] Taken from Sverjensky et al. (1997).
[(6)] Derived using the logK data from Busey and Mesmer (1977).
[(7)] Taken from Shock et al. (1989).

J/(mol·K) and 65.6 J(mol·K) (Shomate and Cook 1946; Takahashi et al. 1973) compared with 37.2 J/(mol·K) and 54.2 J/(mol·K) (Hemingway et al. 1991) selected for the present study. Verdes et al. (1992) attributed these differences to the possible presence of a small amount of excess water in the boehmite samples used by Shomate and Cook (1946) and Takahashi et al. (1973), while this contamination was not present in the samples studied calorimetrically by Hemingway et al. (1978). As highlighted by Tagirov and Schott (2001), there is no experimental evidence that gibbsite is converted to boehmite below 80 °C, but the existing thermodynamic data predict that boehmite is more stable than gibbsite below this temperature. One explanation for this could be that kinetic factors have affected the relative stability of gibbsite and boehmite in the experiments. The Ostwald step rule would predict that the formation of the mineral with the fastest crystallization rate (gibbsite) is favored, while the conversion to the thermodynamically stable phase (boehmite) can be extremely slow (Morse and Casey, 1988).

A substantial proportion of the experiments constraining aluminum solubility are those involving gibbsite and boehmite. They are not included into the HP02 mineral dataset, but offer essential information on the stability of aluminum speciation over the entire pH range. The solubility experiments on diaspore, corundum or other minerals present in the HP02 database are not sufficient to independently constrain the properties of all relevant aluminum species present under acidic to alkaline conditions. Therefore, we have adopted the following data refinement strategy for the Al species. In a first step, all hydrolysis constants of Al^{3+} were refined using the selected solubility experiments of gibbsite and boehmite (Table 3). The new hydrolysis constants were then subsequently used to independently refine the properties of Al^{3+} from experiments that involve the solubility of Al minerals in the HP02 dataset (diaspore, corundum). When refining the $\Delta_f G^0_{298,1}$ of Al^{3+}, we have included all Al hydroxide complexes in the speciation model and adjusted their $\Delta_f G^0_{298,1}$ based on the hydrolysis constants (and their temperature dependence) that were fixed to the values obtained from the gibbsite and boehmite solubility data. While the absolute values of $\Delta_f G^0_{298,1}$ of all aluminum species are dependent on the mineral properties, the aluminum hydrolysis constants are independent of the chosen mineral properties. This can be shown by the following set of chemical reactions for the species $Al(OH)_2^+$, where the mineral properties obviously cancel out:

$$AlOOH_{(cryst.)} + 3\ H^+ = Al^{3+} + 2\ H_2O \quad (5)$$

$$AlOOH_{(cryst.)} + 2\ H^+ = Al(OH)_2^+ + H_2O \quad (6)$$

$$Al(OH)_2^+ + H^+ = Al^{3+} + 2\ H_2O \quad (7)$$

Optimization runs were first performed separately for the gibbsite and boehmite experiments, and subsequently for the remaining Al minerals present in the HP02 database. Finally, the data were

refined in a global optimization run using all experimental data. This permitted to evaluate the level of consistency between the properties of gibbsite and boehmite and the aluminum minerals present in the HP02 database.

The $\Delta_f G^0_{298,1}$ values of several aqueous complexes were constrained using association constants derived from conductance and potentiometric experiments. The $\Delta_f G^0_{298,1}$ of these species were refined in the same way as discussed for the Al hydroxy species above. The independently regressed association constants were then used as reaction constraints. In this way, any change in $\Delta_f G^0_{298,1}$ from fitting solubility data is propagated to the related complexes using the $\Delta_f G^0_{298,1}$ of the reaction (e.g., for the reaction $Na^+ + Cl^- = NaCl^0$). At each optimization step, new $\Delta_f G^0_{298,1}$ values of the reaction constrained complexes are recalculated using the updated properties of the reactant species. The newly derived association constants from conductance measurements were used to constrain the properties of the neutral ion pairs ($NaCl^0$, KCl^0, $NaOH^0$, KOH^0). Reaction constraints were also used for species which are not sensitive to the selected experiments (i.e., they do not form in significant amounts). Important examples are the complexes $NaHSiO_3^0$ and $AlH_3SiO_4^{2+}$, which are linked to simple species by the following reactions:

$$Na^+ + H_2O + SiO_2^0 = NaHSiO_3^0 + H^+ \quad (8)$$

$$Al^{3+} + 2\ H_2O + SiO_2^0 = AlH_3SiO_4^{2+} + H^+ \quad (9)$$

The association constants of these complexes were originally derived from quartz solubility experiments in borate solutions for the $NaHSiO_3^0$ (Seward, 1974) and from the silica injection experiments of Salvi et al. (1998) and potentiometric measurements of Pokrovskii et al. (1996) for $AlH_3SiO_4^{2+}$. An additional reaction constraint was imposed on the $AlOH^{2+}$ species, because its properties are highly correlated with those of Al^{3+}, making it difficult to independently refine the $\Delta_f G^0_{298,1}$ of both species from solubility data alone. We accepted the association constants for $AlOH^{2+}$ from the direct hydrolysis measurements of Palmer and Wesolowski (1993) (Figure 3). The stability of the $HSiO_3^-$ aqueous species was linked to SiO_2^0 trough the reaction logK values determined from the potentiometric measurements (Figure 4) performed by Busey and Mesmer (1977):

$$SiO_2^0 + H_2O = HSiO_3^- + H^+ \quad (10)$$

In contrast, Sverjensky et al. (1997) selected to refine the standard state properties and parameters of $HSiO_3^-$ using the logK data of Seward (1974) derived from quartz solubility in borate solutions. These results were criticized by Busey and Mesmer (1977) for being strongly dependent on the selected properties for aqueous borate speciation equilibria and the method of extrapolation to infinite dilution.

To reproduce those experiments where the actual bulk composition is not directly reported in GEMSFITS (Miron et al., 2015) and GEMS3 (Kulik et al., 2013), the nested regression functionality of GEMSFITS was used. This makes it possible to iteratively adjust the input composition (e.g., amounts of HCl and NaOH) in such a way that reported output compositions (e.g., pH or amount of H^+) are reproduced. The iterative adjustment of the bulk composition was done before each iteration of the global fitting algorithm. In this way the temperature, pressure and also the pH conditions of the simulated experiments matched the reported values.

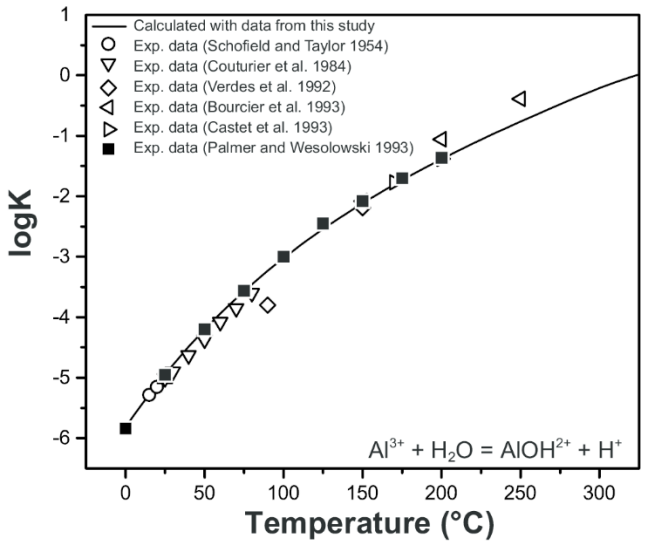

Figure 3. Comparison between calculated and reported literature values for the logK of the first hydrolysis reaction of Al^{3+}.

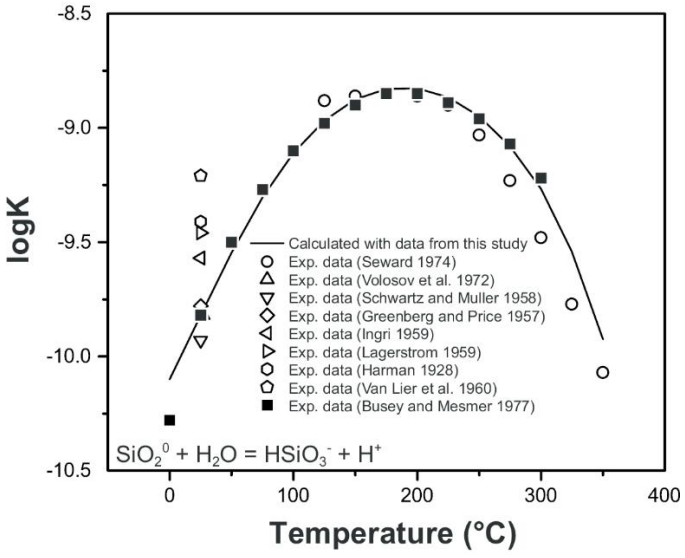

Figure 4. Comparison between calculated and reported literature values for the logK of the SiO_2^0 hydrolysis reaction to form $HSiO_3^-$.

The uncertainties of the final regressed $\Delta_f G^0_{298,1}$ values were evaluated using Monte Carlo simulation of synthetic datasets generated from randomly sampled residuals added to the measured values for each dataset (Miron et al., 2015). The uncertainties of the reaction-constrained species were propagated from the independently fitted species and the average reported error on the reaction logK values. The uncertainties in the calculated standard state Gibbs energies at elevated temperatures and pressures are also affected by the uncertainties in the HKF parameters. If all errors of the HKF parameters would be added up, this would result in a maximum additional error of the $\Delta G^0_{T,P}$ between 2.4 kJ/mol at 500 °C and 2 kbar and 6.0 kJ/mol at 1000 °C and 5 kbar (Shock and Helgeson, 1988). More likely, these additional uncertainties should be typically below 2 kJ/mol (around 0.1 units in logK). This conclusion is supported by the generally good agreement between calculated and measured mineral solubilities, as will be discussed in the following section.

6. Results

The final regressed $\Delta_f G^0_{298,1}$ values of aqueous species generated by global optimization of all mineral solubility data selected for the final database (Tables 2, 3 and 4) are summarized in Table 6. The correlation coefficients between the freely optimized aqueous species are given in Table 7. This table also lists thermodynamic properties of species that were fixed during fitting, and those which were constrained from association reaction constants. The Electronic Supplementary Material lists values for the aluminum aqueous species obtained from fitting them only against gibbsite and boehmite solubility experiments (Table EA2). The resulting properties (logK values) were then used as reaction constraints for the aluminum hydroxy species while the Gibbs energy of the Al^{3+} ion was fitted against the experimental corundum and diaspore solubility data (Table EA3). The $\Delta_f G^0_{298,1}$ obtained for $Al(OH)_4^-$ from independently fitting gibbsite and boehmite solubility was -1305.3 ± 0.3 kJ/mol, while fitting it using corundum and diaspore solubility along with the reaction constraints yielded -1305.2 ± 0.6 kJ/mol. The final value of -1305.1 ± 0.23 kJ/mol (Table 6) was obtained from the global optimization of all solubility experiments (including gibbsite, boehmite, corundum and diaspore solubility data) and is identical within errors with all other fitting results.

Selected experimental datasets that were used in the regression of Gibbs energies are plotted together with datasets that were not used, and are compared to calculations with the final aqueous species dataset in Figures 1 through 20. Filled symbols do always represent experimental data points used during fitting, while open symbols represent experimental data points which were not used. Solid curves represent calculated values using the final aqueous species dataset (Table 6), while

Table 6. Final values of the standard-state molal Gibbs energy for aqueous species, obtained from the global optimization against experimental solubility datasets (Tables 2, 3 and 4). Gibbs energy values need to be combined with standard state entropy, volume, heat capacity and HKF parameters from Table 1 (ion pairs of main electrolytes) and Table 5 (other aqueous species). The standard deviation of parameters was calculated from 500 Monte Carlo simulation runs, and the 95% confidence interval - using the Student's t-distribution.

Species	$\Delta_f G^0_{298,1}$ (J/mol)	Standard deviation	95% confidence interval	Optimization mode
Al^{3+}	-486627	258	507	Optimized
$AlOH^{2+}$	-695574	543	1077	(1)Constrained
$Al(OH)_2^+$	-898295	1339	2627	Optimized
$Al(OH)_3^0$	-1105801	944	1852	Optimized
$Al(OH)_4^-$	-1305097	229	450	Optimized
$NaAl(OH)_4^0$	-1562121	944	1853	Optimized
$AlH_3SiO_4^{2+}$	-1782516	828	1547	(2)Constrained
$KAlO_2^0$	-1100293	2423	4751	Optimized
K^+	-276893	643	1261	Optimized
KOH^0	-431656	-	-	(3)Constrained
KCl^0	-402544	-	-	(3)Constrained
Na^+	-256169	644	1263	Optimized
$NaOH^0$	-411594	-	-	(3)Constrained
$NaCl^0$	-383091	-	-	(3)Constrained
$NaHSiO_3^0$	-1283076	1820	3614	(4)Constrained
$HSiO_3^-$	-1015237	-	-	(5)Constrained
SiO_2^0	-834103	34	67	Optimized
Cl^-	-131290	-	-	(6)Fixed
HCl^0	-127240	-	-	(7)Fixed
OH^-	-157287	-	-	(6)Fixed
H^+	0	-	-	(8)Fixed
H_2O	-237183	-	-	(9)Fixed

(1) Constrained to properties of Al^{3+} by the reaction: $AlOH^{2+} + H^+ = Al^{3+} + H_2O$, using equilibrium constant values from Palmer and Wesolowski (1993).
(2) Constrained to properties of Al^{3+} and SiO_2^0 by the reaction: $Al^{3+} + 2\ H_2O + SiO_2^0 = AlH_3SiO_4^{2+} + H^+$, and equilibrium constants from Tagirov and Schott (2001), extracted from Pokrovskii et al. (1996) and Salvi et al. (1998).
(3) Constrained to properties of Na^+, K^+, OH^-, and Cl^- using the equilibrium constants determined from the new standard state properties of ion pairs extracted from the conductance data (Table 1).
(4) Constrained to properties of Na^+ and SiO_2^0 by the reaction: $Na^+ + H_2O + SiO_2^0 = NaHSiO_3^0 + H^+$, using equilibrium constants from Sverjensky et al. (1997), extracted from Seward (1974).
(5) Constrained to properties of SiO_2^0 by the reaction: $SiO_2^0 + H_2O = HSiO_3^- + H^+$, using equilibrium constants from Busey and Mesmer (1977)
(6) Taken from Shock and Helgeson (1988).
(7) Taken from Tagirov et al. (1997).
(8) Conventional value.
(9) Taken from Johnson et al. (1992).

Table 7. Correlation coefficients between the freely optimized aqueous species. They are calculated from the sensitivity analysis as outlined in Miron et al. (2015).

Species	$Al(OH)_2^+$	$Al(OH)_3^0$	$Al(OH)_4^-$	Al^{3+}	K^+	$KAlO_2^0$	Na^+	$NaAl(OH)_4^0$	SiO_2^0
$Al(OH)_2^+$	1.000	-0.604	0.049	-0.394	-0.004	-0.001	-0.004	-0.014	0.000
$Al(OH)_3^0$	-0.604	1.000	-0.109	0.175	0.003	0.004	0.003	0.027	0.000
$Al(OH)_4^-$	0.049	-0.109	1.000	-0.013	-0.009	-0.022	-0.010	-0.333	-0.002
Al^{3+}	-0.394	0.175	-0.013	1.000	0.005	-0.001	0.004	0.006	-0.001
K^+	-0.004	0.003	-0.009	0.005	1.000	0.062	0.791	0.684	-0.011
$KAlO_2^0$	-0.001	0.004	-0.022	-0.001	0.062	1.000	0.073	0.070	0.001
Na^+	-0.004	0.003	-0.010	0.004	0.791	0.073	1.000	0.864	-0.014
$NaAl(OH)_4^0$	-0.014	0.027	-0.333	0.006	0.684	0.070	0.864	1.000	-0.012
SiO_2^0	0.000	0.000	-0.002	-0.001	-0.011	0.001	-0.014	-0.012	1.000

dashed or dotted curves represent the values calculated with thermodynamic properties of aqueous species from SUPCRT92 (Shock and Helgeson, 1988; Shock et al., 1989; Johnson et al., 1992; Shock et al., 1997; Sverjensky et al., 1997) or other sources. Most importantly, the final aqueous species dataset is able to accurately reproduce the input experimental data largely within their uncertainty and without any systematic deviation. The overall quality of the fit for each individual experimental dataset is reported in Tables 2, 3 and 4 and defined by the normalized-root-mean-square-error (NRMSE):

$$NRMSE = \sqrt{\frac{\sum_{i}^{N}\left[y(i) - f(i)\right]^2}{\sum_{i}^{N} y(i)^2}} \tag{11}$$

where *y(i)* represents the measured (experimental) value of a property (e.g. Si solubiliy), *f(i)* is the calculated value of this property, and *N* the number of experiments in this dataset. This evaluation of the quality of the fit was performed after the GEMSFITS optimization and does not represent the minimized objective function.

The thermodynamic database presented in this study and future updates will be provided at the following web-address: http://gems.web.psi.ch/. The files are compatible with the GEM-Selektor geochemical modeling software (Kulik et al. 2013) and enable calculation of aqueous-mineral equilibria in the system Na-K-Al-Si-O-H-Cl at temperatures up to 1000 °C, pressures up to 5 kbar and salt concentrations up to 5 molal.

6.1. System Si-O-H-Cl

Figure 5 displays the quartz solubilities in pure H_2O over a wide range in temperature and from saturated water vapor pressure to 5 kbar. The calculated solubilities are in excellent agreement with the experimental data that were used in the data regression, but also in good agreement with experimental data that were not used. Figure 5B shows that the experimental data points from Xie and Walther (1993) are inconsistent with all other experimental datasets at the same conditions and that they have a different temperature trend. Other experimental datasets for quartz solubility show only minor differences between calculated and measured values.

6.2. System Al-O-H-Cl

In this section, we present results of the global optimization of all Al solubility data (including boehmite, gibbsite, corundum and diaspore solubility). The majority of experimental gibbsite and boehmite solubility data in acid, neutral and alkaline solutions and at different salt concentrations and

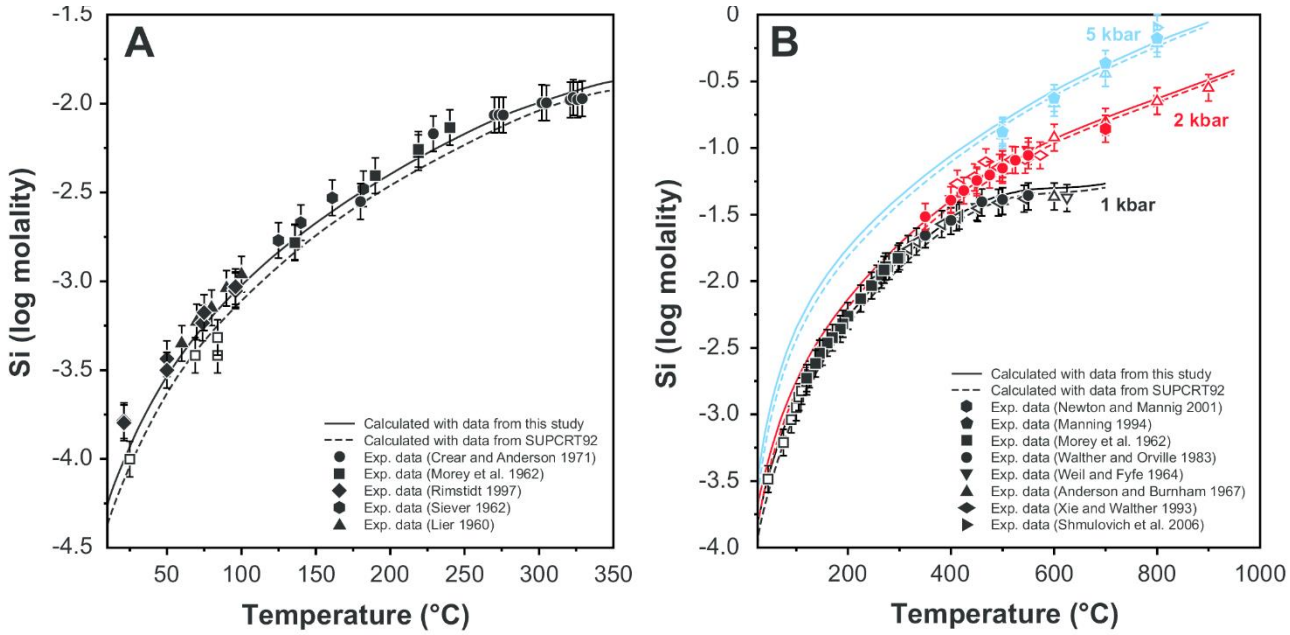

Figure 5. Comparison between calculated and experimentally measured quartz solubility (total dissolved Si concentration) over a wide range in temperature and at pressures up to 5 kbar. Full symbols represent experimental data points used in the global data regression, while open symbols represent experimental data points which were not used. (**A**) Data at saturated water vapor pressure. (**B**) Data at isobars of 1, 2 and 5 kbar.

temperatures are in good mutual agreement and are also in agreement with the diaspore solubility data. Calculated dissolved aluminum concentrations agree well with those determined from gibbsite solubility experiments at temperatures between 25 and 120 °C (Fig. 2). Very good agreement is also observed with the experimental boehmite solubility in alkaline conditions (Fig. 6), especially with the large dataset of Bénézeth et al. (2001) that covers a wide range in temperature and solution pH (Fig. 7). Good agreement between calculations and experiments is also observed for the diaspore solubility in moderately concentrated alkaline solutions (Fig. 8A) and in very dilute solutions (Fig. 8B).

The calculated aluminum concentrations using the new thermodynamic dataset (Table 6) are in very good agreement with the experimental data for corundum solubility in alkaline solutions at high temperatures and pressures (Fig. 9). The main impact on the calculated results comes from the greatly improved properties of the associated species KOH^0 and $NaOH^0$ taking advantage of the new high-quality conductance data. The calculated corundum solubilities are now in very good agreement with their experimental counterparts (Fig. 10). As expected, there is a considerable disagreement with some of the experimental corundum solubility data in H_2O (see discussion of experimental data above). Very good agreement between calculated and experimental corundum solubility is observed for the high-quality datasets of Becker et al. (1983) and Tropper and Manning (2007) when using the properties of $Al(OH)_3^0$ derived in this study.

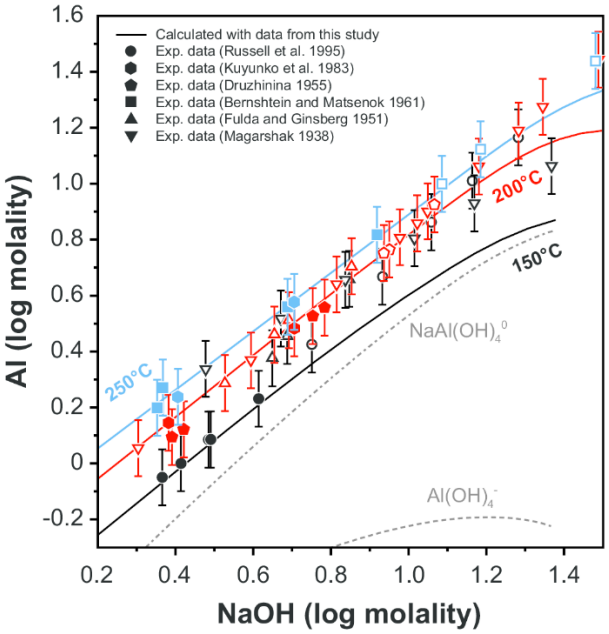

Figure 6. Comparison between calculated and experimentally determined boehmite solubility (Al concentration) as function of NaOH concentration. The data cover temperatures up to 250 °C at saturated water vapor pressure. Full symbols represent experimental data points used in the global data regression, while open symbols represent experimental data points which were not used.

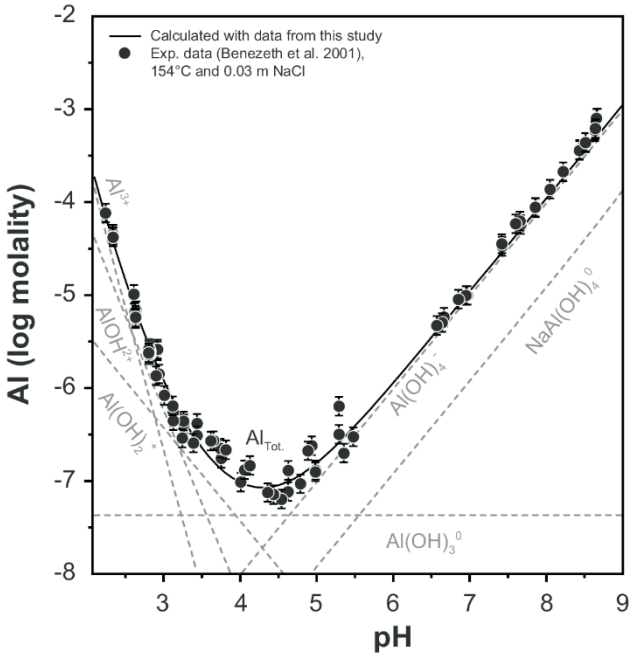

Figure 7. Comparison between calculated and experimentally measured boehmite solubility (Al concentration) as function of solution pH. The experimental data were obtained in 0.03 molal NaCl solutions (Bénézeth et al., 2001).

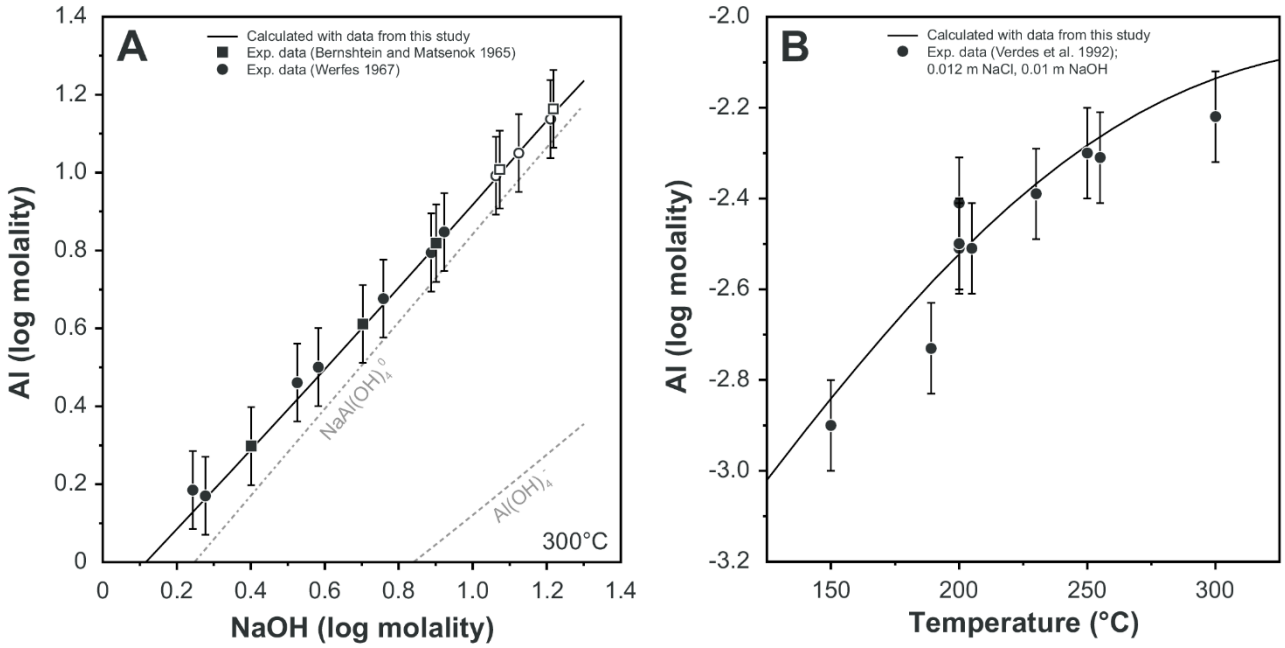

Figure 8. Comparison between calculated and experimentally determined diaspore solubility (Al concentration) as function of (**A**) NaOH concentration at 300 °C, and (**B**) as function of temperature. Full symbols represent experimental data points used in the global data regression, while open symbols represent experimental data points which were not used.

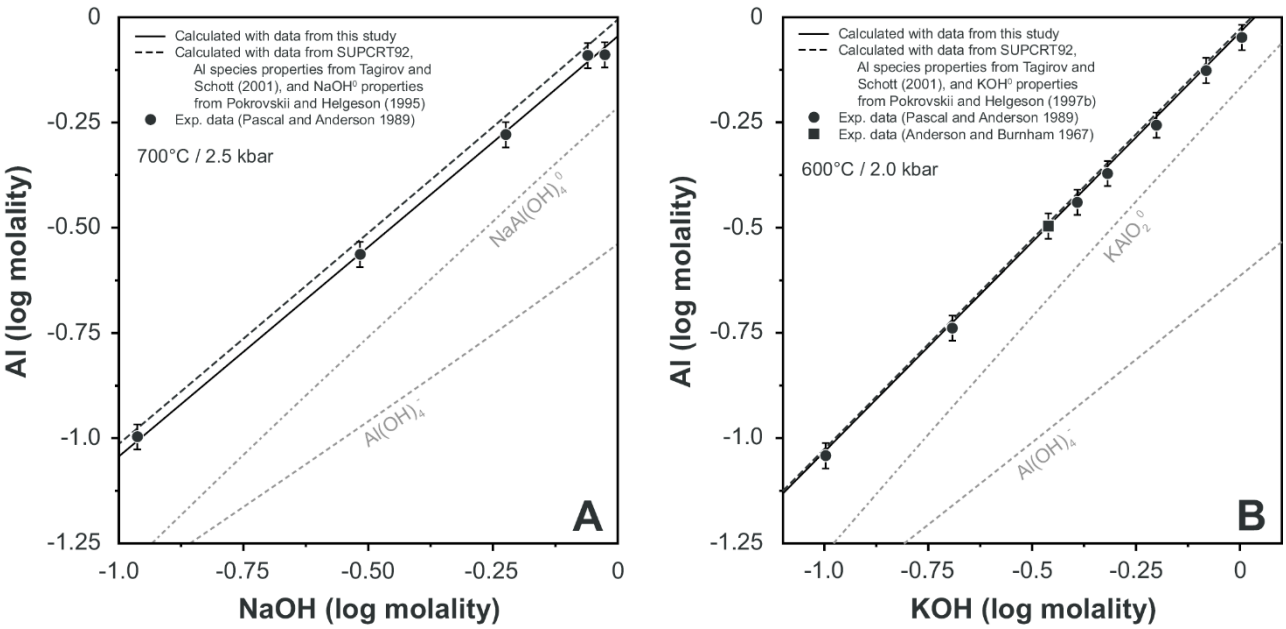

Figure 9. Comparison between calculated and experimentally determined corundum solubility (Al concentration) as function of (**A**) NaOH concentration (at 700°C and 2.5 kbar), and (**B**) KOH concentration (at 600°C and 2.0 kbar). The grey dashed and dash-dotted lines show the relative contributions of the $Al(OH)_4^-$ species and alkali-aluminum ion pairs $NaAl(OH)_4^0$ and $KAlO_2^0$ to total solubility.

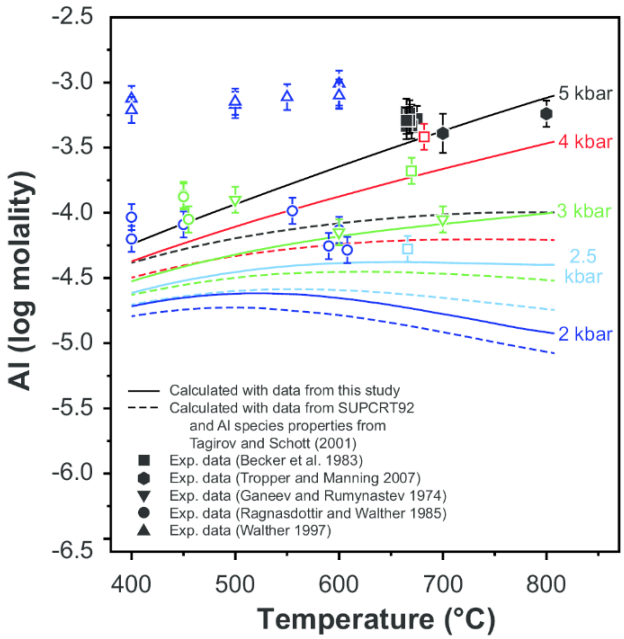

Figure 10. Comparison between calculated and measured corundum solubility (Al concentration) in supercritical water as function of temperature and at different pressures (2.0, 2.5, 3.0, 4.0 and 5.0 kbar). Full symbols represent experimental data points used in the global data regression, while open symbols represent experimental data points which were not used.

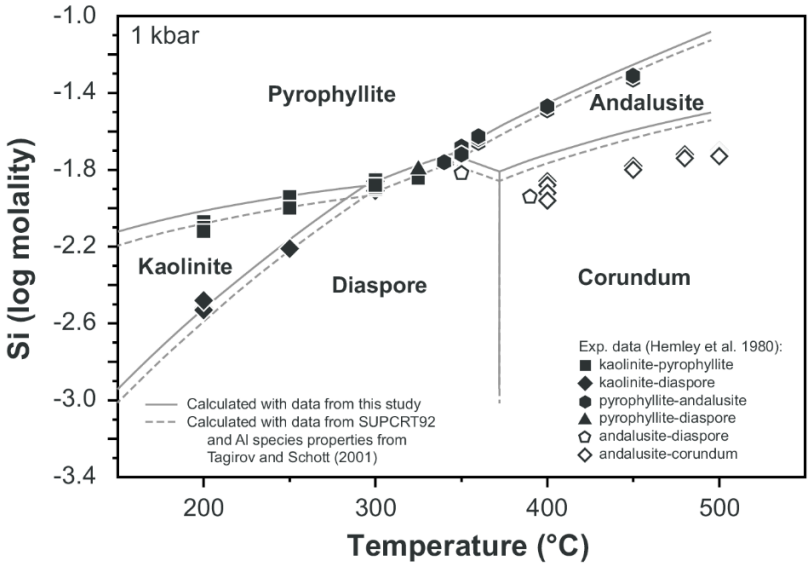

FFigure 11. Comparison between calculated and experimentally determined phase equilibria and Si concentrations in the Si-Al-H-O system (Hemley et al., 1980) as function of temperature (and at 1 kbar pressure).

6.3. System Al-Si-O-H-Cl

There is a fairly good agreement between calculated and experimentally determined solubility data of aluminosilicate mineral pairs (Hemley et al. 1980). The phase equilibria pyrophyllite-kaolinite, pyrophyllite-andalusite and kaolinite-diaspore are mostly reproduced within their experimental uncertainty (Fig. 11). Only the calculated phase equilibria andalusite-corundum and andalusite-

diaspore are slightly offset by a maximum value of 0.2 log units of the dissolved silica molality (Fig. 11).

6.4. System K-Na-Al-Si-O-H-Cl

The only feldspar solubility experiments used for the global regression were those for albite reported by Davis (1972). The agreement between calculated and measured concentrations of Si, Na, and Al is generally very good (Fig. 12). There is not so good agreement with the albite-paragonite-quartz solubility data of Woodland and Walther (1987). While the calculated Si concentrations partly agree with the experimental ones, the Al and Na concentrations show substantial disagreement (Fig. 13). There is not only disagreement in terms of the absolute values of the Al and Na concentrations, but the calculated temperature and pressure trends do also diverge systematically from the experimental data. The experimental data at different pressures above 1.5 kbar appear to be overlapping within their uncertainties.

The new dataset is able to accurately reproduce the phase equilibria and log(Na/H) values from the experimental study of Montoya and Hemley (1975) in the system albite-paragonite-quartz-fluid (Fig. 14). The calculated results are in better agreement with the absolute values of log(Na/H) and their temperature trend than calculations using the SUPCRT92 dataset (Shock and Helgeson, 1988; Shock et al., 1989; Johnson et al., 1992; Shock et al., 1997; Sverjensky et al., 1997) and the HCl^0 properties from Tagirov et al. (1997). There is also fair agreement between calculated and experimental phase equilibria and log(K/H) values (Hemley, 1959; Haselton et al., 1988; Sverjensky et al., 1991; Haselton et al., 1995) in the potassium system (Fig. 15). The agreement between calculated and experimental log(K/H) values is not much improved with the new dataset for this system, but the temperature trends of the reaction boundaries are in better agreement with the experimental data. There is a systematic improvement in both the Na and K systems when the $\Delta_f G^0_{298,1}$ values for K^+ and Na^+ are included into the global regression. In the potassium system (Fig. 15), the only phase boundary that is still not too well reproduced is that of the pyrophyllite-muscovite reaction (Fig. 15). This could be due to possible changes in the structure of phyrophyllite during the experimental runs or some impurities in pyrophyllite or muscovite that would affect their stability.

Most importantly, calculations with the final aqueous species dataset are in very good agreement with the high-temperature solubility experiments in the four-mineral system albite+K-feldspar+andalusite+quartz (Hauzenberger et al., 2001; Pak et al., 2003). Especially the calculated Na and K concentrations are now exactly reproducing the experimental data (Figs. 16, 17 and 18). The Si and Al concentrations are also in good agreement with the experimental data, which are

reproduced within their rather large uncertainties (Figs. 16 and 17). The experimental data for the Si and Al concentrations show a rather large scatter in the experimental dataset. This may reflect the fact that (unlike for the Na and K data), the Si and Al solubility data were not fully reversed in the experiments, and some values might therefore represent minimum concentrations.

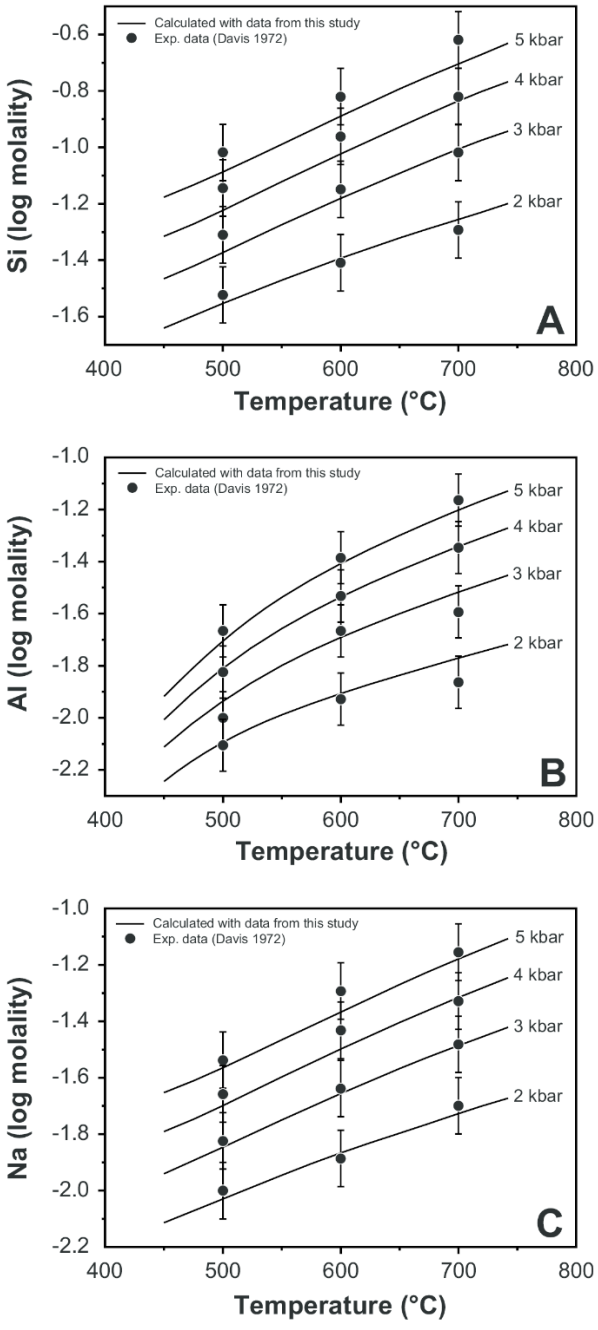

Figure 12. Comparison between calculated and experimentally determined albite solubility data (Davis, 1972) as function of temperature (and pressures of 2.0, 3.0, 4.0 and 5.0 kbar). (**A**) Si concentration. (**B**) Al concentration. (**C**) Na concentration.

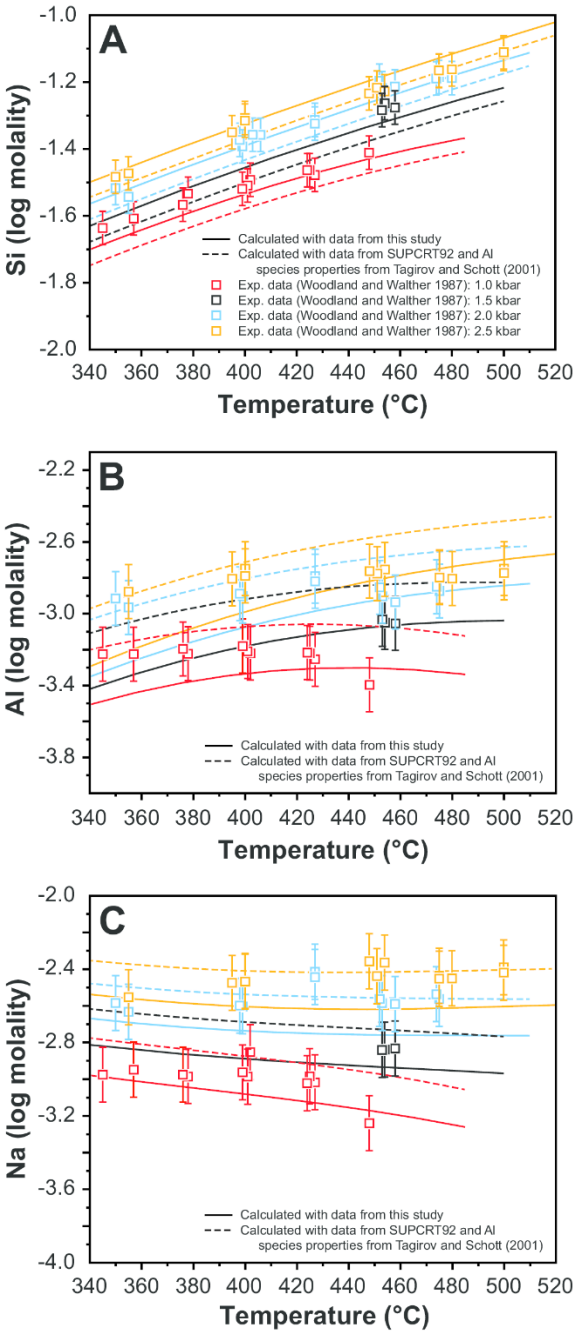

Figure 13. Comparison between calculated and experimentally determined solubility data in the albite-paragonite-quartz-water system (Woodland and Walther, 1987) as function of temperature (and pressures of 1.0, 1.5, 2.0 and 2.5 kbar). (**A**) total dissolved Si concentration. (**B**) Al concentration. (**C**) Na concentration.

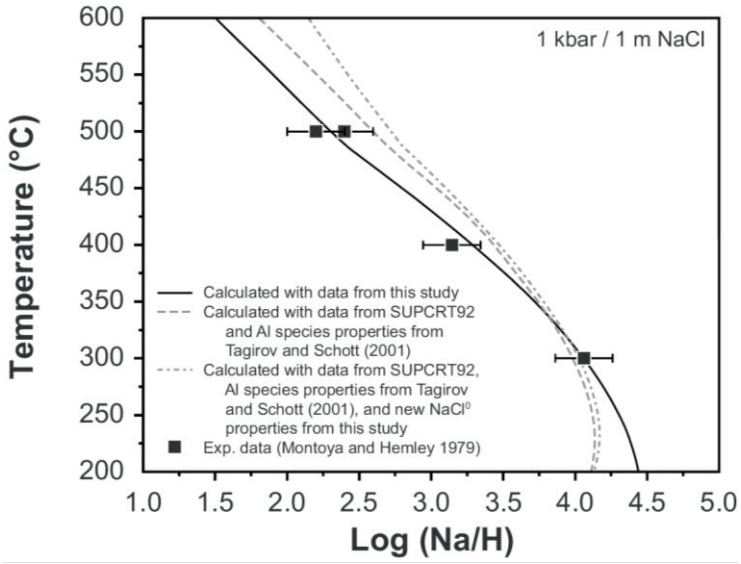

Figure 14. Comparison between calculated and experimentally determined log(Na/H) values for the solubility of albite-paragonite-quartz assemblages (in 1 molal NaCl solution) as function of temperature (and at a pressure of 1 kbar).

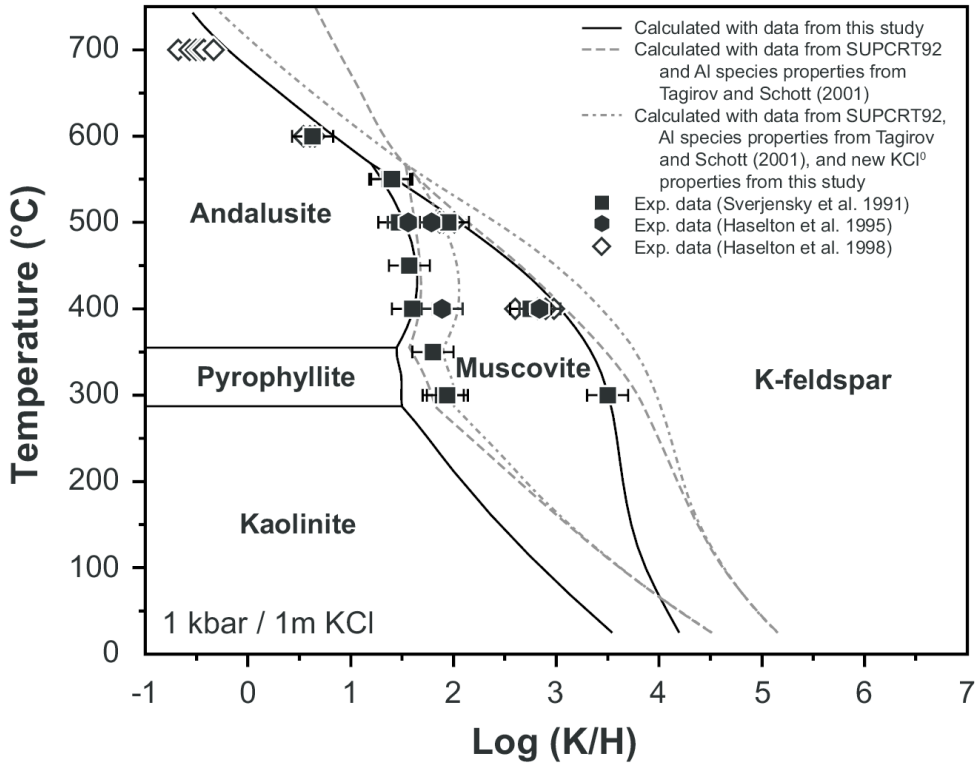

Figure 15. Comparison between calculated and experimentally determined phase equilibria and log(K/H) values in the system Si-Al-K-OH-Cl (in 1 molal KCl solution) as function of temperature (and at a pressure of 1 kbar). Full symbols represent experimental data points which were used in the global data regression, while open symbols represent experimental data points which were not used.

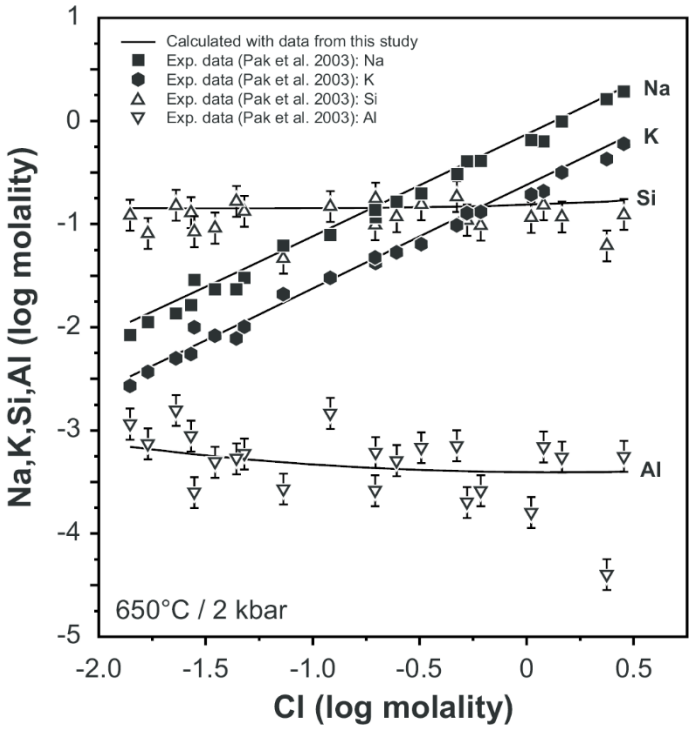

Figure 16. Comparison between calculated and experimentally determined (Pak et al., 2003) concentrations of Na, K Si and Al in a fluid in equilibrium with the mineral assemblage albite+K-feldspar+andalusite+quartz (at 650°C and 2.0 kbar), plotted as function of fluid chlorinity. The total concentrations of N and K in solution increase systematically with solution chlorinity, while the concentrations of Si and Al remain nearly constant.

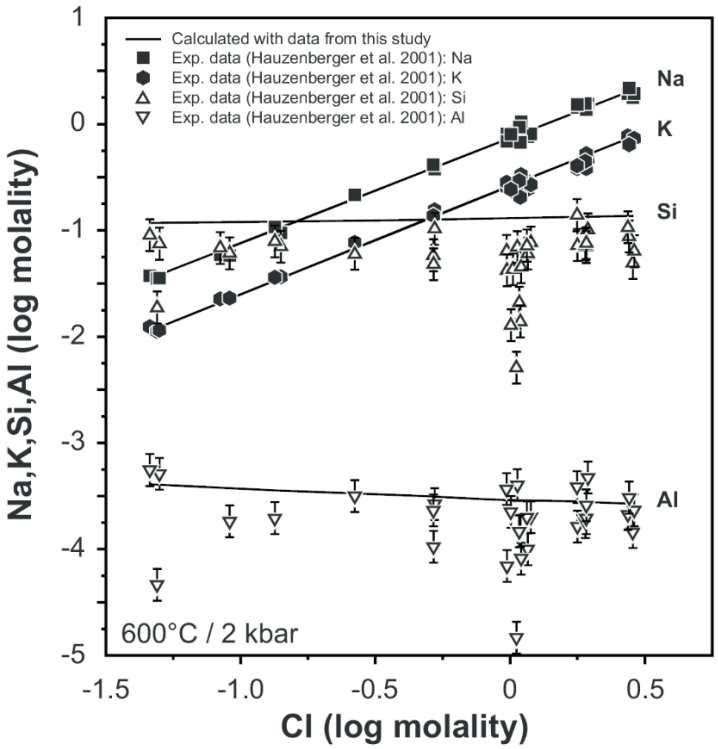

Figure 17. Comparison between calculated and experimentally determined (Hauzenberger et al., 2001) concentrations of Na, K Si and Al in a fluid in equilibrium with the mineral assemblage albite+K-feldspar+andalusite+quartz (at 600°C and 2.0 kbar), plotted as function of fluid chlorinity. The concentrations of N and K in solution increase systematically with solution chlorinity, while the concentrations of Si and Al remain nearly constant.

7. Discussion

In the present study, we have adopted the strategy of refining the standard state Gibbs energies of aqueous ions and complexes by global regression of a large body of critically selected equilibrium solubility data for individual minerals and mineral assemblages. In this process, we have taken advantage of the availability of recent high-precision data for the association constants of aqueous complexes of major electrolytes (NaCl, KCl, NaOH, KOH, HCl) derived from conductance and potentiometric measurements. We have also accepted the thermodynamic properties of the minerals from the internally consistent database of Holland and Powell (1998), as given in the Thermocalc database ds55. This dataset is in very good agreement with the majority of the available calorimetric data and experimental phase equilibria brackets, and is widely used in a great number of petrological applications (e.g. Fabrichnaya et al., 2013; Lanari et al. 2014; Miron et al., 2013; Galvez et al., 2015; Tajčmanová et al. 2015). The Holland-Powell dataset is supported by a comprehensive suite of mineral solid-solution models that account for all essential crystal-chemical substitutions. Because we have accepted the thermodynamic properties of minerals as such, only the standard state thermodynamic properties of aqueous ions and complexes were allowed to adjust to bring them into agreement with the fluid-mineral equilibria experiments.

The problem of consistency between the standard state thermodynamic data of aqueous species and minerals in major geochemical-thermodynamic datasets has been addressed in a number of studies (Sverjensky et al., 1991; Zhu and Sverjensky, 1991; Holland and Powell, 1998; Tutolo et al., 2014). All studies concluded that there are major discrepancies between predictions from calculated fluid mineral-equilibria and experimental mineral solubility studies. Different strategies were then suggested for resolving these discrepancies. In most cases, the properties of aqueous species were accepted from different critical data compilations (e.g., CODATA), and the standard state Gibbs energies of the minerals were then adjusted to bring them into agreement with the experimental solubility data.

Sverjensky et al. (1991) resolved the discrepancies between calculated fluid-mineral equilibria and the respective experimental data by first adjusting the properties of minerals using a selected set of experiments, and then by refining the association constant data for HCl^0. In this process, they retained the standard state thermodynamic properties and HKF parameters of all other aqueous ions and complexes. They adjusted the standard state Gibbs energies of selected minerals (paragonite, albite, muscovite, sanidine) using the thermodynamic datasets of Helgeson et al. (1978) and Berman (1988) as a basis. Zhu and Sverjensky (1991) extended the approach of Sverjensky et al. (1991) and determined the standard state properties of F- and Cl-bearing minerals using results of the F-Cl partitioning experiments between hydrous minerals and aqueous fluid.

The approach of Sverjensky et al. (1991) and Zhu and Sverjensky (1991) has a number of drawbacks. Firstly, the two mineral datasets (Helgeson et al., 1978; Berman, 1988) that were used as a basis for making the adjustments were not updated by taking advantage of more recent mineral phase equilibria experiments. The situation is fundamentally different for the mineral dataset of Holland and Powell (1998), whose recent update (Thermocalc dataset ds55) has incorporated a large body of new experimental phase equilibria data. Secondly, the incremental adjustment to the standard state Gibbs energy of selected minerals breaks the internal consistency of the respective thermodynamic mineral dataset. Thirdly, the properties used for the ion pair association constants of major electrolytes (NaCl, KCl, NaOH, KOH, HCl) are not in agreement with the new conductance and potentiometric data. Fourthly, the choice to use a restricted set of experimental mineral solubility data for determining the magnitude of the Gibbs energy adjustments brings the data into better agreement with these particular experiments, but worsens the agreement with other mineral solubility data (as shown in the results section above).

Taking a different approach, Tutolo et al. (2014) proposed a method that is conceptually similar to the one proposed by Holland and Powell (1985) for producing an internally consistent mineral dataset. They refined the standard state Gibbs energy of some aluminum minerals against phase equilibria, calorimetric data, and also against selected solubility data. During the data optimization, they accepted the thermodynamic data for aqueous species from published sources. While the method used by Tutolo et al. (2014) ensures internal consistency for the system they have considered (they have chosen to adjust the properties of a few minerals in the aluminum system), this may break the thermodynamic consistency with experimental phase equilibria in other chemical systems where these minerals are involved into reactions. Although these authors noted a considerable improvement between calculated and experimental mineral solubility data, they nevertheless reported persisting discrepancies in modeling the Al-Si-Na-K-Cl-OH system using their adjusted mineral data. They further reported a substantial disagreement between the association constant data for the major electrolytes they used (Shock and Helgeson, 1988; Sverjensky et al., 1991) and the new experimental conductance data (Ho et al., 1994; Ho and Palmer, 1996; Ho and Palmer, 1997).

Holland and Powell (1998) presented a preliminary dataset for aqueous species together with their internally consistent database for minerals. They used an equation of state for aqueous species that is a modification of the density model (Anderson et al., 1991). The standard state properties of aqueous species were not refined as part of their simultaneous regression of the mineral thermodynamic data, but they have been collected from different sources and were processed separately. Holland and Powell (1998) compared the calculated fluid-mineral equilibria with the

experimental data for a few selected examples, and demonstrated a reasonable agreement. However, they did not demonstrate that fluid-mineral equilibria calculated using their combined aqueous species and mineral data would be able to reproduce the large body of available mineral solubility data in the Na-K-Al-Si-O-H-Cl system. Furthermore, their data for aqueous ions and complexes are in disagreement with the association constants derived from the new conductance and potentiometric experiments.

Taken together, the previous attempts to address the large discrepancies between the calculated fluid-mineral equilibria and the experimental mineral solubility data have resulted in some improvements, but have not been able to fundamentally resolve the consistency issues in a general way. In our study, we have therefore used a very different approach by global regression of the standard state Gibbs energies of aqueous ions and complexes against a large body of experimental mineral solubility data, while retaining the internally consistent thermodynamic data for minerals, and maintaining full consistency with the association constant data for aqueous complexes.

7.1. System Si-O-H-Cl

There are no major changes to the thermodynamic properties of the silica species, because this system was extensively studied and there is a large amount of high-quality experimental data available. The quartz solubility data in pure water over wide ranges of temperature and pressure are generally in good agreement with each other (with a few exceptions like the dataset of Xie and Walther, 1993) and can be well reproduced by model calculations. The quartz solubility data in KOH solutions (Anderson and Burnham, 1967; Pascal and Anderson, 1989) are systematically underpredicted by the speciation model that only accounts for the SiO_2^0 and $HSiO_3^-$ species. This suggests that the $KHSiO_3^0$ complex may have formed in these experiments, similar to the better established complex $NaHSiO_3^0$ in the Na system, which would account for the difference between the calculated and measured quartz solubilites. More experimental data in the system SiO_2-H_2O-KOH would be needed to evaluate the stability and standard state properties of the $KHSiO_3^0$ complex.

7.2. System Al-O-H-Cl

The experimental solubility data for gibbsite and boehmite were first used to retrieve the stability constants of Al hydroxide complexes $AlOH^{2+}$, $Al(OH)_2^+$, $Al(OH)_3^0$ and $Al(OH)_4^-$. These were then used together with the experimental corundum and diaspore solubility data to refine the $\Delta_f G^0_{298,1}$ values of all Al species (Tables 5 and 6). When we initially fitted the corundum and diaspore solubility data separately, we noticed that the resulting $\Delta_f G^0_{298,1}$ for those Al species that are significant in the

experiments were different by only a few hundred joules (but still within the 1 sigma error of the parameters), compared to the results obtained from the global fit that included the solubility data for all aluminum minerals. This suggests that the standard state properties of gibbsite and boehmite (Robie and Hemingway, 1995) are essentially consistent with the properties of corundum and diaspore in the HP02 dataset.

The extended Debye-Hückel aqueous activity model (Helgeson et al., 1981; Oelkers and Helgeson, 1990) is considered appropriate for aqueous solutions up to moderate salt concentrations. At higher salt concentration exceeding about 5 molal, the calculated activity coefficients start to deviate from experimental data (Sharygin et al., 2002; Hingerl et al., 2014; Appelo, 2015), resulting in a steeper increase in the calculated solubility compared to the experimentally measured values (Figs. 2, 5, and 6). We have, however, observed that the extended Debye-Hückel model is able to predict the experimental aluminum hydroxide solubilities in alkaline (NaOH and KOH) solutions reasonably well, even at higher salt concentrations. We attribute this to the predominance of associated neutral species at higher temperatures, which reduces the effective ionic strength to values within the applicability limits of the extended Debye-Hückel model.

Many studies have concluded that corundum solubility in water is controlled by the two species $Al(OH)_3^0$ and $Al(OH)_4^-$, with $Al(OH)_3^0$ becoming predominant at temperatures exceeding 400 °C and pressures above 1.0 kbar (Pokrovskii and Helgeson, 1995; Tropper and Manning, 2007; Sverjensky et al., 2014). When using the thermodynamic properties for $Al(OH)_3^0$ from Pokrovskii and Helgeson (1995), the calculated aluminum concentrations at near-neutral pH are about 1.5 orders of magnitude higher than those determined in the experiments (Tagirov and Schott, 2001). Using the thermodynamic data for Al species from Tagirov and Schott (2001) results in calculated corundum solubilities that are lower by around 0.7 log units than measured in the high-quality solubility experiments of Becker et al. (1983) and Tropper and Manning (2007). This most likely reflects that Tagirov and Schott (2001) derived the thermodynamic properties of $Al(OH)_3^0$ only from boehmite solubility experiments up to 350 °C and SWVP. Therefore, calculated Al solubilities diverge increasingly from experimental ones at higher temperatures and pressures. To resolve this disagreement, we have refitted the standard state properties and HKF parameters of $Al(OH)_3^0$ using both low- and high-temperature experiments. We accepted the standard state partial heat capacity and volume data of $Al(OH)_3^0$ from Pokrovskii and Helgeson (1995) as initial values and then refined the $\Delta_f G^0_{298,1}$ in the global regression.

7.3. System Al-Si-O-H-Cl

The discrepancies between the calculated and the experimentally determined Si concentrations in equilibrium with the assemblages corundum+andalusite and disapore+andalusite cannot be resolved by adjusting the standard state properties of the SiO_2^0 species (Fig. 11). We suspect that most likely additional Si-Al complexes that were not accounted for in our speciation model like $AlSiO_4^-$ or $HAlSiO_4^0$ (Manning, 2007) have contributed to enhanced silica solubility. Because of insufficient data to constrain the thermodynamic properties of these species, we were not able to include them into our model.

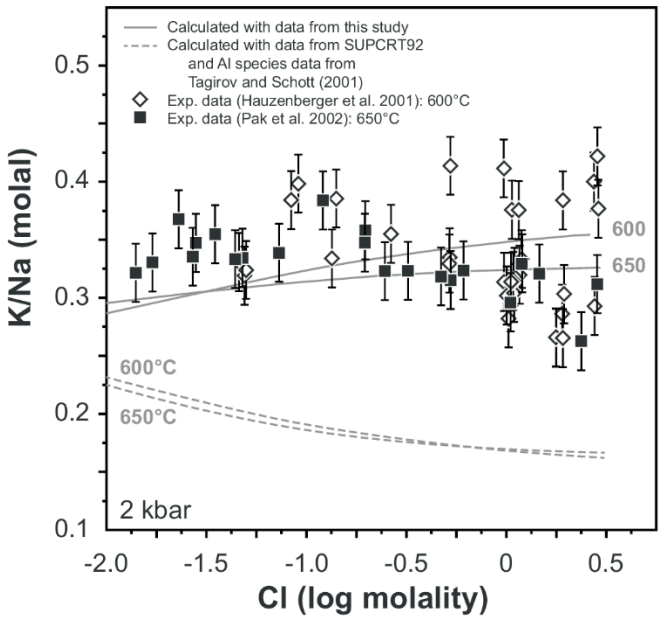

Figure 18. Comparison between calculated and measured molal (K/Na) ratios for the reversed solubility experiments in the system albite-K-feldspar-andalusite-quartz-fluid (Hauzenberger et al., 2001; Pak et al., 2003). The molal K/Na ratios are plotted as function of solution chlorinity.

7.4. System K-Na-Al-Si-O-H-Cl

The calculated log(K/H), log(Na/H) and K/Na ratios in chlorine bearing systems (Figs. 14, 15 and 18) are determined by the thermodynamic properties of Na^+, K^+, $NaCl^0$, KCl^0, HCl^0, and those of the buffering minerals. Because we have adopted the strategy of using fixed thermodynamic properties of minerals, adjusting the properties of aqueous ions and complexes was the only possibility to bring the calculated fluid-mineral equilibria into agreement with the experimental solubility data. Because we wanted to maintain consistency with the association constant data $NaCl^0$, KCl^0 and HCl^0 at elevated temperatures and pressures derived from conductance experiments, we had to adjust the thermodynamic properties of the Na^+ and K^+ ions. This was done by regressing their $\Delta_f G^0_{298,1}$ values against a large body of solubility data for Na-K-aluminosilicate mineral assemblages in chloride

solutions (Montoya and Hemley, 1975; Haselton et al., 1988; Sverjensky et al., 1991; Haselton et al., 1995).

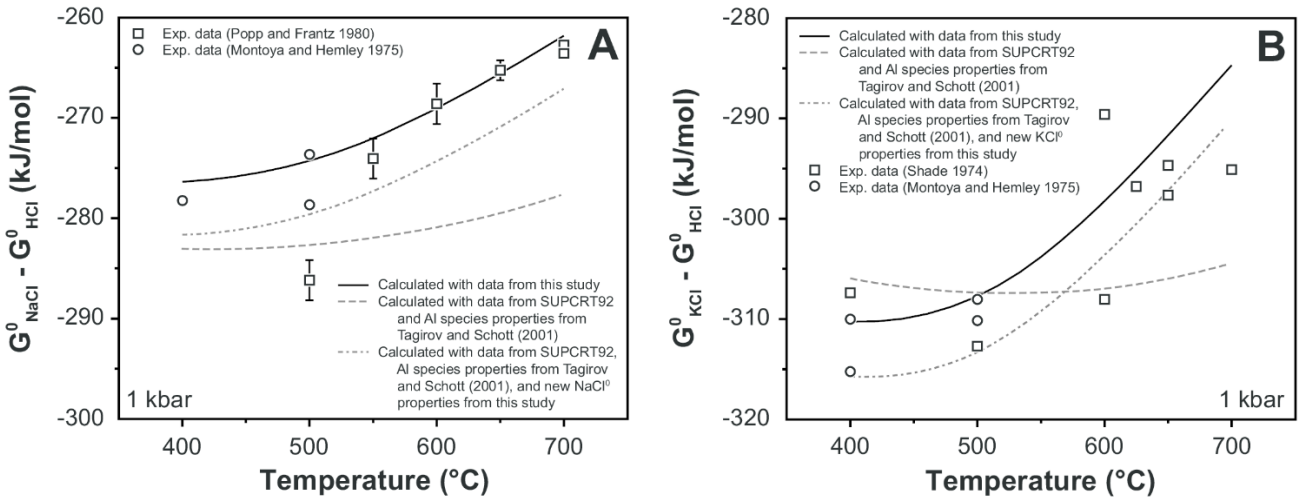

Figure 19. (**A**) Comparison between calculated $(G^0_{\mathrm{NaCl}} - G^0_{\mathrm{HCl}})$ values and their counterparts extracted from solubility experiments in the system Na-Al-Si-O-H-Cl (Montoya and Hemley, 1975; Popp and Frantz, 1980). The data are plotted as function of temperature (and at a pressure of 1 kbar). Popp and Franz (1980) suggested that their data point at 500°C is inconsistent with the remainder of their data. (**B**) Comparison between calculated $(G^0_{\mathrm{KCl}} - G^0_{\mathrm{HCl}})$ values and their counterparts extracted from solubility experiments in the system K-Al-Si-O-H-Cl (Montoya and Hemley, 1975; Shade 1974). The data are plotted as function of temperature (and at a pressure of 1 kbar).

The calculated K/Na ratios are now in good agreement with the experimental data from Hauzenberger et al. (2001) and Pak et al. (2003). This is largely due to the improved thermodynamic properties of the KCl^0 and $NaCl^0$ species. This leads to the conclusion that during optimization of the $\Delta_f G^0_{298,1}$ values of the ions, every adjustment to K^+ must be accompanied by an adjustment to Na^+ of similar magnitude. This is essential for maintaining the agreement with the experimental K/Na partitioning data (Hauzenberger et al., 2001; Pak et al., 2003). This further leads to the prediction that an adjustment in the $\Delta_f G^0_{298,1}$ of K^+ and Na^+ of similar magnitude should then simultaneously improve the agreement between calculated and experimentally measured log(K/H) and log(Na/H) values. This is exactly what is observed as a key result from the final global data regression of this study. Figures 14 and 15 show that the agreement between calculated and experimentally measured data is considerably better in both the K- and the Na-system, while the good agreement with the experimental K/Na partitioning data is maintained (Fig. 16 and 17). This result can be further analyzed by looking at the relative Gibbs energy differences $(G^0_{\mathrm{NaCl}} - G^0_{\mathrm{HCl}})$ and $(G^0_{\mathrm{KCl}} - G^0_{\mathrm{HCl}})$ extracted by Popp and Frantz (1980) from experimental studies (Fig. 19). The agreement with the temperature trends is

already greatly improved by using the KCl^0 and $NaCl^0$ association constant data from this study, but good agreement with the absolute values is only achieved after optimization of the $\Delta_f G^0_{298,1}$ values of K^+ and Na^+.

An empirical test for the quality of the new thermodynamic dataset is provided by a comparison of calculated K/Na ratios for a fluid in equilibrium with the assemblage K-feldspar+albite+muscovite+quartz with the natural data from geothermal waters (Fig. 20). The calculated data are in excellent agreement with the natural K/Na ratios, which have been used by Can (2002) to develop an empirical solute thermometer for geothermal exploration.

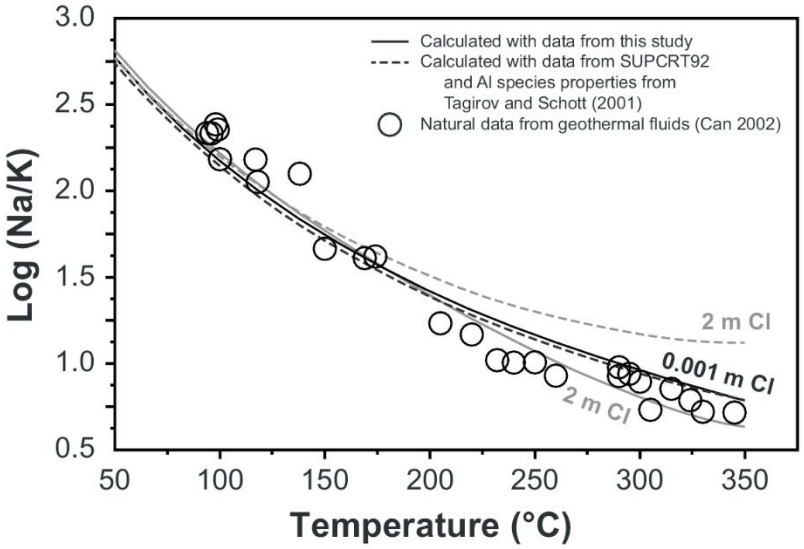

Figure 20. Comparison between calculated log(K/Na) ratios and those measured from natural geothermal fluids (Can, 2002), plotted as function of temperature (and at saturated water vapor pressure). The calculations were performed for fluid salinities of 0.001 and 2.0 molal NaCl, assuming equilibrium with the mineral assemblage K-feldspar+albite+muscovite+quartz.

7.5. Thermodynamics of the aqueous K^+ and Na^+ ions

The experiments that largely determine the adjustments to the $\Delta_f G^0_{298,1}$ values of the K^+ and Na^+ ions were performed at elevated temperature and pressure conditions. Therefore, it could be argued that a good agreement with the experimental data could have been achieved by adjusting the standard state entropy, volume, heat capacity or the HKF parameters for the ions. These properties were obtained using the framework of the HKF model by Tanger and Helgeson (1988). They used experimental standard partial molal volumes, isothermal compressibilities, and isobaric heat capacities of several aqueous electrolytes (e.g., HCl, NaCl, KCl, NaOH, KOH; Tanger and Helgeson, 1988) over a range in temperature. From those experimental data, they extracted the HKF equation of state parameters for the electrolytes. When performing regression of the partial molal entropy, volume, heat capacity

and HKF equation of state coefficients for Na^+ and K^+ and other ions, they used the following thermodynamic constraint:

$$\Omega_k = \sum_j \nu_{j,k} \Omega_j \tag{12}$$

where Ω stands for the HKF equation of state coefficients of the *j*th aqueous ion and the *k*th aqueous electrolyte, and $\nu_{j,k}$ is the stoichiometry coefficient of the *j*th ion in the *k*th electrolyte. This means that HKF coefficients for the aqueous ions are directly linked to the values of the corresponding coefficients for aqueous electrolytes. Therefore, any modification of the HKF coefficients of these ions that does not satisfy Eq. (11) will break the fundamental consistency of the HKF model. For example, if the values of some HKF coefficient for K^+ will be changed, this will result in an adjustment to the corresponding HKF coefficients of Cl^-. Because the HKF coefficients of Cl^- are also linked to those of HCl(aq) through Eq. (11), this change in the HKF coefficients of Cl^- will then violate the fundamental convention that all properties of the H^+ ion are zero at any temperature and pressure.

Accepting these thermodynamic constraints, the only feasible strategy was to adjust the $\Delta_f G^0_{298,1}$ values of the K^+ and Na^+ ions. We will now discuss how this adjustment is justified in view of the sources for the $\Delta_f G^0_{298,1}$ values of K^+ and Na^+ that are found in the geochemical and chemical literature. The $\Delta_f G^0_{298,1}$ values of the Na^+ and K^+ ions used in most geochemical databases are accepted from CODATA (Cox et al., 1989). The sources for these values are ultimately calorimetric data for the heats of reaction and hydrolysis of solid Na and K metals with H_2O, and standard electrode potential measurements (Smith and Taylor 1940; Gunn and Green 1958; Cerquetti et al., 1968; Dill et al., 1968). These heats of reaction were combined with the heats of formation of H_2O(aq), that of OH^-, the heats of dilution and the standard state entropies for the elements from the NBS tables (Wagman et al., 1982) to derive the heats of formation for the K^+ and Na^+ ions at infinite dilution. The standard state Gibbs energy of formation and the standard state entropy were then calculated from standard electrode potential measurements (Smith and Taylor 1940; Dill et al., 1968). When reviewing the basic literature data on the electrode potential measurements related to Na^+ and K^+, it becomes clear that the maximum error that could arise from the experimental measurements and the data processing should not exceed about 0.5 kJ/mol.

Another reason for adjustments of $\Delta_f G^0_{298,1}$ values of the Na^+ and K^+ ions could be our incomplete understanding of the speciation and activity coefficients of aqueous species in hydrothermal solutions. The HKF model parameters also introduce errors in the properties of the species, and the model itself has several limitations. While the HKF model was developed using the

physically sound Born solvation theory for charged species, it was subsequently extended to nonelectrolytes and neutral species as well (Shock et al., 1989). However, it has been demonstrated theoretically and using experimental data that the Born-type model is not really suitable for calculating and predicting thermodynamic properties of neutral species, especially at near-critical and supercritical conditions (Akinfiev and Diamond, 2003; Plyasunov, 2015; Plyasunov and Shock, 2001).

7.6. Thermodynamics of Na- and K-bearing minerals

The overall success of the Holland-Powell mineral thermodynamic datasets (Holland and Powell, 1985, 1990, 1998, 2011) is based on their internal consistency and the close agreement with a large amount of phase equilibria experiments, rather than on the agreement of individual values for the standard enthalpies of formation with calorimetric data. This makes these datasets extremely valuable and successful in pertological and geochemical applications where phase equilibria of complex rock-dominated systems are modeled. Favoring internal consistency rather than accuracy for individual enthalpy values is also the key reason, why subsequent versions of the database show large differences (up to ca. 7.0 kJ/mol and more) in standard enthalpies for some individual minerals. For example, the standard enthalpy of muscovite is 7.6 kJ/mol higher in Holland and Powell (2011) compared to Holland and Powell (1998), and that of paragonite is 3.4 kJ/mol higher. These differences do not have any visible impact when modeling phase equilibria for metamorphic rocks because essentially the same experimental dataset was used to refine the parameters in both versions of the database, and the agreement with these experimental data is very good. The changes in absolute values of enthalpies of formation for the minerals just reflect changes to the equations of state and phase transition models that were used, e.g. the new thermal equation of state and the symmetric formalism for modeling order-disorder in Holland and Powell (2011).

When optimizing the standard enthalpies of minerals, Holland and Powell (1998, 2011) have mainly used experimental phase equilibria data, but also mineral calorimetry data (Robie et al., 1979; Robie and Hemingway, 1995) as a set of rather loose constraints. The calorimetric constraints have a variable impact on the final regressed enthalpy values. In most cases, the mineral end-members with calorimetric constraints display the smallest change between different versions of the dataset. Most of the adjustments arising from the experimental phase equilibria data are assimilated by the standard enthalpies of mineral end-members without calorimetric constraints (e.g. muscovite, paragonite). As a result, the mineral end-members with no loose calorimetric constraints are typically those showing the largest differences between subsequent versions of the Holland-Powell database. For example, the substantial change in the standard enthalpy of microcline between Holland and Powell (1990) and

Holland and Powell (1998) was due to a change in the calorimetric data that were used. In Holland and Powell (2011), the calorimetric constraint for microcline is retained, and the shift of the enthalpy value is just -280 J/mol compared to Holland and Powell (1998). By contrast, the difference in the standard enthalpy of muscovite, which did not have any calorimetric constraints, is -2.5 kJ/mol between Holland and Powell (1998) and Holland and Powell (1990), and 7.6 kJ/mol between Holland and Powell (2011) and Holland and Powell (1998). These substantial differences between versions of the Holland-Powell mineral dataset are also reflected by the rather large errors reported for the final values of the enthalpies of formation. These amount to 5.8, 6.1, 3.8 and 4.0 kJ/mol for microcline, muscovite, albite and paragonite, respectively (Holland and Powell, 1990, 1998, 2011).

Calorimetric values reported in compilations of Robie et al. (1979) and Robie and Hemingway (1995) do not come from direct measurements, but are based on calculation of thermochemical cycles using heats of reactions measured by HF dissolution or molten-salt calorimetry. The thermochemical cycle for calculating the standard enthalpy of formation of microcline, given in Hemingway and Haselton (1994), involves 13 reactions. Each reaction has an associated experimental error of several kJ/mol, and some reaction enthalpies may be affected by systematic errors as well. The change of 6.9 kJ/mol for microcline in Robie and Hemingway (1995) was related to a systematic error in calorimetric measurements of the enthalpy of solution of aluminium chloride hexahydrate in HF. Considering that errors in calorimetric measurements of just one reaction are so large and that 13 reactions are involved in the thermochemical cycle, the uncertainty interval for the standard enthalpy of microcline and other rock-forming silicate minerals is at least of the order of 10 kJ/mol. This warrants adjustments to the enthalpies of formation of similar magnitude, when thermodynamic data for minerals are refined against experimental phase equilibria data via an internally-consistent data regression procedure.

In our study, we have selected the Holland-Powell mineral dataset as a hard constraint. Fitting the properties of the mineral end-members together with those of the aqueous species would have involved all the experimental phase equilibria data that were also used in optimizing the parameters in the Holland-Powell dataset. This formidable task was far beyond the scope of this study, because initially we did not see any need for refining the mineral properties, given that Holland and Powell (1990, 1998, 2011) have demonstrated that they are able to reproduce all available experimental phase equilibria data within their uncertainty brackets. The focus of our study was rather to model complex fluid-rock systems at hydrothermal conditions, taking advantage of the already refined and highly successful Holland-Powell database for minerals. We have therefore optimized the standard Gibbs energies for the aqueous species against the solubility experiments. We recognized that, in fact, the absolute values of standard enthalpies of formation for the K- and Na-bearing minerals are much less

constrained than those for the Na^+ and K^+ ions. However, we accepted that as a consequence of our approach, the Gibbs energies of formation for the K^+ and Na^+ ions had to be adjusted to bring about a good agreement between calculated and experimentally determined fluid-mineral equilibria data.

7.7. Internally consistent thermodynamic database

Internally consistent thermodynamic data are not necessarily in best agreement with all of the experimental solubility data or with other types of data such as calorimetric or electromotive force measurements. Because the equations of state and thermodynamic models used in calculations have associated errors and because the data fixed during the regression process (e.g. equilibrium constants for complexes derived from conductance data, the thermodynamic data for minerals) contribute additional errors, the accumulated discrepancies are assimilated by the adjustable parameters i.e. standard Gibbs energies of the aqueous species in this work. Therefore, internally consistent datasets may actually show significant differences between modeled and measured properties of individual substances. The major advantage of an internally consistent dataset is the ability to reproduce a large range of experimental data and to model complex natural systems in a robust and accurate way, in contrast with plain compilations of thermodynamic data collected from different sources, which may have been derived from individual experiments using vastly different assumptions and models. While some of these data compilations (e.g. CODATA) may be in good agreement with selected precisely measured thermodynamic properties, they are clearly not fully consistent with the large body of experimental solubility, conductance and calorimetric data and can therefore not be used directly to model complex geochemical fluid-mineral equilibria.

This clearly highlights that it is not sensible to model complex geochemical systems at hydrothermal conditions using thermodynamic properties of minerals and aqueous species assembled from several data sources that are not linked to each other by a consistent data treatment procedure. The only feasible approach for overcoming these limitations is to derive thermodynamic data through an internally consistent regression procedure, as performed in this study. The resulting values may not be the most accurate ones for each and every specific chemical system, and the refined properties of some aqueous species may differ from the values accepted in major compilations like CODATA. Nevertheless, the new dataset can be successfully used to model complex multi-component, multi-phase geochemical systems, including mineral solubility and aqueous speciation, at a level of confidence and accuracy that was hardly possible before.

7.8. Agreement with CODATA for Na^+ and K^+ ions

Because we have adopted the strategy to keep the thermodynamic properties of minerals fixed during the global regression of solubility data, the discrepancies between calculated and experimentally determined fluid-mineral equilibria were translated into adjustments to the values of the standard state Gibbs energy of formation aqueous species including those of the Na^+ and K^+ ions. This has the result that their $\Delta_f G^0_{298,1}$ values are not any more in agreement with the CODATA recommended values. However, even if we would have included the $\Delta_f G^0_{298,1}$ of minerals along with those of aqueous species into the regression process (and fitting them against mineral solubility data and mineral reaction phase equilibria), this would not guarantee the outcome that the refined $\Delta_f G^0_{298,1}$ values of K^+ and Na^+ ions would be equal to those from CODATA. Acknowledging that many aqueous and hydrothermal geochemists consider the agreement with CODATA values as highly important, we have generated an alternative converted thermodynamic dataset where the $\Delta_f G^0_{298,1}$ values of K^+ and Na^+ from CODATA were retained, but the properties of the K- and Na-bearing minerals were shifted accordingly (Table EA-4). This was done by adjusting the $\Delta_f G^0_{298,1}$ values of all K- and Na-bearing minerals by 5569 and 5712 J per mole of K and Na in their formula, respectively. A similar adjustment method was proposed by Sverjensky et al. (1991). This alternative dataset provides the same level of internal consistency and quality in terms of the agreement with experimental solubility and fluid-mineral equilibria data. This is because the reaction equilibrium constants between any K and/or Na –bearing aqueous ions, species, and minerals in the two datasets are not affected. The alternative dataset represents a workaround for matching the recommended CODATA values of Na^+ and K^+ aqueous ions. We, nevertheless, recognize the shortcomings of this formal conversion, and suggest that the next generation of internally consistent thermodynamic datasets for fluid-rock interaction should take advantage of both experimental mineral reaction brackets and fluid-mineral equilibria data. The properties of aqueous species and mineral end-members should be simultaneously refined, but the properties of the basic ions such as K^+ and Na^+ should be used as anchors, because they are well-constrained from highly accurate experiments.

8. Conclusions and outlook

(1) A large amount of critically evaluated experimental solubility data covering the entire Na-K-Al-Si-O-H-Cl system over a wide range in temperatures and pressures was used to simultaneously refine, in an internally consistent way, the standard state Gibbs energies of aqueous ions and complexes. An

astonishing degree of consistency with a large body of fluid-mineral equilibria data is obtained. This is achieved by adjusting the standard state Gibbs energies of the aqueous species.

(2) The global optimization of standard state Gibbs energies of aqueous species was set up in such a way that the association equilibria for ion pairs and complexes independently derived from conductance and potentiometric data are always maintained. This was achieved by introducing reaction constraints into the optimization problem, which adjust the standard state Gibbs energies of complexes by their respective Gibbs energy of reaction whenever the properties of the reactant species (ions) are changed. Optimized parameters can therefore be reported with calculated parameter confidence intervals and correlation coefficients.

(3) The new dataset is inherently consistent with the Holland and Powell (1998) mineral dataset (Thermocalc dataset ds55) and with all experimental mineral phase equilibria used to derive these data, as well as with experimental constraints on aqueous speciation equilibria. The dataset reproduces all available fluid-mineral phase equilibria and mineral solubility data with good accuracy over a wide range in temperature, pressure and composition (25 to 800 °C; 1 bar to 5 kbar; salt concentrations up to 5 molal).

(4) This work serves as a proof of concept for the optimization strategy that is feasible and successful in generating a thermodynamic dataset reproducing all fluid-mineral and aqueous speciation equilibria essentially within their experimental uncertainties. The core dataset in the system Na-K-Al-Si-O-H-Cl can be further extended using the same strategy to include additional rock-forming elements such as Ca, Mg, Fe, Mn, Ti, S, C and B. Work is currently in progress to incorporate Ca, Mg and C into the dataset, taking advantage of new experimental data for the solubility of Ca and Mg carbonate and silicate minerals.

(5) The global data optimization process implemented for this study can be repeated when an extension to new chemical elements and species is needed, when new experimental data become available, or when different aqueous activity models should be used. From a conceptual point of view, it is desirable that in the future also mineral phase equilibria and stability data and mineral partitioning data would be added to the experimental database. Then the standard-state properties of minerals and aqueous species could be simultaneously optimized to create a next-generation internally consistent dataset for fluid-mineral equilibria.

(6) The new geochemical-thermodynamic dataset for fluid-mineral equilibria, which resolves the existing data discrepancies, will help dramatically improve the quality and robustness of the next generation of geochemical and reactive transport models. This is a crucial step in gaining in-depth understanding of fluid-rock reaction processes such as formation of hydrothermal ore deposits,

evolution of natural and engineered geothermal reservoirs, and fluid chemistry in compressional orogenic belts, subduction zones, and mid-ocean ridges.

(7) Simultaneous parameter fitting in multicomponent and P-T space provides a clear guide to future experimentation, by highlighting the most sensitive gaps in fluid-mineral phase equilibria experiments. The thermodynamic database for aqueous species can be further improved when new solubility experiments become available, such as those involving feldspar and aluminosilicate assemblages in pure water but also in salt solutions. Experimental data on the solubilities of minerals at hydrothermal conditions are still needed to resolve some of the persisting discrepancies between available studies. New data on the speciation in the hydrothermal fluids especially on the association properties of species like $AlSiO_4^-$, $HAlSiO_4^0$, and $KSiOH_3^0$ are also needed to improve the agreement between calculations and experiments.

Acknowledgements

This project was supported by funding from ETH Zurich, ETHIIRA grant number ETH-19 11-2.

References

Adcock, S.W., 1985. The solubulity of some alumosilicate minerals in supercritical water - An experimental and thermodynamic study. Ph.D. thesis, Dep. of Geol., Carleton University, Ottawa, Ontario, 337 pp.

Akinfiev, N.N., Diamond, L.W., 2003. Thermodynamic description of aqueous nonelectrolytes at infinite dilution over a wide range of state parameters. Geochim. Cosmochim. Acta 67, 613-629.

Akinfiev, N.N., Diamond, L.W., 2009. A simple predictive model of quartz solubility in water–salt–CO_2 systems at temperatures up to 1000 °C and pressures up to 1000 MPa. Geochim. Cosmochim. Acta 73, 1597-1608.

André, L., Spycher, N., Xu, T., Vuataz F.D., Pruess, K., 2006. Modeling brine-rock interactions in an enhanced geothermal systemdeep fractured reservoir at Soultz-Sous-Forets (France): a joint approachusing two geochemical codes: FRACHEM and TOUGHREACT. Technical report, Center of Geothermal Research, Switzerland, 71 pp.

Anderson, G.M., 2005. Thermodynamics of Natural Systems, Second Ed., Cambridge University Press, Cambridge, 648 pp.

Anderson, G. M., Burnham, C.W., 1965. The solubility of quartz in super-critical water. Amer. J. Sci. 263, 494-511.

Anderson, G.M., Burnham, C.W., 1967. Reactions of quartz and corundum with aqueous chloride and hydroxide solutions at high temperatures and pressures. Amer. J. Sci. 265, 12-27.

Anderson, G.M., Burnham, C.W., 1983. Feldspar solubility and the transport of aluminum under metamorphic conditions. Amer. J. Sci. 283A, 283-297.

Anderson, G.M., Castet, S., Schott, J., Mesmer R.E., 1991. The density model for estimation of thermodynamic parameters of reactions at high temperatures and pressures. Geochim. Cosmochim. Acta 55, 1769-1779.

Anderson, G.M., Pascal, M.L., Rao, J., 1987. Aluminum speciation in metamorphic fluids. In Chemical Transport in Metasomatic Processes (ed. Helgeson H.), Springer Netherlands, 297-321.

Antignano, A., Manning, C.E., 2003. Solubility of albite + paragonite ± quartz in H_2O at 1 GPa, 580° C: Implications for metamorphic fluids. AGU Fall Meeting Abstracts 01/2003.

Audetat, A., Keppler, H., 2005. Solubility of rutile in subduction zone fluids, as determined by experiments in the hydrothermal diamond anvil cell. Earth Planet. Sci. Lett. 232, 393-402.

Appelo, C.A.J., 2015. Principles, caveats and improvements in databases for calculating hydrogeochemical reactions in saline waters from 0 to 200 °C and 1 to 1000 atm. Appl. Geochem. 55, 62-71.

Apps, J.A., 1970. The Stability field of analcime. Ph.D. Thesis, Harvard University, 347 pp.

Apps, J.A., Neill, J.M., 1990. Solubilities of aluminum hydroxides and oxihydroxides in alkaline solutions. Correlation with thermodynamic properties of $Al(OH)_4^-$. In: Chemical Modelling of Aqueous Systems II, 414-428.

Apps, J.A., Neill, J.M., Jun, C.H., 1988. Thermochemical properties of gibbsite, bayerite, boehmite, diaspore, and the aluminate ion between 0 and 350 °C. Technical Report, Lawrence Berkeley National Laboratory, 350 pp.

Arcis, H., Zimmerman, G.H., Tremaine, P.R., 2014. Ion-pair formation in aqueous strontium chloride and strontium hydroxide solutions under hydrothermal conditions by AC conductivity measurements. Phys. Chem. Chem. Phys. 16,17688-17704.

Armbruster, M.H., Crenshaw, J.L., 1934. A Thermodynamic Study of liquid potassium amalgams. J. Am. Chem. Soc. 56, 2525-2534.

Azaroual, M., Pascal, M.L., Roux, J., 1996. Corundum solubility and aluminum speciation in KOH aqueous solutions at 400°C from 0.5 to 2.0 kbar. Geochim. Cosmochim. Acta 60, 4601-4614.

Azimov, P., Bushmin, S., 2007. Solubility of minerals of metamorphic and metasomatic rocks in hydrothermal solutions of varying acidity: Thermodynamic modeling at 400-800°C and 1-5 kbar. Geochem. Internat. 45, 1210-1234.

Bandura, A.V., Lvov, S.N., 2006. The ionization constant of water over wide ranges of temperature and density. J. Phys. Chem. Ref. Data 35, 15-30.

Barns, R.L., Laudise, R.A., Shields, R.M., 1963. The solubility of corundum in basic hydrothermal solvents. J. Phys. Chem. 67, 835-839.

Bastrakov, E., Shvarov, Y., Girvan, S., Cleverley, J., McPhail, D., Wyborn, L.A.I., 2005. FreeGs: A web-enabled thermodynamic database for geochemical modelling. Geochim. Cosmochim. Acta, 69 (Suppl. 1), A845.

Bates, R.G., Bower, V.E., 1954. Standard potential of the silver-silver-chloride electrode from 0° to 95° C and the thermodynamic properties of dilute hydrochloric acid solutions. J. Res. National Bureau Standards 53, 283-290.

Bates, S.J., Kirschman, H.D., 1919. The vapor pressures and free energies of the hydrogen halides in aquoues solution; the free energy of formation of hydrogen chloride. J. Amer. Chem. Soc. 41, 1991-2001.

Becker, K.H., Cemic, L., Langer, K., 1983. Solubility of corundum in supercritical water. Geochim. Cosmochim. Acta 47, 1573-1578.

Bénézeth, P., Palmer, D.A., Wesolowski, D.J., 2001. Aqueous high-temperature solubility studies. II. The solubility of boehmite at 0.03 m ionic strength as a function of temperature and pH as determined by in situ measurements. Geochim. Cosmochim. Acta 65, 2097-2111.

Bénézeth, P., Dandurand, J.L., Harrichoury, J.C., 2009. Solubility product of siderite ($FeCO_3$) as a function of temperature (25–250 °C). Chem. Geol. 265, 3-12.

Bénézeth, P., Saldi, G.D., Dandurand, J.L., Schott, J., 2011. Experimental determination of the solubility product of magnesite at 50 to 200°C. Chem. Geol. 286, 21-31.

Berecz, E., Szita, L., 1970. Electrochemical method for the solubility and dissolution of solid compounds. Some thermodynamic properties of the system $Al(OH)_3$-NaOH-H_2O. Electrochim. Acta 15, 1407-1419.

Berman, R.G., Brown, T.H., 1985. Heat capacity of minerals in the system Na_2O-K_2O-CaO-MgO-FeO-Fe_2O_3-Al_2O_3-SiO_2-TiO_2-H_2O-CO_2: representation, estimation, and high temperature extrapolation. Contrib. Mineral. Petrol. 89, 168-183.

Berman, R.G., 1988. Internally-consistent thermodynamic data for minerals in the system Na_2O-K_2O-CaO-MgO-FeO-Fe_2O_3-Al_2O_3-SiO_2-TiO_2-H_2O-CO_2. J. Petrol. 29, 445-522.

Berman, R.G., Engi, M., Greenwood, H.J., Brown, T.H., 1986. Derivation of internally-consistent thermodynamic data by the technique of mathematical programming: a review with application the System MgO-SiO_2-H_2O. J. Petrol. 27, 1331-1364.

Bernshtein, V.A., Matsenok, Y.A., 1965. Equilibrium in the interaction of diaspore with solutions of sodium hydroxide at temperatures of 250 and 300 °C. J. Appl. Chem. USSR 38,1898-1901.

Bernshtein, V.A., Matsenok, Y.A., 1961. Solubility of boehmite in alkaline solution at 250 and 300°C. Zhurnal Prikladnoi Khimii 34, 982-986 (in Russian).

Bourcier, W.L., Knauss, K.G., Jackson, K.J., 1993. Aluminum hydrolysis constants to 250°C from boehmite solubility measurements. Geochimica et Cosmochimica Acta 57, 747-762.

Brown, G.C., Fyfe, W.S., 1971. Kyanite-andalusite equilibrium. Contrib. Mineral. Petrol 33, 227-231.

Burnham, C.W., Ryzhenko, B.N., Schitl, D., 1973. Water solubility of corundum at 500-800°C and 6 kbar. Geochem. Intern. 10 (6), 1374.

Busey, R.H. and Mesmer, R.E. (1977) Ionization equilibriums of silicic acid and polysilicate formation in aqueous sodium chloride solutions to 300 ºC. Inorg. Chem. 16, 2444-2450.

Can, I. (2002) A new improved Na/K geothermometer by artificial neural networks. Geothermics 31, 751-760.

Castet, S., Dandurand, J.L., Schott, J., Gout, R., 1993. Boehmite solubility and aqueous aluminum speciation in hydrothermal solutions (90-350°C): Experimental study and modeling. Geochim. Cosmochim. Acta 57, 4869-4884.

Cerquetti, A., Longhi, P., Mussini, T., 1968. Thermodynamics of aqueous hydrochloric acid from the emf. of hydrogen-chlorine cells. J. Chem. Eng. Data 13, 458-461.

Chang, B.T., Pak, L.H., Li, Y.S., 1979. Solubilities and rates of dissolution of diaspore in NaOH aqueous solutions. Bull. Chem. Soc. Japan 52, 1321-1326.

Chatterjee, N., Miller, K., Olbricht, W., 1994. Bayes estimation: A novel approach to derivation of internally consistent thermodynamic data for minerals, their uncertainties, and correlations. Part II: Application. Phys. Chem. Miner. 21, 50-62.

Chatterjee, N.D., Krüger, R., Haller, G., Olbricht, W., 1998. The Bayesian approach to an internally consistent thermodynamic database: theory, database, and generation of phase diagrams. Contrib. Mineral. Petrol. 133, 149-168.

Cloke, P.L., 1954. Quartz solubility in potassium hydroxide solutions under elevated pressures and temperatures with some geological applications. Ph.D. Thesis, Massachusetts Institute of Technology, 87 pp.

Couturier, Y., Michard, G., Sarazin, G., 1984. Constantes de formation des complexes hydroxydés de l'aluminium en solution aqueuse de 20 a 70°C. Geochimica et Cosmochimica Acta 48, 649-659.

Cox, J.D., Wagman, D.D., Medvedev, V.A., 1989. CODATA Key Values for Thermodynamics. Hemisphere Publishing Company, New York.

Crear, D.A., Anderson, G.M., 1971. Solubility and solvation reactions of quartz in dilute hydrothermal solutions. Chem. Geol. 8, 107-122.

Currie, K.L., 1968. On the solubility of albite in supercritical water in the range of 400 degrees to 600 degrees C and 750 to 3500 bars. Amer. J. Sci. 266, 321-341.

Davis, N.F., 1972. Experimental studies in the system $NaAlSi_3O_8$-H_2O. Ph.D. Thesis, Pensylvenia State University, 319 pp.

Delany, J.M., Lundeen, S.R., 1990. The LLNL thermochemical database. Lawrence Livermore National Laboratory, Report UCRL-21658.

Diakonov, I., Pokrovski, G., Schott, J., Castet, S., Gout, R., 1996. An experimental and computational study of sodium-aluminum complexing in crustal fluids. Geochim. Cosmochim. Acta 60, 197-211.

Dill, A.J., Itzkowitz, L.M., Popovych, O., 1968. Standard potentials of potassium electrodes and activity coefficients and medium effects of potassium chloride in ethanol-water solvents. J. Phys. Chem. 72, 4580-4586.

Dolejs, D., Manning, C.E., 2010. Thermodynamic model for mineral solubility in aqueous fluids: theory, calibration and application to model fluid-flow systems. Geofluids 10, 20-40.

Dolejs, D., Wagner, T., 2008. Thermodynamic modeling of non-ideal mineral-fluid equilibria in the system Si-Al-Fe-Mg-Ca-Na-K-H-O-Cl at elevated temperatures and pressures: Implications for hydrothermal mass transfer in granitic rocks. Geochim. Cosmochim. Acta 72, 526-553.

Druzhinina, N.K., 1955. Solubility of diaspore in aluminate solutions. Tsvetnyye Metally 1, 54-56 (in Russian).

Engi, M., 1992. Thermodynamic data for minerals: a critical assessment, In: Price, G., Ross, N. (Eds.), The Stability of Minerals. Springer Netherlands, 267-328.

Fabrichnaya, O., Saxena, S.K., Richet, P., Westrum, E.F., 2013. Thermodynamic data, models, and phase Diagrams in multicomponent oxide systems: an assessment for materials and planetary scientists based on calorimetric, volumetric and phase equilibrium data. Springer, Berlin, 198 pp.

Fournier, R.O., Rosenbauer, R.J., Bischoff, J.L., 1982. The solubility of quartz in aqueous sodium chloride solution at 350°C and 180 to 500 bars. Geochim. Cosmochim. Acta 46, 1975-1978.

Franck, E.U., 1956. Hochverdichteter Wasserdampf. III. Ionendissoziation von HCl, KOH und H_2O in überkritischem Wasser. Z. Phys. Chem. 8, 192-206.

Frantz, J.D., Marshall, W.L., 1984. Electrical conductances and ionization constants of salts, acids, and bases in supercritical aqueous fluids. I. Hydrochloric acid from 100 ºC to 700 ºC and at pressures to 4000 bars. Amer. J. Sci. 284, 651-667.

Fricke, R., Jucaitis, P., 1930. Untersuchungen über die Gleichgewichte in den Systemen Al_2O_3-Na_2O-H_2O and Al_2O_3-K_2O-H_2O. Z. Anorg. Allgem. Chem. 191, 129-149.

Galvez, M.E., Manning, C.E., Connolly, J.A.D., Rumble D., 2015. The solubility of rocks in metamorphic fluids: A model for rock-dominated conditions to upper mantle pressure and temperature. Earth and Planetary Science Letters, In Press. http://dx.doi.org/10.1016/j.epsl.2015.06.019

Gottschalk, M., 1997. Internally consistent thermodynamic data for rock-forming minerals in the system SiO_2-TiO_2-Al_2O_3-CaO-MgO-FeO-K_2O-Na_2O-H_2O-CO_2. Eur. J. Mineral. 9, 175-223.

Greenberg S. A., Price E. W., 1957. The solubility of silica in solutions of electrolytes. J. Phys. Chem. 61, 1539-1541.

Gruszkiewicz, M.S., Wood, R.H., 1997. Conductance of dilute LiCl, NaCl, NaBr, and CsBr solutions in supercritical water using a flow conductance cell. J. Phys. Chem. B 101, 6549-6559.

Gunn, S.R., Green, L.G., 1958. The heats of formation at 25° of the crystalline hydrides and deuterides and aqueous hydroxides of lithium, sodium and potassium. J. Am. Chem. Soc. 80, 4782-4786.

Gunter, W.D., Eugster, H.P., 1981. Mica-feldspar equilibria in supercritical alkali chloride solutions. Contrib. Mineral. Petrol. 75, 235-250.

Harman R. W., 1928. Aqueous solutions of sodium silicates: Part VIII. J. Phys. Chem. 32, 44-60.

Haselton, H.T., Cygan, G.L., and D'Angelo, W.M., 1988. Chemistry of aqueous solutions coexisting with fluoride buffers in the system K_2O-Al_2O_3-SiO_2 -H_2O-F_2O_{-1} (1 kbar, 400 ºC - 700 ºC). Econ. Geol. 83,163-173.

Haselton, H.T., Cygan, G.L., Jenkins, D.M., 1995. Experimental study of muscovite stability in pure H_2O and 1 molal KCl-HCl solutions. Geochim. Cosmochim. Acta 59 429-442.

Hauzenberger, C.A., Baumgartner, L.P., Pak, T.M., 2001. Experimental study on the solubility of the "model"-pelite mineral assemblage albite + K-feldspar + andalusite + quartz in supercritical chloride-rich aqueous solutions at 0.2 GPa and 600 °C. Geochim. Cosmochim. Acta 65, 4493-4507.

Hayden, L.A., Manning, C.E., 2011. Rutile solubility in supercritical $NaAlSi_3O_8$-H_2O fluids. Chem. Geol. 284, 74-81.

Helgeson, H.C., 1969. Thermodynamics of hydrothermal systems at elevated temperatures and pressures. Amer. Jour. Sci. 267, 729–804.

Helgeson, H.C., Kirkham, D.H., 1974a. Theoretical prediction of the thermodynamic behavior of aqueous electrolytes at high pressures and temperatures. I. Summary of the thermodynamic/electrostatic properties of the solvent. Amer. J. Sci. 274, 1089-1198.

Helgeson, H.C., Kirkham, D.H., 1974b. Theoretical prediction of the thermodynamic behavior of aqueous electrolytes at high pressures and temperatures. II. Debye-Huckel parameters for activity coefficients and relative partial molal properties. Amer. J. Sci. 274, 1199-1261.

Helgeson, H.C., Kirkham, D.H., Flowers, G.C., 1981. Theoretical prediction of the thermodynamic behavior of aqueous electrolytes by high pressures and temperatures. IV. Calculation of activity coefficients, osmotic coefficients, and apparent molal and standard and relative partial molal properties to 600 ºC and 5kb. Amer. J. Sci. 281, 1249-1516.

Helgeson, H.C., Delaney, J.M., Nesbitt, H.W., Bird, D.K., 1978. Summary and critique of the thermodynamic properties of rock-forming minerals. Amer. J. Sci. 278A, 1-229.

Hemingway, B.S., Haselton Jr, H.T., 1994. A reevaluation of the calorimetric data for the enthalpy of formation of some K- and Na-bearing silicate minerals. U.S. Geological Survey, 33 pp.

Hemingway, B.S., Robie, R.A., Kittrick, J.A., 1978. Revised values for Gibbs free-energy of formation of $Al(OH)_4(aq)$, diaspore, boehmite and bayerite at 298.15 K and 1 bar, thermodynamic properties of kaolinite to 800 K and 1 bar, and heats of solution of several gibbsite samples. Geochim. Cosmochim. Acta 42, 1533-1543.

Hemingway, B.S., Robie, R.A., Apps, J.A., 1991. Revised values for the thermodynamic properties of boehmite, AlOOH and related species and phases in the system Al-H-O. Amer. Mineral. 76, 445-457.

Hemley, J.J., 1959. Some mineralogical equilibria in the system K_2O-Al_2O_3-SiO_2-H_2O. Amer. J. Sci. 257, 241-270.

Hemley, J.J., Montoya, J.W., Marinenko, J.W., Luce, R.W., 1980. Equilibria in the system Al_2O_3-SiO_2-H_2O and some general implications for alteration/mineralization processes. Econ. Geol. 75, 210-228.

Hingerl, F.F., Wagner, T., Kulik, D.A., Thomsen, K., Driesner, T., 2014. A new aqueous activity model for geothermal brines in the system Na-K-Ca-Mg-H-Cl-SO_4-H_2O from 25 to 300 °C. Chem. Geol. 381, 78-93.

Hitch, B.F., Mesmer, R.E., Baes, C.F., Sweeton, F.H., 1980. The solubility of Gibbsite (α- $Al(OH)_3$) in 1 molal NaCl as a function of pH and temperature. Oak Ridge National Laboratory Report ORNL-5623, 35 pp.

Ho, P., Bianchi, H., Palmer, D.A., Wood, R., 2000a. Conductivity of dilute aqueous electrolyte solutions at high temperatures and pressures using a flow cell. J. Solut. Chem. 29, 217-235.

Ho, P.C., Palmer, D.A., Wood, R.H., 2000. Conductivity measurements of dilute aqueous LiOH, NaOH, and KOH solutions to high temperatures and pressures using a flow-through cell. J. Phys. Chem. B 104, 12084-12089.

Ho, P., Palmer, D.A., 1996. Ion association of dilute aqueous sodium hydroxide solutions to 600°C and 300 MPa by conductance measurements. J. Solut. Chem. 25, 711-729.

Ho, P., Palmer, D.A., Mesmer, R., 1994. Electrical conductivity measurements of aqueous sodium chloride solutions to 600°C and 300 MPa. J. Solut. Chem. 23, 997-1018.

Ho, P.C., Palmer, D.A., 1997. Ion association of dilute aqueous potassium chloride and potassium hydroxide solutions to 600°C and 300 MPa determined by electrical conductance measurements. Geochim. Cosmochim. Acta 61, 3027-3040.

Ho, P.C., Palmer, D.A., Gruszkiewicz, M.S., 2001. Conductivity measurements of dilute aqueous HCl solutions to high temperatures and pressures using a flow-through cell. J. Phys. Chem. B 105, 1260-1266.

Holland, T.J.B., 1989. Dependence of entropy on volume for silicate and oxide minerals; a review and predictive model. Amer. Mineral. 74, 5-13.

Holland, T.J.B., Powell, R., 1985. An internally consistent thermodynamic dataset with uncertainties and correlations. 2. Data and results. J. Metam. Geol. 3, 343-370.

Holland, T.J.B., Powell, R., 1990. An enlarged and updated internally consistent thermodynamic dataset with uncertainties and correlations: the system K_2O–Na_2O–CaO–MgO–MnO–FeO–Fe_2O_3–Al_2O_3–TiO_2–SiO_2–C–H_2–O_2. Journal of Metamorphic Geology 8, 89-124.

Holland, T.J.B., Powell, R., 1991. A compensated-Redlich-Kwong (CORK) equation for volumes and fugacities of CO_2 and H_2O in the range 1 bar to 50 kbar and 100-1600 °C. Contrib. Mineral. Petrol 109, 265-273.

Holland, T.J.B., Powell, R., 1998. An internally consistent thermodynamic data set for phases of petrological interest. J. Metam. Geol. 16, 309-343.

Holland, T.J.B., Powell, R., 2011. An improved and extended internally consistent thermodynamic dataset for phases of petrological interest, involving a new equation of state for solids. J. Metam. Geol. 29, 333-383.

Ikkatai, T., Okada, N., 1962. Viscosity, specific gravity and equilibrium concentrations of sodium aluminate solutions. In: Gerhard, G., Stroup, P.T. (Eds.) Extractive Metallurgy of Aluminum. New York, Interscience Publishers, pp. 159-173.

Ingri N., 1959. Equilibrium studies of polyanions IV. Silicate ions in NaC1 medium. Acta Chem. Scand. 13, 758-775.

Johnson, J.W., Oelkers, E.H., Helgeson, H.C., 1992. SUPCRT92: A software package for calculating the standard molal thermodynamic properties of minerals, gases, aqueous species, and reactions from 1 to 5000 bar and 0 to 1000 °C. Comp. Geosci. 18, 899-947.

Kennedy, G.C., 1950. A portion of the system silica-water. Econ. Geol. 45, 629-653.

Kestin, J., Sengers, J.V., Kamgar-Parsi, B., Levelt-Sengers, J.H.M., 1984. Thermophysical properties of fluid H_2O. J. Phys. Chem. Ref. Data 13, 175-183.

Kitahara, S., 1960. The solubility of quartz in water at high temperatures and high pressures. Review Phys. Chem. Japan 30, 109-114.

Korzhinskiy, M.A., 1987. The solubility of corundum in HCl fluid and forms taken by Al. Geochem. Intern. 24, 105-110.

Kulik, D.A., Wagner, T., Dmytrieva, S.V., Kosakowski, G., Hingerl., F.F., Chudnenko, K.V., Berner, U., 2013. GEM-Selektor geochemical modeling package: revised algorithm and GEMS3K numerical kernel for coupled simulation codes. Computat. Geosci. 17, 1-24.

Kuyunko, N.S., Malinin, S.D., Khodakovsky, I.L., 1983. An experimental study of aluminum ion hydrolysis at 150, 200, and 250 ºC. Geochem. Intern. 20, 76-86.

Lagerström G., 1959. Equilibrium studies of polyanions III. Silicate ions in $NaClO_4$ medium. Acta. Chem. Scand. 13, 722-736.

Lanari, P., Wagner, T., Vidal, O., 2014. A thermodynamic model for di-trioctahedral chlorite from experimental and natural data in the system MgO-FeO-Al_2O_3-SiO_2-H_2O: applications to P-T sections and geothermometry. Contrib. Mineral. Petrol. 167, 1-19.

Leal, A.M.M., Blunt, M.J., LaForce, T.C., 2014. Efficient chemical equilibrium calculations for geochemical speciation and reactive transport modelling. Geochim. Cosmochim. Acta. 131, 301-322.

Lichtner, P.C., Steefel, C.I., Oelkers, E.H., 1997. Reactive transport in porous media. Rev. Mineral. Geochem. 34, 448 pp.

Lier, J.A.V., Bruyn, P.L.D., Overbeek, J.T.G., 1960. The solubility of quartz. J. Phys. Chem. 64, 1675-1682.

Lukashov, Y.M., Komissarov, K.B., Golubev, B.P., Smirnov, S.N., Svistunov, E.P., 1975. An experimental investigation of the electrolytic properties of uni-univalent electrolytes at high parameters of state. Thermal Eng. 22, 79-82.

Lyapunov, A.N., Khodakova, A.G., Galkina, Z.G., 1964. Solubility of hydrargillite in NaOH solutions, containing soda or sodium chloride, at 60°C and 95°C. Tsvetnyye Metally 38, 48-51.

Magarshak, G.K., 1938. Polytherms in the Al_2O_3-Na_2O-H_2O System at 30-200°C. Legkiye Metally 7, 12-16 (in Russian).

Manning, C.E., 1994. The solubility of quartz in H_2O in the lower crust and upper mantle. Geochim. Cosmochim. Acta 58, 4831-4839.

Manning, C.E., 2007. Solubility of corundum + kyanite in H_2O at 700°C and 10 kbar: evidence for Al-Si complexing at high pressure and temperature. Geofluids 7, 258-269.

Manning, C.E., Antignano, A., Lin, H.A., 2010. Premelting polymerization of crustal and mantle fluids, as indicated by the solubility of albite-paragonite-quartz in H_2O at 1 GPa and 350-620 °C. Earth Planet. Sci. Lett. 292, 325-336.

Marshall, W.L., Franck, E.U., 1981. Ion product of water substance, 0-1000 °C, 1-10,000 bars, new international formulation and its background. J. Phys. Chem. Ref. Data 10, 295-304.

Méndez De Leo, L.P., Wood, R.H., 2005. Conductance study of association in aqueous $CaCl_2$, $Ca(CH_3COO)_2$, and $Ca(CH_3COO)_2 \cdot nCH_3COOH$ from 348 to 523 K at 10 MPa. J. Phys. Chem. B 109, 14243-24250.

Miron, G.D., Kulik, D.A., Dmytrieva, S.V., Wagner, T., 2015. GEMSFITS: Code package for optimization of geochemical model parameters and inverse modeling. Appl. Geochem. 55, 28-45.

Miron, G.D., Wagner, T., Wälle, M., Heinrich, C.A., 2013. Major and trace-element composition and pressure-temperature evolution of rock-buffered fluids in low-grade accretionary-wedge metasediments, Central Alps. Contrib. Mineral. Petrol 165, 981-1008.

Montoya, J.W., Hemley, J.J., 1975. Activity relations and stabilities in alkali feldspar and mica alteration reactions. Econ. Geol. 70, 577-583.

Mookherjee, M., Keppler, H., Manning, C.E., 2014. Aluminum speciation in aqueous fluids at deep crustal pressure and temperature. Geochim. Cosmochim. Acta 133, 128-141.

Morey, G.W., Fournier, R.O., Rowe, J.J., 1962. The solubility of quartz in water in the temperature interval from 25° to 300° C. Geochim. Cosmochim. Acta 26, 1029-1043.

Morse, J.W., Casey, W.H., 1988. Ostwald processes and mineral paragenesis in sediments. Amer. J. Sci. 288, 537-560.

Newton, R.C., Manning, C.E., 2000. Quartz solubility in H_2O-NaCl and H_2O-CO_2 solutions at deep crust-upper mantle pressures and temperatures: 2-15 kbar and 500-900 °C. Geochim. Cosmochim. Acta 64, 2993-3005.

Novgorodov, P.G., 1975. Solubility of quartz in H_2O-CO_2 mixtures at 700 °C and pressures of 3 and 5 kbar. Geochem. Internat. 12, 122-126.

Novgorodov, P.G., 1977. On the solubility of quartz in $H_2O + CO_2$ and H_2O + NaCl at 700 °C and 1.5 kb pressure. Geochem. Internat. 14, 191-193.

Oelkers, E.H., Helgeson, H.C., 1988. Calculation of the thermodynamic and transport properties of aqueous species at high pressures and temperatures: Aqueous tracer diffusion coefficients of ions to 1000 °C and 5 kb. Geochim. Cosmochim. Acta 52, 63-85.

Oelkers, E.H., Helgeson, H.C., 1990. Triple-ion anions and polynuclear complexing in supercritical electrolyte solutions. Geochim. Cosmochim. Acta 54, 727-738.

Oelkers, E.H., Helgeson, H.C., Shock, E.L., Sverjensky, D.A., Johnson, J.W., Pokrovskii, V.A., 1995. Summary of the apparent standard partial molal Gibbs free energies of formation of aqueous species, minerals, and gases at pressures 1 to 5000 bars and temperatures 25 to 1000 °C. J. Phys. Chem. Ref. Data 24, 1401-1560.

Ostapenko, G.T., Khetchikov, L.N., Balitskiy, V.S., 1969. Hydrolysis of aqueous solutions of sodium sulfide and solubility of quartz in these solutions. Geochem. Internat. 6, 22-28.

Ostapenko, G.T., Arapova, M.A., 1971. Solubility of kyanite, corundum, quartz and amoprhous silica in aqueous hydrochloric acid solutions at 285 °C and 485 bars. Geochem. Internat. 8, 482-488.

Ostapenko, G.T., Timoshkova, L.P., Tsymbal, S.N., 1978. Gibbs energy of sillimanite from data on its solubility in water at 530 °C and 1300 bars. Intern. Geol. Review 20, 864-866.

Pak, T.M., Hauzenberger, C.A., Baumgartner, L.P., 2003. Solubility of the assemblage albite+K-feldspar+andalusite+quartz in supercritical aqueous chloride solutions at 650 °C and 2 kbar. Chem. Geol. 200, 377-393.

Palmer, D.A., Bénézeth, P., Wesolowski, D.J., 2001. Aqueous high-temperature solubility studies. I. The solubility of boehmite as functions of ionic strength (to 5 molal, NaCl), temperature (100-290°C), and pH as determined by in situ measurements. Geochim. Cosmochim. Acta 65, 2081-2095.

Palmer, D.A., Wesolowski, D.J., 1992. Aluminum speciation and equilibria in aqueous solution: II. The solubility of gibbsite in acidic sodium chloride solutions from 30 to 70 °C. Geochim. Cosmochim. Acta 56, 1093-1111.

Palmer, D.A., Wesolowski, D.J., 1993. Aluminum speciation and equilibria in aqueous solution: III. Potentiometric determination of the first hydrolysis constant of aluminum(III) in sodium chloride solutions to 125 °C. Geochim. Cosmochim. Acta 57, 2929-2938.

Pascal, M.L., Anderson, G.M., 1989. Speciation of Al, Si, and K in supercritical solutions: Experimental study and interpretation. Geochim. Cosmochim. Acta 53, 1843-1855.

Plumridge, J., Arcis, H., Tremaine, P.R., 2015. Limiting conductivities of univalent cations and the chloride ion in H_2O and D_2O under hydrothermal conditions. J. Solut. Chem. 44, 1062-1089.

Plyasunov, A.V., 1988. Estimation for dissociation constants for symetrical electrolytes on the basis of stoichiometric activity coefficients. Russ. J. Phys. Chem. 62, 622-625.

Plyasunov, A.V., 2015. Correlation and prediction of thermodynamic properties of nonelectrolytes at infinite dilution in water over very wide temperature and pressure ranges (2000 K and 10 GPa). Geochim. Cosmochim. Acta 168, 236-260.

Plyasunov, A.V., Shock, E.L., 2001. Correlation strategy for determining the parameters of the revised Helgeson-Kirkham-Flowers model for aqueous nonelectrolytes. Geochim. Cosmochim. Acta 65, 3879-3900.

Pokrovskii, G.S., Schott, J., Harrichoury, J.C., Sergeyev, A.S., 1996. The stability of aluminum silicate complexes in acidic solutions from 25 to 150 °C. Geochim. Cosmochim. Acta 60, 2495-2501.

Pokrovskii, V.A., Helgeson, H.C., 1995. Thermodynamic properties of aqueous species and the solubilities of minerals at high pressures and temperatures; the system Al_2O_3-H_2O-NaCl. Amer. J. Sci. 295, 1255-1342.

Pokrovskii, V.A., Helgeson, H.C., 1997a. Calculation of the standard partial molal thermodynamic properties of KCl^0 and activity coefficients of aqueous KCl^0 at temperatures and pressures to 1000 °C and 5 kbar. Geochim. Cosmochim. Acta 61, 2175-2183.

Pokrovskii, V.A., Helgeson, H.C., 1997b. Thermodynamic properties of aqueous species and the solubilities of minerals at high pressures and temperatures: the system Al_2O_3-H_2O-KOH. Chem. Geol. 137, 221-242.

Popp, R.K., Frantz, J.D., 1980. Mineral-solution equilibria. III. The system Na_2O-Al_2O_3-SiO_2-H_2O-HCl. Geochim. Cosmochim. Acta 44, 1029-1037.

Powell, R., Holland, T.J.B., 1985. An internally consistent thermodynamic dataset with uncertainties and correlations: 1. Methods and a worked example. J. Metam. Geol. 3, 327-342.

Quist, A.S., Marshall, W.L., 1969. Electrical conductances of some alkali metal halides in aqueous solutions from 0 to 800 ºC and at pressures to 4000 bars. J. Phys. Chem. 73, 978-985.

Ragnarsdóttir, K.V., Walther, J.V., 1985. Experimental determination of corundum solubilities in pure water between 400-700 °C and 1-3 kbar. Geochim. Cosmochim. Acta 49, 2109-2115.

Reed, M.H, 1982. Calculation of multicomponent chemical equilibria and reaction processes in systems involving minerals, gases and an aqueous phase. Geochim. Cosmochim. Acta 46, 513-528.

Reukov, V.V., Zotov, A.V., 2006. Determination of the HCl dissociation constant at a temperature of 350°C and 200 bars of pressure by the potentiometric method using a ceramic electrode. Geol. Ore Depos. 48, 144-150.

Rimstidt, J.D., 1997. Quartz solubility at low temperatures. Geochim. Cosmochim. Acta 61, 2553-2558.

Robie, R.A., Hemingway, B.S., Fisher, J.R., 1979. Thermodynamic Properties of Minerals and Related Substances at 298.15 K and 1 Bar (10^5 Pascals) Pressure and at Higher Temperatures, U.S. Geological Survery Buletin, Washington, 452 pp.

Robie, R.A., Hemingway, B.S., 1995. Thermodynamic Properties of Minerals and Related Substances at 298.15 K and 1 Bar (10^5 Pascals) Pressure and at Higher Temperatures. U.S. Geol. Survey Bull. 2131, 461 pp.

Roedder, E., 1984. Fluid inclusions. Rev. Mineral. Geochem. 12, 464 pp.

Ruaya, J.R., Seward, T.M., 1987. The ion-pair constant and other thermodynamic properties of HCl up to 350°C. Geochim. Cosmochim. Acta 51, 121-130.

Russell, A.S., Edwards, J.D., Taylor, C.S., 1955. Solubility and density of hydrated alumina in NaOH solutions. Journal of Metals 7, 1123-1128.

Salvi, S., Pokrovski, G.S., Schott, J., 1998. Experimental investigation of aluminum-silica aqueous complexing at 300°C. Chem. Geol. 151, 51-67.

Sassani, D.C., Shock, E.L., 1992. Estimation of standard partial molal entropies of aqueous ions at 25°C and 1 bar. Geochim. Cosmochim. Acta 56, 3895-3908.

Sato, T., 1954. Hydrolysis of sodium aluminate solution. XIII. Effect of decomposition temperature. J. Chem. Soc. Japan Ind. Chem. Sect. 57, 805-808.

Schofield, R.K., Taylor, A.W., 1954. The hydrolysis of aluminium salt solutions. Journal of the Chemical Society (Resumed), 4445-4448.

Schott, J., Pokrovsky, O.S., Oelkers, E.H., 2009. The link between mineral dissolution/precipitation kinetics and solution chemistry. Rev. Mineral. Geochem. 70, 207-258.

Schwarz, R., Müller, W.D., 1958. Zur Kenntnis der Kieselsäuren. XIV. Die wasserlösliche Monokieselsäure. Z Anorg Allg Chem 296, 273-279.

Seward, T.M., 1974. Determination of the first ionization constant of silicic acid from quartz solubility in borate buffer solutions to 350°C. Geochim. Cosmochim. Acta 38, 1651-1664.

Shade, J.W., 1974. Hydrolysis reactions in the SiO_2-excess portion of the system K_2O-Al_2O_3-SiO_2-H_2O in chloride fluids at magmatic conditions. Econ. Geol. 69, 218-228.

Sharygin, A.V., Mokbel, I., Xiao, C.B., Wood, R.H., 2001. Tests of equations for the electrical conductance of electrolyte mixtures: Measurements of association of NaCl(aq) and Na_2SO_4(aq) at high temperatures. J. Phys. Chem. B 105, 229-237.

Sharygin, A.V., Wood, R.H., Zimmerman, G.H., Balashov, V.N., 2002. Multiple ion association versus redissociation in aqueous NaCl and KCl at high temperatures. J. Phys. Chem. B 106,7121-7134.

Shinohara, H., Fujimoto, K., 1994. Experimental study in the system albite-andalusite-quartz-NaCl-HCl-H_2O at 600°C and 400 to 2000 bars. Geochim. Cosmochim. Acta 58, 4857-4866.

Shmulovich, K., Graham, C., Yardley, B., 2001. Quartz, albite and diopside solubilities in H_2O-NaCl and H_2O-CO_2 fluids at 0.5-0.9 GPa. Contrib. Mineral. Petrol 141, 95-108.

Shmulovich, K.I., Yardley, B.W.D., Graham, C.M., 2006. Solubility of quartz in crustal fluids: experiments and general equations for salt solutions and H_2O-CO_2 mixtures at 400-800°C and 0.1-0.9 GPa. Geofluids 6, 154-167.

Shock, E.L., Helgeson, H.C., 1988. Calculation of the thermodynamic and transport properties of aqueous species at high pressures and temperatures: Correlation algorithms for ionic species and equation of state predictions to 5 kb and 1000°C. Geochim. Cosmochim. Acta 52, 2009-2036.

Shock, E.L., Helgeson, H.C., Sverjensky, D.A., 1989. Calculation of the thermodynamic and transport properties of aqueous species at high pressures and temperatures: Standard partial molal properties of inorganic neutral species. Geochim. Cosmochim. Acta 53, 2157-2183.

Shock, E.L., Oelkers, E.H., Johnson, J.W., Sverjensky, D.A., Helgeson, H.C., 1992. Calculation of the thermodynamic properties of aqueous species at high pressures and temperatures. Effective electrostatic radii, dissociation constants and standard partial molal properties to 1000 °C and 5 kbar. J. Chem. Soc. Faraday Trans. 88, 803-826.

Shock, E.L., Sassani, D.C., Willis, M., Sverjensky, D.A., 1997. Inorganic species in geologic fluids: Correlations among standard molal thermodynamic properties of aqueous ions and hydroxide complexes. Geochim. Cosmochim. Acta 61, 907-950.

Shomate, C.H., Cook, O.A., 1946. Low-temperature heat capacities and high-temperature heat contents of $Al_2O_3 \cdot 3H_2O$ and $Al_2O_3 \cdot H_2O$. J. Amer. Chem. Soc. 68, 2140-2142.

Shvarov, Y., 2015. A suite of programs, OptimA, OptimB, OptimC, and OptimS compatible with the Unitherm database, for deriving the thermodynamic properties of aqueous species from solubility, potentiometry and spectroscopy measurements. Appl. Geochem. 55, 17-27.

Siever, R., 1962. Silica solubility, 0-200° C, and the diagenesis of siliceous sediments. J. Geol. 70, 127-150.

Simonson, J.M., Holmes, H.F., Busey, R.H., Mesmer, R.E., Archer, D.G., Wood, R.H., 1990. Modeling of the thermodynamics of electrolyte solutions to high temperatures including ion association. Application to hydrochloric acid. J. Phys. Chem. 94, 7675–7681.

Smith, E.R., Taylor, J.K., 1940. Standard electrode potential of sodium. J. Res. National Bureau Standards 25, 731-744.

Sretenskaya, N.G., 1992. The dissociation constant of hydrochloric acid from the electrical conductance data for HCl solutions in water-dioxane mixtures. Geochem. Internat. 29, 447-453.

Steefel, C.I., Maher, K., 2009. Fluid-rock interaction: a reactive transport approach. Rev. Mineral. 70, 485-532.

Stefánsson, A., 2001. Dissolution of primary minerals of basalt in natural waters: I. Calculation of mineral solubilities from 0°C to 350°C. Chem. Geol. 172, 225-250.

Sverjensky, D., Shock, E.L., Helgeson, H.C., 1997. Prediction of the thermodynamic properties of aqueous metal complexes to 1000°C and 5 kb. Geochim. Cosmochim. Acta 61, 1359-1412.

Sverjensky, D.A., Harrison, B., Azzolini, D., 2014. Water in the deep Earth: The dielectric constant and the solubilities of quartz and corundum to 60kb and 1200°C. Geochim. Cosmochim. Acta 129, 125-145.

Sverjensky, D.A., Hemley, J.J., D'Angelo, W.M., 1991. Thermodynamic assessment of hydrothermal alkali feldspar-mica-aluminosilicate equilibria. Geochim. Cosmochim. Acta 55, 989-1004.

Tajčmanová, L., Vrijmoed, J., Moulas, E., 2015. Grain-scale pressure variations in metamorphic rocks: implications for the interpretation of petrographic observations. Lithos 216-217, 338-351.

Tagirov, B.R., Schott, J., 2001. Aluminum speciation in crustal fluids revisited. Geochim. Cosmochim. Acta 65, 3965-3992.

Tagirov, B.R., Zotov, A.V., Akinfiev, N.N., 1997. Experimental study of dissociation of HCl from 350 to 500°C and from 500 to 2500 bars: Thermodynamic properties of HCl°(aq). Geochim. Cosmochim. Acta 61, 4267-4280.

Takahashi, Y., Yamada, K., Fukunaga, T., Mukaibo, T., 1973. Heat capacity of hydrated and crystalline aluminas. Denki Kagaku 41, 287–290.

Tanger, J.C., Helgeson, H.C., 1988. Calculation of the thermodynamic and transport properties of aqueous species at high pressures and temperatures; revised equations of state for the standard partial molal properties of ions and electrolytes. Amer. J. Sci. 288, 19-98.

Thien, B.M.J., Kulik, D.A., Curti, E., 2014. A unified approach to model uptake kinetics of trace elements in complex aqueous - solid solution systems. Appl. Geochem. 41, 135-150.

Tropper, P., Manning, C.E., 2007. The solubility of corundum in H_2O at high pressure and temperature and its implications for Al mobility in the deep crust and upper mantle. Chem. Geol. 240, 54-60.

Tsirlina, S.M., 1936. The solubility of aluminum hydroxides in sodium hydroxide solutions. (System AI(OH)-NaOH-H_2O). Legkiye Metally 5, 10.

Tutolo, B.M., Kong, X.Z., Seyfried, W.E., Saar, M.O., 2014. Internal consistency in aqueous geochemical data revisited: Applications to the aluminum system. Geochim. Cosmochim. Acta 133, 216-234.

Vanderzee, C.E., Nutter, J.D., 1963. Heats of solution og gaseous hydrogen chloride and hydrogen bromide in water at 25°C. J. Phys. Chem. 67, 2521-2523.

Verdes, G., Gout, R., Castet, S., 1992. Thermodynamic properties of the aluminate ion and of bayerite, boehmite, diaspore and gibbsite. Eur. J. Mineral. 4, 767-792.

Volosov A.G., Khodakovskiy I.L., Ryzhenko B.N., 1972. Equilibria in the system SiO_2-H_2O at elevated temperatures along the lower three-phase curve. Geochem. Intl. 9, 362-377

Wagman, D.D., Evans, W.H., Parker, V.B., Schumm, R.H., Halow, I., Bailey, S.M., Churney, K.L. Nuttal, R.L., 1982, The NBS tables of chemical thermodynamic properties. Selected values for inorganic and C1, and C2 organic substances in SI units. J. Phys. Chem. Ref. Data 11 (Suppl. 2), 392 pp.

Wagner, T., Kulik, D.A., Hingerl, F.F., Dmytrieva, S.V., 2012. GEM-Selektor geochemical modeling package: TSolMod library and data interface for multicomponent phase models. Can. Mineral. 50, 1173-1195.

Walther, J.V., Orville, P.M., 1983. The extraction-quench technique for determination of the thermodynamic properties of solute complexes: application to quartz solubility in fluid mixtures. Amer. Mineral. 68, 731-741.

Walther, J.V., 1997. Experimental determination and interpretation of the solubility of corundum in H_2O between 350 and 600°C from 0.5 to 2.2 kbar. Geochim. Cosmochim. Acta 61, 4955-4964.

Walther, J.V., 2001. Experimental determination and analysis of the solubility of corundum in 0.1 and 0.5 m NaCl solutions between 400 and 600°C from 0.5 to 2.0 kbar. Geochim. Cosmochim. Acta 65, 2843-2851.

Walther, J.V., Woodland, A.B., 1993. Experimental determination and interpretation of the solubility of the assemblage microcline, muscovite, and quartz in supercritical H_2O. Geochim. Cosmochim. Acta 57, 2431-2437.

Wefers, K., 1967. Zur chemischen Technologie des Bauxitaufschlusses. Teil 1: Das System N_2Q-Al_2O_3-H_2O. Metallography 21, 1-10.

Weill, D.F., Fyfe, W.S., 1964. The solubility of quartz in H_2O in the range 1000-4000 bars and 400-550°C. Geochim. Cosmochim. Acta 28, 1243-1255.

Wesolowski, D.J., 1992. Aluminum speciation and equilibria in aqueous solution: I. The solubility of gibbsite in the system Na-K-Cl-OH-$Al(OH)_4$ from 0 to 100°C. Geochim. Cosmochim. Acta 56, 1065-1091.

Wintsch, R.P., Merino, E., Blakely, R.F., 1980. Rapid-quench hydrothermal experiments in dilute chloride solutions applied to the muscovite-quartz-sanidine equilibrium. Amer. Mineral. 65, 1002-1011.

Wohlers, A., Manning, C.E., Thompson, A.B., 2011. Experimental investigation of the solubility of albite and jadeite in H_2O, with paragonite-quartz at 500 and 600°C, and 1-2.25 GPa. Geochim. Cosmochim. Acta 75, 2924-2939.

Woodland, A.B., Walther, J.V., 1987. Experimental determination of the solubility of the assemblage paragonite, albite, and quartz in supercritical H_2O. Geochim. Cosmochim. Acta 51, 365-372.

Wyart, J., Sabatier, G., 1955. Nouvelles mesures de la solubilite du quartz, de la tridymite et de la cristobalite dans l'eau sous pression au-dessus de la temperature critique. Compt. Rendus Acad. Sci. 240, 1905-1907.

Xie, Z., Walther, J.V., 1993. Quartz solubilities in NaCl solutions with and without wollastonite at elevated temperatures and pressures. Geochim. Cosmochim. Acta 57, 1947-1955.

Xu, T., Sonnenthal, E., Spycher, N., Pruess, K., Brimhall, G., Apps, J., 2001. Modeling multiphase non-Isothermal fluid flow and reactive geochemical transport in variably saturated fractured rocks: 2. Applications to supergene copper enrichment and hydrothermal flows. Amer. J. Sci. 301, 34-59.

Xu, T., Spycher, N., Sonnenthal, E., Zhang, G., Zheng, L., Pruess, K., 2011. TOUGHREACT Version 2.0: A simulator for subsurface reactive transport under non-isothermal multiphase flow conditions. Comp. Geosci. 37, 763-774.

Yalman, R.G., Shaw, E.R., Corwin, J.F., 1960. The effect of pH and fluoride on the formation of aluminum oxides. J. Phys. Chem. 64, 300-303.

Yamaguchi, G., Yanagida, H., Soejima, S., 1962. On the solubility and the velocity of dissolution of corundum under hydrothermal conditions. Bull. Chem. Soc. Japan 35, 1789-1794.

Yardley, B.W.D, 1997. The evolution of fluids through the metamorphic cycle. In: Jamtveit, B., Yardley, B.W.D. (Eds.) Fluid Flow and Transport in Rocks, pp. 139-147.

Zhang, Z., Duan, Z., 2005. Prediction of the PVT properties of water over wide range of temperatures and pressures from molecular dynamics simulation. Phys. Earth Planet. Inter. 149, 335-354.

Zhang, L., Soong, Y., Dilmore, R., Lopano, C. (2015) Numerical simulation of porosity and permeability evolution of Mount Simon sandstone under geological carbon sequestration conditions. Chem. Geol. 403, 1-12.

Zheng, L., Apps, J.A., Zhang, Y., Xu, T., Birkholzer, J.T., 2009. On mobilization of lead and arsenic in groundwater in response to CO_2 leakage from deep geological storage. Chem. Geol. 268, 281-297.

Zhu, C., Sverjensky, D.A., 1991. Partitioning of F-Cl-OH between minerals and hydrothermal fluids. Geochim. Cosmochim. Acta 55, 1837-1858.

Zhu, C., Anderson, G., 2002. Environmental Applications of Geochemical Modeling, Cambridge University Press, 300 pp.

Zimmermann, R., Gottschalk, M., Heinrich, W., Franz, G., 1997. Experimental Na-K distribution between amphiboles and aqueous chloride solutions, and a mixing model along the richterite – K-richterite join. Contrib. Mineral. Petrol. 126, 252-264.

Zimmerman, G.H., Scott, P.W., Greynolds, W., 2007. A new flow instrument for conductance measurements at elevated temperatures and pressures: Measurements on NaCl(aq) to 458 K and 1.4 MPa. J. Solut. Chem. 36, 767-786.

Table EA1. Standard state properties (Gibbs energy of formation, partial molal entropy, heat capacity and volume) for mineral end members used in this study. The values were taken as such from Holland and Powell database (dataset ds55 2002). These values were not optimized during the global optimization.

					$Cp^0 = a_0 + a_1 \cdot T + a_2 \cdot T^{-2} + a_3 \cdot T^{-0.5} + a_4 \cdot T^2$					
	$\Delta_f G^0_{298,1}$	$S^0_{298,1}$	$Cp^0_{298,1}$	$V^0_{298,1}$	a_0	$a_1 \cdot 10^5$	a_2	a_3	a°	κ
	(J/mol)	(J/mol·K)	(J/mol·K)	(J/bar)	(kJ/K)	(kJ/K^2)	(kJ·K)	(kJ/K$^{0.5}$)	(K^{-1})	(kbar)
albite	-3711996	210.1	207.725	10.006	0.4520	-1.3364	-1275.9	-3.9536	4.56	593
albite high	-3706202	223.4	204.694	10.109	0.4520	-1.3364	-1275.9	-3.9536	4.56	593
analcite (analcime)	-3091093	232	211.729	9.740	0.6435	-1.6067	9302.3	-9.1796	5.00	400
andalusite	-2441050	92.7	122.594	5.153	0.2773	-0.6588	-1914.1	-2.2656	4.11	1334
coesite	-850864	40.8	45.0974	2.064	0.0965	-0.0577	-448.8	-0.7982	1.80	1000
cristobalite	-853084	46.5	44.919	2.610	0.0979	-0.3350	-626.2	-0.7740	0.81	600
corundum	-1581808	50.9	79.4529	2.558	0.1395	0.5890	-2460.6	-0.5892	4.19	2520
diaspore	-920825	35	53.4369	1.776	0.1451	0.8709	584.4	-1.7411	7.97	2300
jadeite	-2849218	133.5	159.915	6.040	0.3011	1.0143	-2239.3	-2.0551	4.66	1284
kalsilite	-2006218	134	118.477	6.040	0.2420	-0.4482	-859.8	-1.9358	5.76	590
kaolinite	-3801669	203.7	224.553	9.934	0.4367	-3.4295	-4055.9	-2.6991	5.10	645
kyanite	-2442617	83.5	121.564	4.414	0.2794	-0.7124	-2055.6	-2.2894	4.04	1590
leucite	-2866366	200	162.794	8.828	0.3698	-1.6332	684.7	-3.6831	3.67	630
microcline	-3750316	216	204.267	10.892	0.4488	-1.0075	-1007.3	-3.9731	3.35	574
muscovite	-5603884	292	321.881	14.083	0.7564	-1.9840	-2170	-6.9792	5.96	490
nepheline	-1980505	124.4	114.290	5.419	0.2727	-1.2398	0	-2.7631	8.10	600
paragonite	-5565263	276	323.97	13.211	0.8030	-3.1580	217	-8.1510	7.74	550
pyrophyllite	-5266775	239.4	293.738	12.810	0.7845	-4.2948	1251	-8.4959	7.50	525
quartz	-856433	41.5	44.8909	2.2688	0.1107	-0.5189	0	-1.1283	0.65	750
sanidine	-3744340	230	204.367	10.900	0.4488	-1.0075	-1007.3	-3.9731	3.35	574
sillimanite	-2438765	95.5	124	4.986	0.2802	-0.6900	-1375.7	-2.3994	2.21	1320
shistovite	-816165	24.5	42.8835	1.401	0.0681	0.6010	-1978.2	-0.0821	2.50	3160

Table EA1. *(continued)*

					$Cp^0 = a_0 +$					
	$\Delta_f G^0_{298,1}$ (J/mol)	$S^0_{298,1}$ (J/mol·K)	$Cp^0_{298,1}$ (J/mol·K)	$V^0_{298,1}$ (J/bar)	a_0 (kJ/K)	$a_1 \cdot 10^5$ (kJ/K^2)	a_2 (kJ·K)	a_3 (kJ/K$^{0.5}$)	a° (K^{-1})	κ (kbar)
[1]boehmite	-918400	37.19	54.2399	1.954	0.205721	-3.4921	1026.66	-2.63527	-	-
[1]gibbsite	-1154900	68.4	91.7203	3.196	0.0546974	17.0272	-1221.73	0	-	-

(1) Taken from Robie and Hemingway (1995), heat capacity polynomial coefficients for gibbsite from Pokrovskii and Helgeson (1995). a° is the thermal expansion parameter; κ is the bulk modulus (incompressibility) at 298K.

Table EA2. The values for the standard sate molal Gibbs free energy for the aluminium aqueous species which resulted after the optimization against gibbsite and boehmite solubility experiments.

Species	$\Delta_f G^0_{298,1}$ (J/mole)	Standard Deviation	95% confidence	Optimization mode
Al^{3+}	-486513	352	691	Optimized
$AlOH^{2+}$	-695460	652[(2)]	3749	[(1)]Constrained
$Al(OH)_2^+$	-898674	486	955	Optimized
$Al(OH)_3^0$	-1105180	1923	3775	Optimized
$Al(OH)_4^-$	-1305337	343	673	Optimized
$NaAl(OH)_4^0$	-1567809	1103	2165	Optimized

(1) Constrained to Al^{3+} by the reaction: $AlOH^{+2} + H^+ = Al^{3+} + H_2O$, and the logK values from Palmer and Wesolowski (1993)
(2) Calculated using the error for the Al^{3+} and the reported error for the logK at 298.15 K of about 0.05

Table EA3. Values of the standard sate molal Gibbs energy for the aqueous species, which resulted after the optimization against the solubility experiments for minerals present in the HP02 database, but with the values for aluminium hydrolysis species constrained through reactions using logK values (Table EA2) derived from fitting those for aluminium species against gibbsite and boehmite solubility experiments.

Species	$\Delta_f G^0_{298,1}$ (J/mole)	Standard Deviation	95% confidence	Optimization mode
Al^{3+}	-486338	282	554	Optimized
$AlOH^{2+}$	-695153	934	1858	(1)Constrained
$Al(OH)_2^+$	-898500	768	1509	(1)Constrained
$Al(OH)_3^0$	-1105006	2205	4329	(1)Constrained
$Al(OH)_4^-$	-1305163	625	1227	(1)Constrained
$NaAl(OH)_4^0$	-1561967	1984	3895	(1)Constrained
$AlH3SiO_4^{2+}$	-1782276	916	1720	(2)Constrained
$KAlO_2^0$	-1100302	932	1831	(3)Constrained
K^+	-276768	650	1277	Optimized
KOH	-431534			(4)Constrained
KCl	-393258			(4)Constrained
Na^+	-256212	599	1176	Optimized
NaOH	-411737			(4)Constrained
NaCl	-383234			(4)Constrained
$NaHSiO_3^0$	-1283195	1805	3586	(5)Constrained
$HSiO_3^-$	-1018600	314	616	Optimized
SiO_2^0	-834063	64	126	Optimized
Cl^-	-131290			(6)Fixed
HCl^0	-127240			(7)Fixed
OH^-	-157287			(6)Fixed
H_2O(aq)	-237183	(8)100		(8)Fixed

(1) Constrained to Al^{3+} by the following reactions: (a) $AlOH^{2+} + H^+ = Al^{3+} + H_2O$; (b) $Al(OH)_2^+ + H^+ = AlOH^{2+} + H_2O$; (c) $Al(OH)_3^0 + H^+ = Al(OH)_2^+ + H_2O$; (d) $Al(OH)_4^- + H^+ = Al(OH)_3^0 + H_2O$; (e) $NaAl(OH)_4^0 = Al(OH)_4^- + Na^+$; and the logK values calculated using the values in Table EA1 and their corresponding HKF parameters and other standard state properties for the values at elevated temperatures and pressures

(2) Constrained to Al^{3+} and SiO_2^0 by the reaction: $Al^{3+} + 2\ H_2O + SiO_2^0 = AlH_3SiO_4^0 + H^+$, and the logK from Tagirov and Schott (2001), extracted from Pokrovskii et al. (1996) and Salvi et al. (1998)

(3) Constrained to K^+ and Al_3^+ by the reaction: $K^+ + Al_3^+ + 2\ H_2O = KAlO_2^0 + 4\ H^+$

(4) Constrained to Na^+, K^+, OH^-, and Cl^- using the logK determined from the new standard state properties properties of the ion pairs extracted from conductance data (Table 1)

(5) Constrained to Na^+ and SiO_2^0 by the reaction: $Na^+ + H_2O + SiO_2^0 = NaHSiO_3^0 + H^+$, and the logK from Sverjensky et al. (1997), extracted from Seward (1974)

(6) Shock and Helgeson (1988)

(7) Tagirov et al. (1997)

(8) Johnson et al. (1992)

Table EA4. Alternative thermodynamic dataset for aqueous species and minerals, converted to restore the CODATA recommended $\Delta_f G^0_{298,1}$ values for Na+ and K+ aqueous ions.

Aqueous Species	$\Delta_f G^0_{298,1}$ (J/mol)	Mineral end-members	$\Delta_f G^0_{298,1}$ (J/mol)
Al^{3+}	-486627	(3)albite	-3706284
$AlOH^{2+}$	-695574	(3)albite high	-3700490
$Al(OH)_2^+$	-898295	(3)analcite (analcime)	-3085381
$Al(OH)_3^0$	-1105801	andalusite	-2441050
$Al(OH)_4^-$	-1305097	boehmite	-918400
(1)$NaAl(OH)_4^0$	-1567833	coesite	-850864
$AlH_3SiO_4^{2+}$	-1782516	cristobalite	-853084
(2)$KAlO_2^0$	-1105862	corundum	-1581808
$Al(OH)_4^-$	-1305097	diaspore	-920825
(2)K^+	-282462	gibbsite	-1154900
(2)KOH^0	-437225	(3)jadeite	-2843506
(2)KCl^0	-408113	(4)kalsilite	-2000649
(1)Na^+	-261881	kaolinite	-3801669
(1)$NaOH^0$	-417306	kyanite	-2442617
(1)$NaCl^0$	-388803	(3)leucite	-2860654
(1)$NaHSiO_3^0$	-1288788	(4)microcline	-3744747
$HSiO_3^-$	-1015237	(4)muscovite	-5598315
SiO_2^0	-834103	(3)nepheline	-1974793
Cl^-	-131290	(3)paragonite	-5559551
HCl^0	-127240	pyrophyllite	-5266775
OH^-	-157287	quartz	-856433
H^+	0	(4)sanidine	-3738771
H_2O	-237183	sillimanite	-2438765
		shistovite	-816165
		topaz-OH	-2690013
		tridymite	-853665

(1) $\Delta_f G^0_{298,1}$ (Table 6) -5712; (2) $\Delta_f G^0_{298,1}$ (Table 6) -5569; (3) $\Delta_f G^0_{298,1}$ (HP98, ds55 2002) +5712; (4) $\Delta_f G^0_{298,1}$ (HP98, ds55 2002) +5569. The standard Gibbs energy values for Na^+ and K^+ aqueous ions and species, reported in Table 6 (main text), were adjusted by adding -5712 and -5569 J/mol, respectively. The standard Gibbs energy values for Na and K-bearing minerals from Holland and Powell (1998) database (ds55), reported in Table EA1, were adjusted with +5712 and +5569 J/mol per mol of Na and K in the mineral formula. The remaining (unchanged) thermodynamic properties and HKF parameters of the aqueous species are reported in Tables 1 and 5 in the manuscript; those of minerals (unchanged) are reported in Table EA1 of the electronic supplementary material. The reaction constants between any K and Na aqueous ions, species, and minerals in this database remain the same as in the database reported in the main text (Table 6 for aqueous species and Table AE1 for minerals).